



**HAL**  
open science

## **Lagrangian ocean analysis: Fundamentals and practices**

Erik van Sebille, Stephen Griffies, Ryan Abernathey, Thomas Adams, Pavel Berloff, Arne Biastoch, Bruno Blanke, Eric Chassignet, Yu Cheng, Colin J Cotter, et al.

► **To cite this version:**

Erik van Sebille, Stephen Griffies, Ryan Abernathey, Thomas Adams, Pavel Berloff, et al.. Lagrangian ocean analysis: Fundamentals and practices. *Ocean Modelling*, 2018, 121, pp.49-75. 10.1016/j.ocemod.2017.11.008 . hal-02106837

**HAL Id: hal-02106837**

**<https://hal.science/hal-02106837>**

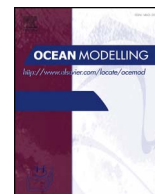
Submitted on 6 Apr 2021

**HAL** is a multi-disciplinary open access archive for the deposit and dissemination of scientific research documents, whether they are published or not. The documents may come from teaching and research institutions in France or abroad, or from public or private research centers.

L'archive ouverte pluridisciplinaire **HAL**, est destinée au dépôt et à la diffusion de documents scientifiques de niveau recherche, publiés ou non, émanant des établissements d'enseignement et de recherche français ou étrangers, des laboratoires publics ou privés.



Distributed under a Creative Commons Attribution - NoDerivatives 4.0 International License



## Review

## Lagrangian ocean analysis: Fundamentals and practices



Erik van Sebille<sup>\*,a,b</sup>, Stephen M. Griffies<sup>c</sup>, Ryan Abernathey<sup>d</sup>, Thomas P. Adams<sup>e</sup>, Pavel Berloff<sup>f</sup>, Arne Biastoch<sup>g</sup>, Bruno Blanke<sup>h</sup>, Eric P. Chassignet<sup>i</sup>, Yu Cheng<sup>j</sup>, Colin J. Cotter<sup>f</sup>, Eric Deleersnijder<sup>k,l</sup>, Kristofer Döös<sup>n</sup>, Henri F. Drake<sup>o,p</sup>, Sybren Drijfhout<sup>q</sup>, Stefan F. Gary<sup>e</sup>, Arnold W. Heemink<sup>l</sup>, Joakim Kjellsson<sup>r,t</sup>, Inga Monika Koszalka<sup>g,aa</sup>, Michael Lange<sup>a,s</sup>, Camille Lique<sup>h</sup>, Graeme A. MacGilchrist<sup>u</sup>, Robert Marsh<sup>q</sup>, C. Gabriela Mayorga Adame<sup>v</sup>, Ronan McAdam<sup>a</sup>, Francesco Nencioli<sup>w</sup>, Claire B. Paris<sup>j</sup>, Matthew D. Piggott<sup>s</sup>, Jeff A. Polton<sup>v</sup>, Siren Rühls<sup>g</sup>, Syed H.A.M. Shah<sup>m,l</sup>, Matthew D. Thomas<sup>x</sup>, Jinbo Wang<sup>y</sup>, Phillip J. Wolfram<sup>z</sup>, Laure Zanna<sup>t</sup>, Jan D. Zika<sup>a,bb</sup>

<sup>a</sup> Grantham Institute & Department of Physics, Imperial College London, UK

<sup>b</sup> Institute for Marine and Atmospheric Research, Utrecht University, Utrecht, Netherlands

<sup>c</sup> NOAA / Geophysical Fluid Dynamics Laboratory, Princeton, USA

<sup>d</sup> Department of Earth and Environmental Sciences, Columbia University, NY, USA

<sup>e</sup> Scottish Association for Marine Science, Oban, UK

<sup>f</sup> Department of Mathematics, Imperial College London, UK

<sup>g</sup> GEOMAR Helmholtz Centre for Ocean Research Kiel, Kiel, Germany

<sup>h</sup> Laboratoire d'Océanographie Physique et Spatiale, UMR 6523, CNRS-IFREMER-IRD-UBO, Brest, France

<sup>i</sup> Center for Ocean-Atmospheric Prediction Studies, Florida State University, Tallahassee, FL, USA

<sup>j</sup> Department of Ocean Sciences, Rosenstiel School of Marine and Atmospheric Science, University of Miami, USA

<sup>k</sup> Université catholique de Louvain, Institute of Mechanics, Materials and Civil Engineering (IMMC) & Earth and Life Institute (ELI), Louvain-la-Neuve, Belgium

<sup>l</sup> Delft Institute of Applied Mathematics (DIAM), Delft University of Technology, Netherlands

<sup>m</sup> Department of Mathematics, Sukkur Institute of Business Administration, Pakistan

<sup>n</sup> Department of Meteorology, Bolin Centre for Climate Research, Stockholm University, Sweden

<sup>o</sup> Department Atmospheric and Oceanic Sciences, Princeton University, USA

<sup>p</sup> Currently at Massachusetts Institute of Technology and Woods Hole Oceanographic Institution Joint Program in Oceanography, USA

<sup>q</sup> University of Southampton, UK

<sup>r</sup> British Antarctic Survey, Cambridge, UK

<sup>s</sup> Department of Earth Science and Engineering, Imperial College London, UK

<sup>t</sup> Department of Physics, University of Oxford, UK

<sup>u</sup> Department of Earth Sciences, University of Oxford, UK

<sup>v</sup> National Oceanography Centre, Liverpool, UK

<sup>w</sup> Remote Sensing Group, Plymouth Marine Laboratory, Plymouth, UK

<sup>x</sup> School of Geology and Geophysics, Yale University, USA

<sup>y</sup> Jet Propulsion Laboratory, California Institute of Technology, USA

<sup>z</sup> Climate, Ocean and Sea Ice Modeling, Theoretical Division: Fluid Dynamics and Solid Mechanics, Los Alamos National Laboratory, Los Alamos, NM, USA

<sup>aa</sup> Christian-Albrechts University of Kiel, Kiel, Germany

<sup>bb</sup> School of Mathematics and Statistics, University of New South Wales, Sydney, Australia

## ARTICLE INFO

## Keywords:

Ocean circulation  
Lagrangian analysis  
Connectivity  
Particle tracking  
Future modelling

## ABSTRACT

Lagrangian analysis is a powerful way to analyse the output of ocean circulation models and other ocean velocity data such as from altimetry. In the Lagrangian approach, large sets of virtual particles are integrated within the three-dimensional, time-evolving velocity fields. Over several decades, a variety of tools and methods for this purpose have emerged. Here, we review the state of the art in the field of Lagrangian analysis of ocean velocity data, starting from a fundamental kinematic framework and with a focus on large-scale open ocean applications. Beyond the use of explicit velocity fields, we consider the influence of unresolved physics and dynamics on particle trajectories. We comprehensively list and discuss the tools currently available for tracking virtual particles. We then showcase some of the innovative applications of trajectory data, and conclude with some open questions and an outlook. The overall goal of this review paper is to reconcile some of the different techniques

\* Corresponding author at: Institute for Marine and Atmospheric Research, Utrecht University, Utrecht, Netherlands.  
E-mail address: [E.vanSebille@uu.nl](mailto:E.vanSebille@uu.nl) (E. van Sebille).

and methods in Lagrangian ocean analysis, while recognising the rich diversity of codes that have and continue to emerge, and the challenges of the coming age of petascale computing.

## 1. Introduction

The ocean exhibits a huge range of dynamical motions, spanning scales from millimetres to thousands of kilometres. As seawater moves, each fluid particle carries tracers such as salt, nutrients, heat, as well as particulate matter such as plankton and marine debris. For various theoretical and practical applications, we are interested in how water moves between ocean regions. That is, we are interested in mapping out pathways of seawater motion, since the transport of seawater and its tracer content, as well as the pathways and timescales for that transport, are key facets in how the ocean plays a role in climate and marine ecology.

### 1.1. Estimating pathways

There are two general methods for estimating pathways in the ocean. One method makes use of tracers, such as the multitude of age tracers described by Mouchet et al. (2016) and references therein. Tracer studies are well suited for Eulerian methods, which make direct use of ocean velocity fields on their native grids.

The second approach makes exclusive use of the Lagrangian perspective of fluid dynamics (e.g., Bennett, 2006). This method employs an ensemble of virtual (passive) Lagrangian particles of zero spatial extent whose trajectories are determined by the velocity field.<sup>1</sup> The velocity fields that are used to move the particles often come from OGCMs, although there are interesting applications using observational-based velocities such as surface geostrophic velocities based on satellite altimetry (e.g. d'Ovidio et al., 2009; Klocker and Abernathy, 2014), or measured by high frequency (HF) radar (e.g. Ullman et al., 2006).

Trajectories for virtual particles map out pathlines of the velocity field, often including the effect of subgrid scale diffusion. Statistics of the trajectories then define particle pathways and their associated time scales. By following the flow of virtual particles, and possibly assigning non-zero transports and other properties to them in post-processing, questions about pathways and flow connectivity can be addressed.

This review focuses on Lagrangian analysis methods facilitated by virtual particles in the open ocean. We are partly motivated by the growing array of floating instruments in the ocean along with the improving Lagrangian simulation capabilities. There is a corresponding need to review the methods and foster new ideas for extracting information about the ocean circulation from the entangled trajectories of floats and/or simulated particles. We thus aim to summarize the state of the science in Lagrangian modelling and analysis, focussing on the large scale open ocean circulation, hoping to support a new generation of scientists contributing to the development and use of the methods.

Our presentation is aimed at graduate students, though any large-scale oceanographer or mathematician with an interest in virtual particle analysis could use this paper as a starting point. In that sense, this paper is intended as an accompanying paper to Griffies et al. (2000), which provided an introduction to primitive equation ocean models and to Ådlandsvik et al. (2009), which gave an overview of Lagrangian modelling practice from a marine biology perspective.

### 1.2. Overview of Lagrangian ocean analysis

Observationalists have been tracking the ocean in a Lagrangian fashion since the very early ages of oceanography. Movements of the

currents were documented using either ship drift or the drift of purposely built (subsurface) floats (e.g., Swift and Riser, 1994). Many observations remain inherently Lagrangian, such as the trajectories of surface drifters shown in Fig. 1 (Lumpkin and Pazos, 2007), the subsurface Argo floats (Lebedev et al., 2007; Ollitrault and Rannou, 2013), and the tracking of fish larvae (Paris et al., 2013a) and turtle hatchlings (Scott et al., 2014).

Lagrangian analysis through virtual particle tracking within OGCMs began in the 1980s, on small-scale structures, with studies on a theoretical box-model (Awaji et al., 1980) as well as a model that incorporated hydrographic data and realistic topography (Imasato et al., 1980). The Lagrangian framework of these small-scale examples was then applied to the velocity-field output of basin-scale, three-dimensional numerical experiments. Examples include regional deep ocean circulation (Fujio and Imasato, 1991), western boundary currents (Imasato and Qiu, 1987), fronts (Pavia and Cushman-Roisin, 1988) and gyre transport (Böning and Cox, 1988). Particle trajectories in global ocean circulation models, driven by global hydrographic and wind observations, were first achieved in the 1990s (Fujio et al., 1992; Döös, 1995; Drijfhout et al., 1996; Blanke and Raynaud, 1997).

In recent years, more than 100 articles per year are published with the words 'Lagrangian Ocean Modelling' as the topic, according to the Web of Science. These papers include studies on the pathways of virtual particles that simulate sea water pathways, as well as explicit tracking of tracers such as nutrients (e.g. Chenillat et al., 2015; Jönsson et al., 2011) and particulates such as larvae (e.g. Cowen et al., 2006; Paris et al., 2005; Teske et al., 2015; Cetina-Heredia et al., 2015; Phelps et al., 2015), plastics (e.g. Lebreton et al., 2012), microbes (e.g. Hellweger et al., 2014), planktic foraminifera (e.g. van Sebille et al., 2015), jellyfish (e.g. Dawson et al., 2005), icebergs (e.g. Marsh et al., 2015), surface drifters (e.g. Kjellsson and Döös, 2012b), oil droplets (e.g. Paris et al., 2012), eel (e.g. Baltazar-Soares et al., 2014), pumice (e.g. Jutzeler et al., 2014) and many more.

The ocean circulation covers an enormous range of scales and regions. As said above, in this review we focus primarily on applications on the basin and global scales. However, it should be noted that there is also extensive Lagrangian analysis work done on smaller scales, such as in coastal zones and recently in the Gulf of Mexico through interest in dispersion of the DeepWater Horizon oil spill (e.g. Beron-Vera and LaCasce, 2016; Haza et al., 2016).

The Lagrangian framework is not only used to analyse velocity fields by computing their integral curves, but also to directly solve for the trajectory by casting the equations of motion in a Lagrangian framework (Bennett, 2006). Lagrangian methods are widely used in engineering, including Discrete Element Methods (e.g. Kruggel-Emden et al., 2008) and Smoothed Particle Hydrodynamics (e.g. Cummins et al., 2012). While advances in this field have been made in large scale oceanography, both for sub-components of ocean models (e.g. Bates et al., 2012) and for fully Lagrangian ocean models (Haertel and Randall, 2002; Haertel and Fedorov, 2012), this topic is not the focus of this review. Instead, we focus on Lagrangian diagnostic methods to identify oceanic pathways.

The Lagrangian framework for analysing pathways is complementary to the analysis of tracers. One of the key differences is the computational cost. For each time step, movement of a Lagrangian particle takes only one set of computations. In contrast, the advection-diffusion of a tracer concentration takes  $N$  sets of computation, where  $N$  is the number of discrete ocean grid cells. While one Lagrangian particle trajectory does not allow for meaningful analysis of ocean pathways, this comparison does show that the computational scaling of the two

<sup>1</sup>Lagrangian particles are also sometimes called 'e-floats' by, for example, Bower et al. (2009).

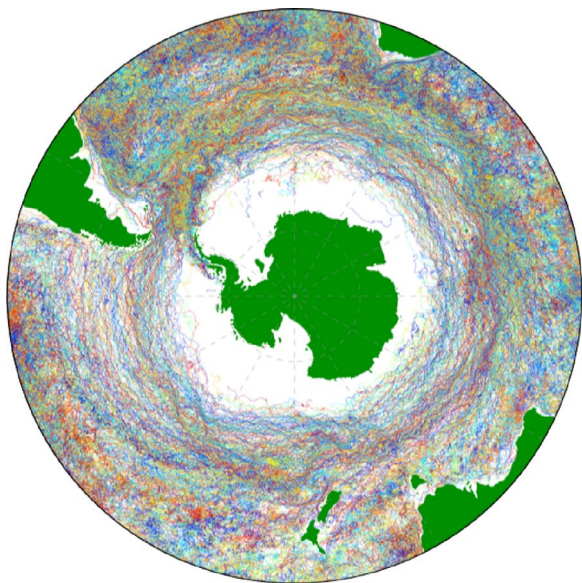


Fig. 1. Map of all the Southern Ocean observational Lagrangian surface drifters in the NOAA GDP Data Set (Lumpkin and Pazos, 2007). Each drifter is geo-located every 6 h and has a randomly assigned colour. (For interpretation of the references to colour in this figure legend, the reader is referred to the web version of this article.)

methods is very different.

Furthermore, the experimental design is different for tracer and particle experiments. Exclusive to particle experiments is that the entire trajectory history of the virtual particles can in principle be stored. This history allows for *a posteriori* analysis of ‘connectivity’ between different regions of the ocean (e.g., Sections 4.5 and 4.6) and ‘conditional statistics’ (e.g. Koszalka et al., 2013b; van Sebille et al., 2013; 2014; von Appen et al., 2014; Gary et al., 2014; Durgadoo et al., 2017), where subsets of particles can be analysed that obey certain conditions based on their properties. For example, in van Sebille et al. (2013), particles in the Southern Ocean were analysed for how often they looped around Antarctica in their journey from the Antarctic slope to the deep subtropical basins. Such an analysis would be hard to do with tracer fields, although the latter has its own advantages, including a more natural alignment with the treatment of advection and diffusion within models.

Finally, another great advantage of Lagrangian particle experiments is that particles can be advected, at least in offline mode when velocity fields are stored, backwards in time. This reverse-time analysis allows one to investigate where water masses found within a model at a certain location come from.

### 1.3. Structure of this paper

This paper is structured as follows. In Section 2 we introduce a kinematic framework used for thinking about Lagrangian particles. In Section 3 we detail how to compute and interpret Lagrangian particles, including an overview of the available Lagrangian diagnostic tools. In Section 4, we highlight applications of how virtual particle trajectories can be analysed to reveal quantitative and qualitative information about the flow. In Section 5, we conclude the main part of the paper with future outlooks. A selection of appendices then provide examples and detailed discussion of topics introduced earlier in the paper, as well as brief descriptions of the different numerical codes introduced in Section 3.

## 2. Kinematic framework

We here introduce a kinematic framework to describe fluid motions. The ideas are fundamental to how we make use of both Eulerian and Lagrangian methods for analysing ocean circulation. We make

connections to Lagrangian analysis methods, though reserve algorithmic details for later sections.

### 2.1. Lagrangian and Eulerian reference frames

A Lagrangian kinematic approach is based on a description of the fluid in a reference frame that is moving with an infinitesimal fluid particle (equivalently a “fluid parcel”). Fluid motion is thus the accumulation of continuum particle motion. The fluid particle framework that forms the basis for Lagrangian kinematics offers a powerful conceptual picture of fluid motion (e.g., Salmon, 1998; Bennett, 2006), with this picture taken as the basis for Lagrangian methods of analysis.

Eulerian kinematics is a complement to Lagrangian kinematics. The Eulerian approach is based on describing fluid motion in a reference frame that is fixed in space. Eulerian kinematics is the basis for most numerical ocean circulation models, in which the horizontal position of grid cells is held fixed in time.<sup>2</sup> Quite generally, the technical aim of Lagrangian ocean analysis is to estimate the trajectory of virtual fluid particles by making use of Eulerian fluid information, i.e., the velocity field.

### 2.2. Trajectories or material pathlines

The motion of a classical point particle is described by knowledge of its position vector,  $\mathbf{X}(t)$ , which provides the position of the particle at time  $t$ . As the particle moves, it traces out a curve in space referred to as a *trajectory*. When describing  $N$  discrete particles, we add a discrete label to each of the particle positions,  $\mathbf{X}^{(n)}(t)$ . For continuum matter, such as seawater, the discrete label  $n$  becomes a continuous vector,  $\mathbf{X}(\mathbf{a}, t)$ , with  $\mathbf{a} = \mathbf{X}(t = t_0)$  a common (though not necessary) choice. In general, the label vector,  $\mathbf{a}$ , is referred to as the *material coordinate* (e.g., Salmon, 1998), since this coordinate distinguishes between infinitesimal particles comprising the continuum.

A fluid particle is conceived of as a microscopically large collection of many molecules, whose velocity is formally determined as a mass weighted mean of the velocity of the individual molecules (i.e., *barycentric* velocity as defined in Section II.2 of DeGroot and Mazur (1984) and Section 1.9 of Salmon (1998)). Alternatively, by making the continuum hypothesis, we dispense with molecular degrees of freedom, so that a particle is considered a macroscopically small material fluid volume, treated as a mathematical continuum and labelled by the material coordinate  $\mathbf{a}$ . For an incompressible fluid, the fluid particle has constant volume; however, its constituents do not remain fixed, as they are generally exchanged with adjacent particles through mixing, thus changing the particle’s tracer content (e.g., water, salt, nutrients), as well as altering its heat, all the while maintaining a constant volume.

The velocity of a fluid particle is the time derivative of the trajectory, computed with the material coordinate held fixed. The mathematical connection between Lagrangian and Eulerian descriptions is enabled by equating the particle velocity crossing a point in space,  $\mathbf{X}(\mathbf{a}, t) = \mathbf{x}$ , to the fluid velocity field at that point

$$\left( \frac{\partial \mathbf{X}(\mathbf{a}, t)}{\partial t} \right)_{\mathbf{a}} = \mathbf{v}(\mathbf{x}, t) \quad \text{where } \mathbf{X}(\mathbf{a}, t) = \mathbf{x}. \quad (1)$$

The relation (1) provides a starting point for Lagrangian fluid analysis. Note that the resulting fluid particle trajectories are sometimes called material pathlines in the fluid mechanics literature (e.g., Aris, 1962; Batchelor, 1967).

<sup>2</sup> The top and bottom faces of grid cells are generally moving, since the general vertical coordinates defining these surfaces need not be static. For example, these cell faces may be defined according to constant pressure, constant potential density, or constant rescaled ocean depth.



### 2.3. The material time derivative without trajectories

A kinematic description requires time changes of an arbitrary function,  $\Psi$ , evaluated along trajectories,  $\Psi[\mathbf{X}(\mathbf{a}, t), t]$ . Use of the chain rule leads to

$$\frac{\partial \Psi[\mathbf{X}(\mathbf{a}, t), t]}{\partial t} = \left[ \left( \frac{\partial}{\partial t} \right)_{\mathbf{x}} + \mathbf{v}[\mathbf{X}(\mathbf{a}, t), t] \cdot \nabla \right] \Psi[\mathbf{X}(\mathbf{a}, t), t]. \quad (2)$$

Note that, when trajectories are dispensed with (as in the Eulerian description), we recover the more succinct expression for the material time derivative

$$\frac{D\Psi(\mathbf{x}, t)}{Dt} = \left( \frac{\partial}{\partial t} + \mathbf{v}(\mathbf{x}, t) \cdot \nabla \right) \Psi(\mathbf{x}, t), \quad (3)$$

where all expressions on the right hand side are taken with respect to the fixed Eulerian reference frame.<sup>3</sup> The symbol  $D$  is commonly used to distinguish the material time derivative from a more general time derivative that is not necessarily following a material fluid particle. To illustrate this formalism, consider  $\Psi(\mathbf{x}, t) = \mathbf{x}$ . In this case, the material time derivative is given by the velocity field at that point

$$\frac{D\mathbf{x}}{Dt} = \mathbf{v}(\mathbf{x}, t). \quad (4)$$

### 2.4. Steady-state volume transport pathways defined by streamtubes

Within Lagrangian Ocean Analysis, there is a long history of interpreting particle trajectories as streamtubes, and using this interpretation to compute volume transports (Döös, 1995; Blanke and Raynaud, 1997, see also Section 3.2.3). Formally, the equivalence between streamtubes and material pathways is only valid for steady-state flows (i.e. where the flow is constant in time). Originally, the streamtube calculations were indeed performed on time-mean, steady-state velocity fields, but they were soon extended to time-varying flows, for example by assuming piecewise steady flow (Blanke and Raynaud, 1997, cf. Section 3.2.3). Over the last two decades, however, the approach has been widely used in studies of large-scale ocean transports (see e.g. Section 4.5), justifying a discussion of the mathematical underpinning of streamtubes for steady-state flows here in this review manuscript.

The ocean is a nearly incompressible fluid. Thus, for this review we consider an incompressible (Boussinesq) fluid, which means that the velocity field is non-divergent

$$\nabla \cdot \mathbf{v} = 0. \quad (5)$$

Consequently, the volume of a material fluid particle remains constant (i.e., it is incompressible).

A streamtube is a bundle of streamlines, so that streamtube sides are parallel to the velocity (see e.g. Fig. 3.6 in Kundu et al., 2012).<sup>4</sup> For a steady flow, streamlines are equivalent to material pathlines, in which case streamtubes are material tubes. It is for the steady case that we can make use of streamtubes to map out volume transport pathways in an incompressible fluid. We see this property by integrating the non-divergence constraint, Eq. (5), over the streamtube, and making use of Gauss's Law. Doing so reveals that volume transport (volume per time) through the two streamtube ends balances exactly

$$\int_{A_1} \mathbf{v} \cdot \hat{\mathbf{n}} \, dA + \int_{A_2} \mathbf{v} \cdot \hat{\mathbf{n}} \, dA = 0, \quad (6)$$

<sup>3</sup> An alternative derivation of Eq. (3), which is arguably more straightforward mathematically, dispenses with trajectories from the start, in which case we express the total differential of a function as  $d\Psi(\mathbf{x}, t) = dt \partial_t \Psi + d\mathbf{x} \cdot \nabla \Psi$ . Specifying the spatial increment to correspond to movement of a fluid particle,  $d\mathbf{x} = \mathbf{v}(\mathbf{x}, t) dt$ , leads to Eq. (3). We prefer the derivation using particle trajectories, as it exposes the relation between Lagrangian and Eulerian reference frames.

<sup>4</sup> One may think of streamtubes as the “communication cable lines” within an incompressible fluid, transmitting volume signals within a steady flow.

where  $\hat{\mathbf{n}}$  is the outward normal at the respective end, and  $dA$  the corresponding area. By construction,  $\mathbf{v} \cdot \hat{\mathbf{n}} = 0$  on the streamtube sides, so the sides do not contribute to the balance in Eq. (6). Hence, the volume transport entering one streamtube end equals to that leaving the other end. Furthermore, the area of the streamtube is inversely proportional to the local normal velocity.

The transport constraint (6) holds regardless of whether there is diffusive tracer mixing in the Boussinesq fluid. It follows from the non-divergence property of the velocity field in an incompressible fluid. However, in the presence of diffusive tracer mixing, the actual material entering one end of the streamtube is not necessarily the same as the material exiting the other end (see also Section 2.5).

The above properties make streamtubes useful for understanding the circulation in a steady incompressible fluid. In particular, they provide the mathematical basis for Lagrangian analysis methods that tag particles with volume transport (e.g. Eckart, 1948; Welander, 1955). The aggregated integral curves for such particles define a probability density function (PDF) for volume transport pathways. In the continuum and under the assumption of a steady flow field, volume transport pathways deduced from streamtubes are identical to pathways deduced from particle trajectories determined by time stepping Eq. (1).

We can make use of the volume transport information carried by streamtubes for Lagrangian analysis. To do so, define the starting point for a streamtube by assigning a volume transport to each particle. The assigned volume transport is directly proportional to the transport crossing the grid cell face where the particle is initialized. In principle, we can fill a non-divergent flow field without void between streamtubes. Consequently, we can compute streamtube derived volume transport pathways whether the flow is laminar or turbulent. However, turbulent flow generally requires more streamtubes to develop robust statistics for the transport pathways, and also requires that the flow is assumed piecewise steady (see also Section 3.2.3), as for any transient flow, steady-state streamlines lose their equivalence to pathlines.

### 2.5. An introduction to tracer transport pathways

A finite-size material seawater parcel is comprised of fresh water and tracers of other matter, such as salts and biogeochemical components.<sup>5</sup> Tracer concentration,  $C$ , measures the mass of tracer per parcel mass. The velocity considered in fluid mechanics is the barycentric velocity (Section 2.2), so that the mass (or volume for a Boussinesq fluid) of a material fluid parcel is constant. However, the mass of each trace constituent is not materially constant, since tracers are exchanged between parcels through mixing in the presence of concentration gradients. Since the small-scale motions that govern this mixing are hardly ever resolved in OGCMs, the effect of tracer mixing has to be represented as (resolution-dependent) diffusive transports based on mean distributions.

In Section 2.4, we defined volume transport pathways according to streamtubes in a steady flow. Here, we introduce transport pathways defined by trace constituents. In the presence of diffusive tracer mixing, tracer and volume transport pathways are distinct. The machinery of stochastic differential equations (SDEs) is required to compute tracer transport pathways, with details deferred to Section 3.3. Our purpose here is to anticipate that discussion by introducing various forms of the tracer concentration equation. In so doing, we also introduce the residual mean velocity.

<sup>5</sup> Conservative temperature can also be considered as the concentration of heat in a parcel. The reason is that, to a very good approximation, Conservative Temperature satisfies a source-free tracer equation analogous to salinity (McDougall, 2003; Graham and McDougall, 2013).

### 2.5.1. The tracer equation with subgrid scale transport

Molecular diffusion as well as turbulent subgrid scale transport processes give rise to irreversible (diffusive) transport as well as reversible (advective or skew diffusive) transport. Mathematically, we express the subgrid scale tracer transport through a transport tensor,  $\mathbf{J}$ . The corresponding tracer concentration equation takes the form<sup>6</sup>

$$\left(\frac{\partial}{\partial t} + \mathbf{v} \cdot \nabla\right)C = \nabla \cdot (\mathbf{J} \cdot \nabla C), \quad (7)$$

where the transport tensor  $\mathbf{J}$  has units of squared length per time. It is convenient to split the transport tensor into the sum of a symmetric and anti-symmetric tensor

$$\mathbf{J} = \mathbf{K} + \mathbf{A}. \quad (8)$$

The symmetric tensor,  $\mathbf{K}$ , has components satisfying<sup>7</sup>

$$K_{ij} = K_{ji}. \quad (9)$$

This tensor corresponds to diffusion so long as it is positive definite. The anti-symmetric tensor,  $\mathbf{A}$ , corresponds to skew diffusion or equivalently to advection (e.g., Middleton and Loder, 1989; Griffies, 1998).

Given the decomposition of the transport tensor (8), we find it useful to write the tracer equation in the form

$$\left(\frac{\partial}{\partial t} + \mathbf{v}^\dagger \cdot \nabla\right)C = \nabla \cdot (\mathbf{K} \cdot \nabla C), \quad (10)$$

where

$$\mathbf{v}^\dagger = \mathbf{v} + \mathbf{v}^* \quad (11)$$

defines the *residual-mean velocity* and

$$v_j^* = -\partial_i A_{ij} \quad (12)$$

is known as the eddy-induced velocity.<sup>8</sup> Notably, the eddy-induced velocity is non-divergent due to the anti-symmetry property

$$A_{ij} = -A_{ji} \Rightarrow \nabla \cdot \mathbf{v}^* = 0. \quad (13)$$

Consequently, the tracer Eq. (10) can be written in the flux-form

$$\frac{\partial C}{\partial t} + \nabla \cdot (\mathbf{v}^\dagger C) = \nabla \cdot (\mathbf{K} \cdot \nabla C). \quad (14)$$

Since both  $\mathbf{v}$  and  $\mathbf{v}^\dagger$  are divergence-free, one can define a streamtube in a steady-state flow according to either velocity field. The streamtubes defined by the residual mean velocity are often more relevant than those for the Eulerian time-mean velocity for ocean transport since the residual mean velocity  $\mathbf{v}^\dagger$  incorporates information about subgrid scale eddy advective transport. Drijfhout et al. (2003), for example, explicitly calculated particle trajectories with both Eulerian mean and residual mean velocities and discussed the differences in (overturning) pathways. Particle trajectories using the Eulerian mean exhibit motions that cross mean isopycnal surfaces, whereas trajectories making use of the residual mean better respect the adiabatic nature of the meridional overturning flow.

### 2.5.2. Introducing the Fokker–Planck equation

Anticipating the discussion of Stochastic Differential Equations (SDEs) in Section 3.3.1, we manipulate the diffusive contribution in the tracer Eq. (14). The aim is to write the tracer concentration equation in the form of a Fokker–Planck equation (see Eq. (24)), which describes the time evolution of the probability density function of the tracer. For this purpose, we use the identity

$$\partial_i (K_{ij} \partial_j C) = \partial_i [\partial_j (K_{ij} C) - C \partial_j K_{ij}], \quad (15)$$

<sup>6</sup> We assume a Boussinesq fluid when writing the tracer Eq. (7).

<sup>7</sup> We make use of Cartesian tensors throughout this review, with results generalizable to arbitrary coordinates.

<sup>8</sup> Repeated indices are summed over their range.

so that

$$\frac{\partial C}{\partial t} + \nabla \cdot (\mathbf{v}^{\text{drift}} C) = \partial_{ij} (K_{ij} C), \quad (16)$$

where we introduced the drift velocity

$$\mathbf{v}^{\text{drift}} = \mathbf{v}^\dagger + \nabla \cdot \mathbf{K}. \quad (17)$$

The drift velocity generally has a non-zero divergence

$$\nabla \cdot \mathbf{v}^{\text{drift}} = \partial_{ij} K_{ij}, \quad (18)$$

since  $\partial_{ij} K_{ij}$  does not generally vanish<sup>9</sup>. Eq. (16) is the tracer equation written in the form of a Fokker–Planck equation.

Tracer transport pathways differ from volume transport pathways in the following ways. First, as already mentioned, the drift velocity  $\mathbf{v}^{\text{drift}}$  is generally divergent. Hence, it is not useful to define steady-state “tracer streamtubes” in terms of  $\mathbf{v}^{\text{drift}}$ . Second, even if  $\nabla \cdot \mathbf{K} = 0$  so that the drift velocity is divergent-free (e.g., isotropic diffusion with a constant diffusivity), tracer pathways are affected by diffusive mixing between fluid particles. To represent such diffusion in a Lagrangian trajectory calculation requires a stochastic noise term weighted by the diffusion tensor (Section 3.3). Therefore, whether one considers volume transport pathways or tracer transport pathways depends on the scientific question and the information available to address that question.

### 2.5.3. Using particles to track a tracer patch

There is yet another way to consider tracer transport pathways using Lagrangian analysis. For this approach, we represent a patch of tracer as a collection of Lagrangian particles (e.g. Bennett, 2006; LaCasce, 2008). In this way, Lagrangian analysis can be used to study tracer dispersion (Rossi et al., 2013; Wang et al., 2016). In principle, in the limit of infinite number of particles and knowledge of the velocity field to arbitrarily fine spatial and temporal resolution, the tracer dispersion from Lagrangian particles would have theoretically perfect resolution and controllable numerical diffusion. How achievable this is in real-world simulations remains an area of active research.

A tracer patch can be represented by a cloud of particles. Each particle carries a portion of the total tracer content. Let  $c$  denote the tracer volume per particle. The corresponding Eulerian tracer concentration,  $C(\mathbf{x}, t)$ , can be written

$$C(\mathbf{x}, t) = \sum_{i=0}^N W(\mathbf{x} - \mathbf{x}_i(t))c_i, \quad (19)$$

where  $N$  is the total number of particles,  $\mathbf{x}_i$  is the particle position, and  $W$  is a mapping kernel function (dimensions inverse volume) that maps the particle density to tracer density. The kernel function satisfies the normalization condition required to conserve volume

$$\int_{\Omega} W \, dx \, dy \, dz = 1, \quad (20)$$

where  $\Omega$  is the integral volume in three dimensions. The form of  $W$  has been extensively investigated in the Smoothed Particle Hydrodynamic approach (Monaghan, 1992). Different forms of  $W$  exist with different projection errors.

## 3. Computing Lagrangian particle trajectories

In this section we discuss technical aspects of Lagrangian modelling and analysis, focusing here on the computation of trajectories. We consider how trajectories of virtual Lagrangian particles can be used in mapping both volume transport pathways and tracer transport

<sup>9</sup> One notable case where  $\nabla \cdot \mathbf{v}^{\text{drift}} = 0$  is isotropic diffusion with a constant diffusivity; e.g., molecular diffusion. Molecular diffusion is generally not relevant for large-scale ocean models, as models (and large-scale observations) do not resolve down to the Kolmogorov scales. Hence, large-scale models make use of the far larger, and flow dependent, eddy diffusivities.

**Table 1**  
Summary of the specifications of the offline Lagrangian codes discussed Appendix A

Code name	Ariane	TRACMASS	Octopus	LAMTA	CMS	Parcels
Website	<a href="http://www.univ-brest.fr/lpo/ariane">www.univ-brest.fr/lpo/ariane</a>	<a href="http://tracmass.org">tracmass.org</a>	<a href="https://github.com/jimbow/Octopus">github.com/jimbow/Octopus</a>	<a href="https://bitbucket.org/f_nencio/spasso/overview">bitbucket.org/f_nencio/spasso/overview</a>	<a href="https://github.com/beatrixparis/connectivity-modeling-system">github.com/beatrixparis/connectivity-modeling-system</a>	<a href="http://oceanparcels.org">oceanparcels.org</a>
License	CeCILL ( <a href="http://www.cecill.info">http://www.cecill.info</a> )	open source	MIT	GNU General Public License	GNU GPL v3	MIT
Key citation	Blanke and Raynaud (1997); Blanke et al. (1999)	Doos et al. (2017)	Wang et al. (2016)	d'Ovidio et al. (2015)	Paris et al. (2013b)	Lange and van Sebille (2017)
OGCMs supported	NEMO/OPA, ROMS, Symphonie and any C-grid	NEMO, IFS (AGCM), MOM, MICOM, POM, HYCOM	MITgcm; any C-grid	AVISO satellite velocities; any velocity field on A-grids (euclidean or spherical)	HYCOM, OFES, NEMO, SOSE, MOM, MITgcm	NEMO, OFES, GlobCurrent; customizable to any OGCM with NetCDF data format
Language(s)	Fortran 90/95; Matlab (IDL on request) for visualisation	Fortran	Fortran	GNU/Octave and C++	Fortran	Python user interface, auto-generated C
Primary use	Offline calculation of 3D streamlines in the velocity field at any scale (regional, basin, global); volume transport calculations	3D water mass pathways, particle/tracer dispersion	3D watermass pathway, particle/tracer dispersion, cross-frontal transport, Argo float simulation	Compute satellite based Lagrangian diagnostics to optimize sampling strategy of meso-scale-based field campaign and support interpretation of in-situ observations	Dispersion, connectivity, fate of pollutants; Individual Based Modelling	Large scale oceanography; Individual Based Modelling; teaching (via customizable interface)
Advection method	Analytic	Analytic	RK4	RK4	RK4	RK4, RK45, Explicit Euler; extensible interface for custom advection methods
Diffusion method	No diffusion (purely kinematic method)	Brownian motion for background diffusion with random displacement or randomly added velocities	Brownian motion for background diffusion, random displacement within the mixed layer	Random walk optional	Brownian motion for background diffusion, random displacement within the mixed layer	Extensible interface for Random Walk and custom behaviour
Grids supported	Arakawa C, also tested with Arakawa B interpolated on C-grid, partial cells supported	Arakawa A, B, C. Spatially and temporally varying vertical grids supported (partial cells, $z^*$ , sigma, hybrid) including those for AGCMs	Arakawa C	Arakawa A	Orthogonal (rectangular) Arakawa A, B and C	Arakawa A, B and C; unstructured meshes planned
Key strengths	Almost 25 years of experience with core of the code; easy-to-install, easy-to-use; fast analytical solution; no coast crash; qualitative mode (full details of selected trajectories) and quantitative mode (volume transport calculations); compatible with the conservation laws of the OGCM	Volume conserving, fast analytical solutions without intermediate time steps, works with both OGCMs and AGCMs	Fast using Fortran, supports openMP	Designed to work out-of-the-box with AVISO surface geostrophic velocities. Already configured to compute a broad range of Lagrangian diagnostics (i.e. Finite Time/Size Lyapunov Exponents; longitudinal and latitudinal origin of particles; time of particle retention within mesoscale eddies etc.)	Modular, fast, parallel; Multi-grid support; Used in a wide variety of contexts, from marine ecology to physical oceanography	Ease-of-use, customizable extension interface and automated performance optimization
Shortcomings	No parallel mode; trajectory scheme is somewhat crude beyond the context of 3D water mass tracing	Need of improving the diffusion method	Non-scalable parallelization, not very efficient in reading large model output	Particle advection only 2D; cannot be run in parallel.	No support for non-orthogonal grids; parallel implementation is heavy on I/O	Not yet parallel; support for unstructured meshes in progress

**Table 2**  
Summary of the specifications of the online Lagrangian codes discussed Appendix A

Code name	LIGHT in MPAS-O	NEMO online floats and icebergs	MITgcm	HYCOM Float Package	ROMS online floats
Website License	mpas-dev.github.io Copyright (c) 2013, Los Alamos National Security, LLC (LANL) and the University Corporation for Atmospheric Research (UCAR). Wolfram et al. (2015)	nemo-ocean.eu/About-NEMO/Reference-manuals CeCILL ( <a href="http://www.cecill.info">http://www.cecill.info</a> )	mitgcm.org None	hycom.org None	myroms.org/wiki/floats.in Open source MIT/X
Key citation		Madec and NEMO team (2016) for floats; Marsh et al. (2015) for icebergs	Marshall et al. (1997a)	Halliwel and Garraffo (2002), Garraffo et al. (2001a); 2001b)	Pitones et al. (2011), Narvaez et al. (2012b)
OGCMs supported	Model for Prediction Across Scales Ocean (MPAS-O) (Ringler et al., 2013)	NEMO	MITgcm	Hybrid Coordinate Ocean Model (HYCOM) (Bleck, 2002; Chassignet et al., 2003; 2006)	ROMS
Language(s) Primary use	Fortran (post-processing in python) Large scale oceanography, diagnosing ocean mixing	Fortran Floats: large-scale, eddying ocean circulation. Icebergs: coupling of iceberg fluxes with ocean physics and dynamics and sea ice, via heat, freshwater and momentum fluxes; evaluating/forecasting iceberg hazard Floats: Ariane method or RK4. Icebergs: RK4	Fortran Ocean modelling at all scales, offline advection	Fortran Large scale and coastal oceanography, biology	Fortran Coastal and mesoscale oceanography, Individual Based modelling for biophysical applications
Advection method	Sub-stepped generalized RK for time integration; Wachspress and RBF horizontal interpolation	None	RK4	RK4	4th-order Milne predictor and 4th-order Hamming corrector
Diffusion method	None	None	Brownian motion optional	Brownian motion optional	Vertical random walk optional
Grids supported	Unstructured C-grid	Arakawa C	Arakawa C	Arakawa C	Arakawa C
Key strengths	Fast (minimal cost to OGCM), high temporal and spatial fidelity, computes isopycnal advection by construction, extensible within Fortran framework Currently no explicit offline mode, tied to MPAS framework and presently embedded in MPAS-O	Floats: Analytical advection on model timestep resolution. Icebergs: freshwater flux due to melting icebergs Floats: limited use/publications to date. Icebergs: physics and dynamics subject to several uncertain parameters; giant tabular icebergs not yet represented; interactions with sea ice currently limited	Works well with archived MITgcm velocity fields, scales to very large sizes using MPI and domain tiling Complicated to set up	Stable and relatively easy to use and understand	Reliable since trajectories are coherent with ocean circulation, parallel, easy to set up Computationally expensive since no offline model is available; Large output files for long runs or many particles.
Shortcomings				No parallel mode	



pathways (recall the distinction discussed in Section 2.5).

### 3.1. Basic needs for Lagrangian trajectory calculations

For volume transport pathways, one needs a non-divergent velocity field. A three-dimensional non-divergent velocity can be produced by sampling a Boussinesq ocean model, thus offering a means to compute three-dimensional trajectories. To compute tracer transport trajectories, we need both a velocity field and a diffusion tensor. The diffusion tensor is a function of the often poorly known subgrid scale flow, and it is generally a complex function of the flow field. Consequently, the calculation of tracer transport pathways is somewhat less mature than volume transport pathways (though see Tables 1 and 2).

When using an ocean model, we distinguish between two techniques of Lagrangian integration. The first occurs online, whereby trajectories are computed each time step that the Eulerian model is updated. Examples of such online methods are available for volume transport pathways using the velocity field (see Section 3.5). In contrast, we know of no example of online tracer trajectory calculations making use of both the instantaneous velocity field and the diffusion tensor.

The second method for Lagrangian analysis occurs through off-line trajectory calculations. Off-line methods make use of stored velocity fields sampled from the Eulerian model. Off-line trajectory calculations offer the ability to compute trajectories in a forward mode (from their starting point forward in time) or in a backward mode (from their ending point backward in time).

As an alternative to velocities generated by OGCMs, we may use observation-based data from floats or drifters, which generally give a two dimensional surface velocity (e.g., Koszalka et al., 2011). We may also diagnose a surface geostrophic velocity by differentiating gridded satellite observations of the sea surface height (e.g., Klocker et al., 2012b). Notably, both surface drifter/float velocities and surface geostrophic velocities generally have a non-zero horizontal divergence (surface geostrophic velocities are non-divergent only on an  $f$ -plane), and the corresponding surface trajectories do therefore not map volume transport pathways. Nonetheless, the resulting surface trajectories do map preferred pathways of the surface flow, thus providing useful diagnostic information.

Computation of particle trajectories using a velocity field requires essentially two operations: a way to integrate the trajectory Eq. (1) and a way to interpolate a gridded velocity field to an arbitrary point in space and time. In this section, we detail these aspects.

### 3.2. Temporal integration of the virtual particle trajectory equation

When the  $n$ th virtual seawater particle is located at the point  $\mathbf{X}^{(n)}(t) = \mathbf{x}$ , we can update its position by time stepping the velocity Eq. (1)

$$\mathbf{X}(t + \Delta t) = \mathbf{X}(t) + \int_t^{t+\Delta t} \mathbf{v}(\mathbf{x}(\tau), \tau) d\tau, \quad (21)$$

where we dropped the trajectory super-script  $n$  to simplify notation. Note that the integrand involves the Eulerian velocity field  $\mathbf{v}(\mathbf{x}, \tau)$ , which equals to the Lagrangian velocity  $d\mathbf{X}(t)/dt$  when evaluated at  $\mathbf{X}(t) = \mathbf{x}$ . In some applications of Lagrangian analysis, there is an additional term on the right hand side of Eq. (21) that represents unresolved physics (see Section 3.3.2). We explore various flavours of this discrete time stepping (see also Fig. 2) for estimating virtual particle trajectories, focussing on the most commonly used schemes. However, there are many more schemes than discussed here (e.g., Chu and Fan, 2014; Liu and Chua, 2016).

In general, the accuracy of trajectories computed in OGCM fields depends on accuracy of the time stepping scheme, as well as accuracy of the interpolation scheme used to estimate velocity at the time and position of the particle (see Section 3.4). Note that the first three

methods (explicit, implicit and analytical) discussed below all result in identical trajectories in the continuum. However, the trajectories differ in numerical implementations due to algorithmic differences and truncation errors. For all methods, statistical significance of the diagnosed pathways is enhanced by increasing the number of deployed particles. As a rule of thumb, one has deployed a sufficient numbers of particles when the physical results of interest do not significantly change as the number of particles is increased (e.g., Jones et al., 2016).

The maximum integration time in Eq. (21) is limited to the run time of a given model simulation. A number of oceanic processes, however, have time scales that exceed these run times (e.g., England, 1995; Stouffer, 2004; Danabasoglu, 2004). Using Lagrangian particles to temporally resolve for example the meridional overturning circulation (Blanke et al., 1999; Thomas et al., 2015b) or inter-basin connectivity (Blanke and Speich, 2002) can be difficult with many state of the art climate models. To address this problem, a commonly employed *ad hoc* method is to loop the model data in time such that the velocity and tracer fields are returned to the first time step once the end has been reached (e.g., Döös et al., 2008; van Sebille et al., 2012; Thomas et al., 2015b). This approach thus permits particles to be advected for longer time scales than available from the raw data. However, particle looping can only work if the model has no drift in the velocity or tracer fields, that there are no large unphysical jumps in the fields between the end and the beginning of the model run, and that any unphysical jumps will have a small net effect on the particle pathways.

#### 3.2.1. Explicit time stepping methods

One way to integrate Eq. (21) is to multiply the velocity at a point by a time step,  $\Delta t$ , to estimate the displacement. This approach is known as the Euler method and is correct to first order in  $\Delta t$ . Better accuracy of the trajectories can be obtained by using higher-order methods for the integration of Eq (21). One popular method is the 4<sup>th</sup> order Runge–Kutta scheme (e.g., Butcher, 2016), where information of the

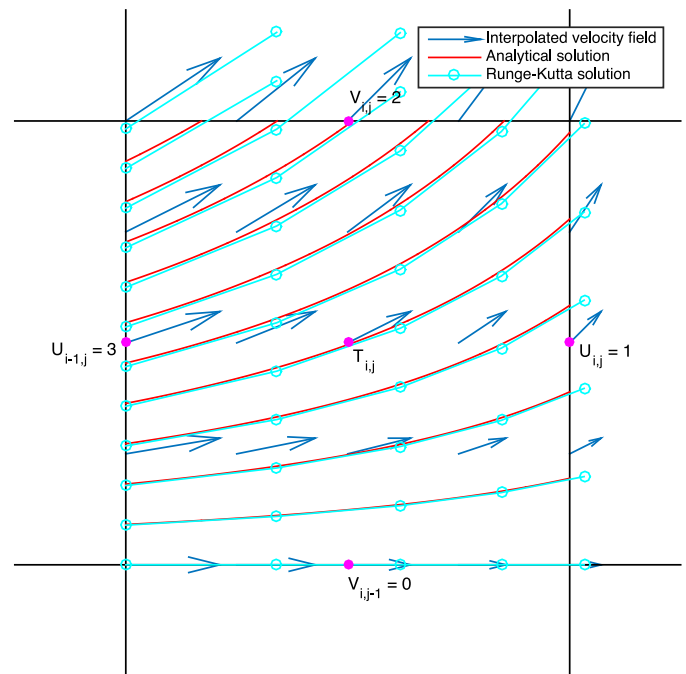


Fig. 2. Illustration of time stepping solutions on an Arakawa C-grid with edges of non-dimensional length = 1. Velocities ( $u, v$ ) across the four edges are given in numbers at the magenta dots. The blue arrows are the linearly interpolated velocities within the grid. Assume particles are released on the  $i - 1$  (left) edge. The red lines are pathlines of the analytical solution for these particles. The cyan piecewise linear lines are the solutions to the RK4 time-stepping with  $dt = 0.1$ . The two types of integration lead to similar solutions. (For interpretation of the references to colour in this figure legend, the reader is referred to the web version of this article.)

(interpolated) velocity field at four increments between time steps  $t_n$  and  $t_{n+1}$  is used.

The fourth order Runge–Kutta method is a member of a family of integrators (Dormand and Prince, 1980). One interesting extension is adaptive timestepping through a RK45-method, where both a fourth order and a fifth order integration are performed. The extra computational cost of a fifth order computation is marginal when a fourth order is already performed. The difference,  $\Delta X = |X_5 - X_4|$ , between the fifth order and fourth order solution can be computed. If  $\Delta X$  is larger than some (pre-chosen) threshold, the time step  $\Delta t$  of Eq. (21) can adaptively be reduced for that particle. Doing so then leads to a straightforward implementation of adaptive timestepping using Runge–Kutta integrators. However, it is not *a priori* clear how the error thresholds for  $\Delta X$  should be chosen.

When working with stored velocity data, as when virtual particle trajectories are computed offline, temporal interpolation is usually required. Interpolation is needed because the interval between consecutive stored velocity fields is generally longer than the time step,  $\Delta t$ , used to advance the particle trajectories in Eq. (21). This temporal interpolation of the velocity fields can be a large source of error, particularly when the interval with which velocity fields are stored becomes longer than a few days (e.g. Valdivieso Da Costa and Blanke, 2004; Qin et al., 2014).

### 3.2.2. Time-implicit discrete integration schemes

To determine volume transport pathways, the volume-preservation properties of numerical integrators becomes an important consideration. Symplectic time integration schemes are one method used to maintain volume conservation for discrete methods. They can be mathematically shown to exactly conserve area in divergence-free 2D fields, meaning that the area bounded by a set of particles will stay constant over time in the absence of turbulent diffusion<sup>10</sup>. Symplectic methods for Lagrangian particles in two dimensions take the same form as symplectic integrators for systems of point vortices, but now the velocity is prescribed (Marsden et al., 1999). The disadvantage of these methods is that they are generally implicit in time. Hence, they require iterative methods. For example, the implicit midpoint rule provides a symplectic integrator for the Lagrangian trajectory equation in two dimensions (McLachlan, 1999; Leimkuhler and Reich, 2004).

In three dimensions, the concept of symplectic integrators must be extended to Lie-Poisson integrators for 3D incompressible velocity fields (McLachlan, 1999; Leimkuhler and Reich, 2004). Few 3D symplectic integrators are known, though the implicit midpoint rule is known to be such an integrator and preserves volume in three dimensions.

### 3.2.3. An analytical discrete streamtube method

Another volume-preserving method to integrate the trajectory Eq. (21) takes advantage of the discrete continuity equation. The resulting virtual particle trajectories respect the volume conservation property of an incompressible Boussinesq fluid, and thereby are particularly suited for experiments where the focus is on the advective component of the flow. In brief, this method analytically computes trajectories across grid cells by making use of the gridded velocity field located on grid cell faces. This approach approximates streamtubes through the use of volume conservation constraints introduced in Section 2.4. While these methods have their origin in applications with steady-state velocity fields, and the streamtube approach is formally only applicable to these cases, there is a large community using extended analytical discrete streamtube methods for time-varying flows too. These applications typically achieve very similar results to the explicit time-stepping schemes.

<sup>10</sup> See Hairer et al. (2006) for a comprehensive description of symplectic time integration schemes, and Leimkuhler and Reich (2004) for an introduction with applications targeted at scientists and engineers.

Algorithms following this approach calculate trajectories for a given steady-state velocity field through analytic computation of three-dimensional streamtubes (Blanke and Raynaud, 1997). If the velocity fields are time-evolving, it is possible to sub-sample them into piecewise steady fields, which are only kept constant in time for a short time; this approach generally increases the computational cost. Another method by de Vries and Döös (2001) allows for analytical trajectories in a time-dependent case that accounts for flow changes across time steps. Döös et al. (2017) showed that the time-dependent trajectory solution is more accurate than the piecewise steady solution, especially in eddying regions, and only at a very small additional computational cost (see also A.1.2).

The analytical calculations are on the scale of a model grid cell for which components of the velocity field, or the volume transports, are typically expressed on a staggered C grid (Mesinger and Arakawa, 1976), i.e., are known over the six faces of the cell (see Fig. 2).<sup>11</sup> The analytical method is enabled by assuming that within a grid cell, the fluid velocity exhibits a linear variation of each velocity component along each corresponding direction, so that

$$\mathbf{v}_{\text{subgrid}} = (u(x), v(y), w(z)). \quad (22)$$

These subgrid scale velocity components ( $u(x)$ ,  $v(y)$ ,  $w(z)$ ) are linear functions of their arguments, with the precise form of these functions determined by the known velocity components on the cell faces. This form of the subgrid scale velocity then allows one to write analytical trajectory equations along the three axes across the grid cell. Analytic time integration of these equations binds each coordinate point ( $x$ ,  $y$ ,  $z$ ) in a grid cell to time in the cell. Grid cell crossing times in each of the three directions are evaluated independently by imposing any of the six grid cell sides as a possible final position. The minimum crossing time specifies the actual crossing time, and hence the trajectory. This approach then allows for an accurate (within the confines of the basic assumption of Eq. (22)) calculation of the final position of a particle on the relevant exit side of the grid cell.

This method for computing volume transport trajectories is both fast and self-consistent. It is fast because it only calculates particle positions on the edge of individual grid cells. It is self-consistent since it respects the local three-dimensional non-divergence of the Boussinesq flow both at the subgrid and the large scale. It therefore provides a judicious method to map volume transport pathways by realizing a discrete implementation of streamtubes introduced in Section 2.4.

Streamtube-based volume transport is reversible, so that backward integrations can be performed to track the origin of a given volume. It is for these reasons that practitioners of discrete streamtube methods generally do *not* introduce diffusion (or stochastic noise) when computing particle trajectories. Rather, the method is focused on determining volume transport pathways defined from the resolved or the residual mean flow.

### 3.3. Computing stochastic trajectories to simulate diffusion and unresolved physics

As noted above, streamtubes track water volume in a steady-state flow. However, in many applications in oceanography, one is interested in tracking tracers such as heat, salt, or nutrients and how they are affected by subgrid scale diffusion and unresolved physics such as mixed layer processes and deep convection (e.g. van Sebille et al., 2013). Tracer concentrations can directly be computed from the spreading of a cloud of particles described by Stochastic Differential Equations (SDEs, see Section 2.5.2), where unresolved physics are represented by stochastic noise.

<sup>11</sup> This method can also be used for A-grid or B-grid stencils, so long as these grids offer conservative volume transport components on tracer cell faces. The use of conservative flux-based transport schemes is a basic property of any finite volume ocean model, regardless the horizontal grid stencil.

Two main approaches can be distinguished in efforts to add diffusion to trajectories. One is to start with the tracer Eq. (16), where the eddy transport is parameterized in terms of the eddy-induced velocity and the appropriate form of the diffusivity tensor in order to derive the SDE for particle trajectories (Section 3.3.1). The second approach (Section 3.3.2) is to use an ‘ad hoc’ SDE where a Markov model is fit to observations from surface drifter trajectories or virtual particles in a much finer resolution velocity field.

It remains an active area of research under which circumstances (e.g. underlying research question, spatial and temporal model data resolutions) and how exactly stochastic noise representing subgrid scale diffusion should be implemented (see also Section 3.3.3).

### 3.3.1. Stochastic trajectories using the Fokker–Planck equation

Here, we provide a brief introduction to the implementation of stochastic terms through the use of a Fokker–Planck Equation. The discussion here makes use of the more thorough discussions provided in the textbooks by Gardiner (1985), Jazwinski (1970), and Kloeden and Platen (1992), as well as the oceanographic review by Visser (2008). Advantages of this Lagrangian SDE approach over Eulerian tracer computations are that it can deal with steep concentration gradients and that tracer concentration can never become negative.

A stochastic differential equation (SDE) for a general trajectory  $\mathbf{X}(t)$  is given by

$$dX_i(t) = a_i(t, \mathbf{X})dt + \sigma_{ik}(t, \mathbf{X})dW_k(t), \quad \mathbf{X}(t_0) = \mathbf{X}_0. \quad (23)$$

In this equation,  $X_i(t)$  are components of the tracer trajectory vector  $\mathbf{X}(t)$ , and  $dX_i(t) = X_i(t + dt) - X_i(t)$  is the stochastic particle displacement during the time interval  $[t, t + dt]$ . The term  $a_i(t, \mathbf{X})$  is a deterministic drift, whereas  $\sigma_{ik}(t, \mathbf{X})$  is related to a tracer diffusion tensor (see Eqs. (25) and (26) below). Finally,  $W_k(t)$  is a Wiener process, or Brownian motion, modelling stochastic fluctuations that represent unresolved motions like eddies, waves or small-scale turbulence. The increment  $dW_k(t) = W_k(t + dt) - W_k(t)$  is a Gaussian variable with zero mean and variance  $dt$ , with non-overlapping increments independent of each other. The stochastic model (23) is Markovian, which means that information on the probability density of the trajectory  $\mathbf{X}(t)$  at time  $t$  is sufficient to make predictions at later times. Non-Markovian models require information at earlier times, which is generally impractical. The presence of the Wiener process means that integrating the equation using deterministic calculus does not produce a unique solution. We make use of ideas proposed by Itô, who developed a stochastic calculus to produce a unique solution of the SDE (23).<sup>12</sup>

A cloud of particles will estimate the probability density  $P(t, \mathbf{x})$  for the stochastic tracer trajectories. Use of an Itô stochastic process  $\mathbf{X}(t)$  ensures that the probability density function evolves according to the following Itô form of the Fokker–Planck or forward Kolmogorov equation

$$\frac{\partial P}{\partial t} = \partial_i(a_i P) + \partial_{ij}(b_{ij} P) \\ P(t_0, \mathbf{x}) = P_0(\mathbf{x}), \quad (24)$$

with

$$2b_{ij} = \sigma_{ik} \sigma_{jk}. \quad (25)$$

We can relate the Fokker–Planck Eq. (24) to the Boussinesq form of the tracer Eq. (16), so that<sup>13</sup>

<sup>12</sup>The Itô calculus used here is but one mathematical approach for realizing a unique solution to a SDE (e.g., Gardiner, 1985). Stratonovich and Itô-backward approaches offer alternative stochastic integration methods, and they can also be used to derive stochastic particle models (Gräwe et al., 2012; Shah et al., 2011; Spivakovskaya et al., 2007a; 2007b). We focus on the Itô calculus as it is well known to physicists, as is the corresponding Fokker–Planck equation. Furthermore, the drift,  $a_i(t, \mathbf{X})$ , of an Itô SDE represents the mean of the stochastic particle tracks. Finally, the well known Euler scheme (see Eq. (28) below) is a straightforward numerical approximation of the Itô SDE, whereas this scheme cannot be used to discretize a Stratonovich or an Itô-backward SDE.

<sup>13</sup>The tensor elements  $\sigma_{ik}(t, \mathbf{X})$  are not uniquely determined by the diffusion tensor  $\mathbf{K}$ .

$$b_{ij} = K_{ij} \\ a_i = v_i^\dagger + \partial_j K_{ij} \\ P = C. \quad (26)$$

The corresponding SDE for the trajectory is given by

$$dX_i(t) = \left( v_i^\dagger + \frac{\partial K_{ij}}{\partial x_j} \right) dt + \sigma_{ik}(t, \mathbf{X})dW_k(t), \\ \mathbf{X}(t_0) = \mathbf{X}_0. \quad (27)$$

It is through this connection that we can derive a stochastic Lagrangian model for any advection-diffusion tracer equation.

Stochastic tracer trajectories can be generated numerically through discrete approximations to the Itô stochastic differential equation (Kloeden and Platen, 1992). Discretizing the continuous stochastic differential Eq. (27) using the Euler scheme leads to

$$X_i(t + \Delta t) = X_i(t) + (v_i^\dagger + \partial_j K_{ij})\Delta t + \sigma_{ik}(t, \mathbf{X})\Delta W_k(t) \\ \mathbf{X}(t_0) = \mathbf{X}_0. \quad (28)$$

In this equation,  $\Delta W_k(t)$  is a Gaussian random variable with zero mean and variance  $\Delta t$ , generated via a random generator. The accuracy of the Euler scheme is  $\mathcal{O}(\Delta t^{1/2})$  in the strong sense; i.e., for approximating the individual particle trajectories. When used to generate many trajectories in order to approximate the probability distribution, or equivalently the tracer concentration, then the Euler scheme is  $\mathcal{O}(\Delta t)$  accurate; i.e. the Euler scheme is  $\mathcal{O}(\Delta t)$  in the weak sense. More accurate numerical schemes have been developed, such as in Gräwe et al. (2012), Shah et al. (2011), Shah et al. (2013) and Spivakovskaya et al. (2005; 2007a; 2007b).

There are methods to compute trajectories directly from a SDE for many applications (e.g., Kloeden and Platen, 1992). Trajectory computation directly from SDEs is less mature in large-scale oceanography where it is often difficult to include a realistic diffusion tensor for subgrid scale tracer transport. Appendix B offers an example of tracer trajectories in the presence of an isopycnal diffusion tensor with a time-constant diffusivity. This application is nontrivial and a major advance in the Lagrangian tracer trajectory method. Unfortunately, it is not fully representative of modern parametrisations for global models, whereby the diffusivity is a function of space and time (Abernathey et al., 2013), and the diffusivity tensor may be anisotropic in the lateral directions as well as between lateral and vertical (Fox-Kemper et al., 2013).

Even with a constant isopycnal diffusivity, sampling components of the  $3 \times 3$  diffusion tensor for offline analysis is a nontrivial computational task, particularly in the presence of realistic temporal variability. Additional difficulty arises from time variations in the diapycnal diffusivity used for planetary boundary layer schemes. Consequently, the current generation of explicit SDEs for tracer trajectories are generally restricted to relatively coarse resolution models with rudimentary subgrid scale parametrisations (e.g., Shah et al., 2017), although efforts are underway to improve this.

### 3.3.2. A hierarchy of Markov models for stochastic trajectories

The second approach to adding the effects of diffusion and unresolved physics to particles is to ‘ad hoc’ find an SDE that matches the statistics - e.g. eddy decorrelation time scales and diffusivity - of the stochastic trajectories with either observations or particles simulated in finer-resolution models. This approach has been developed by Griffa (1996) and further by Berloff and McWilliams (2003) in the context of ocean models. See also Vallis (2006, Section 10.2) and LaCasce (2008) for discussion, and Veneziani et al. (2004) and Koszalka et al. (2013a) for implementations.

A hierarchy of Markov models is considered, whereby the stochastic

(footnote continued)

However, all choices consistent with the relation  $2K_{ij} = \sigma_{ik} \sigma_{jk}$  result in statistically identical diffusion processes.



term is added to either particle displacement (zeroth-order Markov model, corresponding to uncorrelated eddy velocity field), the particle velocity (first-order model, accounting for correlations of the velocity) or the particle accelerations. In most cases, the first-order model is found to best approximate the oceanic mesoscale turbulence introduced by coherent eddies.

In the first-order Markov model (multiplicative noise), stochastic noise is used to modify the present position of a particle when updating to a new position, in which case the trajectory Eq. (21) can be written as

$$\mathbf{X}(t + \Delta t) = \mathbf{X}(t) + (1 + \epsilon) \int_t^{t+\Delta t} \mathbf{v}(\mathbf{x}, \tau) d\tau, \quad (29)$$

where  $\epsilon$  is a random number. Notably, the application of noise in this manner does not ensure that  $\mathbf{X}(t + \Delta t)$  results from time stepping a divergence-free velocity. For that purpose, we consider an alternative approach, whereby we introduce a stochastic divergence-free velocity

$$\mathbf{X}(t + \Delta t) = \mathbf{X}(t) + \int_t^{t+\Delta t} [\mathbf{v}(\mathbf{x}, \tau) + \mathbf{v}_{\text{noise}}(\mathbf{x}, \tau)] d\tau. \quad (30)$$

We can ensure  $\nabla \cdot \mathbf{v}_{\text{noise}} = 0$  by introducing a stochastic vector streamfunction, so that for each grid cell we have

$$\mathbf{v}_{\text{noise}}(\mathbf{x}) = \nabla \wedge \Psi_{\text{noise}}(\mathbf{x}). \quad (31)$$

Since the stochastic velocity remains non-divergent, this approach offers a realisation of stochastic streamtubes in steady-state flows. The choice of either Eq. (29) or (30) depends on the application and will be further discussed in Section 3.3.3.

In the zeroth-order Markov model (additive, or *random walk*, noise), the stochastic noise is added to the particle positions, which is often applied in a rather simple form, by adding an extra term to the trajectory Eq. (21):

$$\mathbf{X}(t + \Delta t) = \mathbf{X}(t) + \int_t^{t+\Delta t} \mathbf{v}(\mathbf{x}, \tau) d\tau + R\sqrt{2K\Delta t}. \quad (32)$$

In this equation,  $R = N(0, 1)$  is a random number taken from the normal distribution with zero mean and unit variance, and  $K$  is a constant tracer diffusivity. A major limitation of this model is that, if the drift term is omitted, Eq. (32) will lead to artificial accumulation of particles in regions of low diffusivity, requiring an enhancement of the random walk model (Hunter et al., 1993; Visser, 1997; Ross and Sharples, 2004; Berloff and McWilliams, 2002)

A myriad of behaviours can be added to a random walk model for capturing the biological characteristic of Lagrangian particles. Examples include diurnal vertical migration, temperature dependent planktonic larval duration and time to settling competency. While it must be noted that enhanced complexity does not necessarily imply enhanced accuracy, studies have shown that even modest vertical migration velocities can significantly alter the dispersal patterns of propagules. For example a recirculation in the Western Irish Sea of northwest Europe, associated with summer stratification, retains surface drifters but does not retain vertically migrating organisms (Phelps et al., 2015).

### 3.3.3. When and how to add stochastic terms?

In the above, we have described a few methods to incorporate mixing through stochastic terms. However, exactly when and how to implement these terms is an open question. It will likely depend on the temporal and spatial resolution of the velocity fields, as well as the unresolved processes that the added stochastic components are intended to reproduce. In particular, the consideration should be whether mesoscale coherent eddies and attendant nonlocal transport properties (velocity correlations and steep Eulerian velocity spectra) are resolved by the ocean model velocity field underlying the Lagrangian simulations.

If a velocity field is available at sufficiently high spatial and temporal resolution, adding a stochastic component may be unnecessary and high numbers of particles may suffice (Koszalka et al., 2013b). If

the available velocity field does not resolve important eddy processes, a first-order or second-order Markov model may need to be used to account for a velocity correlations induced by the mesoscale eddy field (Griffa, 1996; Berloff and McWilliams, 2002; LaCasce, 2008). The applicability of the stochastic simulations should in any case be verified against existing observations (Koszalka et al., 2013a) or high resolution model simulations, if available.

It is also still open how the Fokker–Plank Equation approach (Section 3.3.1) and the ad-hoc Markov model approach (Section 3.3.2) can be combined. While the first approach is more mathematically rigorous, the second provides an insight into the properties of observed or simulated oceanic turbulence on different scales and in different regions, and may be useful in building future parameterizations of eddy induced transport in terms of Lagrangian stochastic parameterizations.

We leave this discussion of diffusivity here, as the research and understanding of this issue is rapidly evolving, and strongly encourage the community to gain a better understanding in how best to implement diffusion and unresolved physics for Lagrangian particles.

### 3.4. Spatial interpolation

The trajectory Eq. (21) is defined on continuous velocity fields. However, all ocean models work with discretized grids, where velocities are only known on either vertices or edges of the grid cells (Griffies et al., 2000). Therefore, computing Lagrangian trajectories from ocean model data requires reconstruction of the continuous velocity field inside grid cells. Bilinear, trilinear, or spline interpolation are viable choices on structured grids. Interpolation on unstructured grids can be accomplished via methods derived from particle-based approaches, e.g., inverse-distance weighting or kernel-based convolutions, or unstructured extension of grid-based spatial interpolation, e.g., Wachspress interpolation (Gillette et al., 2012).

On grids where velocities are defined on the corners of grids (e.g., Arakawa A and B), the reconstruction choices include weak-form reconstruction (Perot, 2000), radial basis functions (Baudisch et al., 2006), or reconstruction via finite-element basis functions (Wang et al., 2011). On grids where velocities are known on the edges of grid cells (e.g., Arakawa C), this reconstruction is often done using simple linear interpolation, although more work needs to be done investigating what the errors are that arise from this.

Horizontal interpolation on arbitrary simplexes from vertex-data is provided by Wachspress interpolation (Gillette et al., 2012), which is a super-linear interpolation scheme for arbitrary simplexes. For triangles, Wachspress interpolation is equivalent to barycentric interpolation, which is commonly used on triangular meshes and readily available in scientific packages (e.g., python-matplotlib). A primary benefit of this approach is that it provides a continuous interpolant, e.g.,  $\mathcal{C}^0$  continuous. Options for higher-order interpolation to obtain  $\mathcal{C}^n$  (for  $n > 1$ ) continuity are more complex and less common, particularly on arbitrary unstructured meshes.

Horizontal interpolation via Wachspress naturally keeps particles within the domain for no-slip conditions where the velocity is zero for boundary points on simplexes. Particles can be constrained to remain within the domain by maintaining  $CFL < 1$ , where  $CFL$  is the Courant–Friedrichs–Lewy condition (e.g., Durran, 1999). This implementation is intrinsically free of if-statements. However, free-slip boundary conditions require further adaptation.

Vertical interpolation choices include linear and spline interpolants. Linear interpolation is a standard approach and is consistent within model accuracy, particularly for fine vertical resolution. Spline interpolation, however, allows representation of vertical curvature, but at the potential cost of artificial maxima and minima.

Particle tracking can employ a spatially-decoupled advection strategy by splitting horizontal and vertical integration steps into sequential operations. The benefit of this approach is that it decouples unstructured interpolants in the horizontal from one-dimensional



interpolation in the vertical and allows different particle behaviours to be employed. For example, vertical interpolation of velocities to specific potential density surfaces allows particles to be advected isopycnally and avoid diapycnal mixing that can occur with neutrally buoyant particle advection (Wolfram et al., 2015).

### 3.5. Available tools

As discussed throughout this section, it is in principle straightforward to compute Lagrangian particle trajectories by time stepping the trajectory Eq. (21). One merely needs to save the velocity field and update the trajectories using available software like Matlab or Python, invoking either rudimentary schemes or built-in functions such as the Matlab ode suite. Several research groups have developed their own virtual particle codes tailored to specific model output format, model grid and boundary conditions. Examples include a 3D Lagrangian Matlab code for the MITgcm used by Koszalka et al. (2013b) and von Appen et al. (2014) and a 2D Matlab code of The Nonlinear Dynamical Systems Group at ETH Zurich (Farazmand and Haller, 2012, <http://georgehaller.com/software/software.html>).

However, significantly more effort is required to develop an analysis code that features a user-friendly interface and thus can be utilized across the modelling communities. Further work is needed to ensure that the code is efficient on data Input/Output. The suite of available tools can roughly be separated into two sets. First, there are large community based Lagrangian codes such as Ariane, TRACMASS, the Connectivity Modelling System (CMS), and the new Parcels code. These are model-independent, run offline (i.e., on stored velocity data) and provide extensive control on particle behaviour. The second set includes Lagrangian codes tied to (and sometimes distributed with) specific models, such as MITgcm, HYCOM, NEMO, ROMS and MPAS-O. These model-specific codes can be run online (i.e., during the computation of the velocity data).

Examples from both types of codes are discussed in Appendix A. These codes are also summarised in Tables 1 and 2. Notably, all of these codes employ either explicit or implicit time integration of volume transports and while some can incorporate additional random terms (Section 3.3.2), there are no community codes available for computing tracer trajectories through the SDE-based methods of Section 3.3.1.

## 4. Applications of Lagrangian particle trajectories

For most applications, the raw particle trajectories output by Lagrangian analysis codes need to be further processed to help answer scientific questions. In this section, we overview ways in which Lagrangian particle trajectories can be used and analysed to improve our understanding of ocean circulation and dynamics.

### 4.1. Dispersion and diffusivity

The ensemble particle dispersion and its rate of change, the diffusivity, are the fundamental Lagrangian diagnostics of use for understanding tracer transport in oceanic flows. Particle trajectories can be used to diagnose eddy diffusivity via single, pair, and cluster techniques. The detailed theoretical and practical underpinnings of these techniques in the context of oceanic flows are summarized by LaCasce (2008); here we reiterate the main points.

The single-particle diffusivity stems from the seminal work of Taylor (1921). It quantifies the ensemble-mean rate of particle dispersion from an initial location, so that we have

$$\kappa(t) \equiv \frac{1}{2} \frac{d}{dt} \langle \mathbf{X}^2(t) \rangle = \langle \mathbf{V}(t) \cdot \mathbf{X}(t) \rangle = \int_0^t \langle \mathbf{V}(t) \cdot \mathbf{V}(\tau) \rangle d\tau. \quad (33)$$

In this equation,  $\mathbf{X}(t)$  is the Lagrangian virtual particle trajectory, and  $\mathbf{V}(t) = d\mathbf{X}(t)/dt$  is the Lagrangian particle velocity.

The Taylor formulation pertains to homogeneous, stationary and

isotropic flows, and is non-trivial to apply in practice. Different approaches to estimation of single-particle statistics for particles deployed in stationary and homogeneous Eulerian flows, with cautious notes on particle deployment strategies and transient behavior, are discussed by Davis (1982) in the context of numerical simulations. For modelled ocean flows of realistic complexity, the estimation of single-particle statistics must be further refined to account for non-stationarity and inhomogeneities of the underlying Eulerian field (Davis, 1983; 1985; 1987; 1991). Under the assumption that the velocity field is slowly-varying with respect to the time increment  $dt$  (in practice,  $dt$  can be the time step of a Lagrangian model) this assumption can be satisfied by segmentation of trajectories over a relevant time scale (e.g., seasonal cycle, the velocity decorrelation time scale), and segregation in space into locally homogeneous regions (Davis, 1991; Koszalka and LaCasce, 2010, see also Section 4.3).

If the focus is on the transport by mesoscale turbulent flows ('eddy diffusivity'), an appropriate technique for 'the mean (or slowly-varying) flow removal' must be applied to the Lagrangian velocity in Eq. (33) (e.g., Berloff et al., 2002; Rypina et al., 2012; Lumpkin and Johnson, 2013). The Lagrangian transport anisotropy can be quantified by using the concept of tensor diffusivity (where Eq. (33) applies to the different velocity vector components) and projection of the flow in the along- and across-flow directions of maximum dispersion (Rypina et al., 2011; 2012; Fox-Kemper et al., 2013; Kamenkovich et al., 2015; Wolfram et al., 2015). In general, anisotropy of the Lagrangian transport arises from spatio-temporal patterns and velocity correlations due to eddies. A significant challenge is that the observed Lagrangian particle dispersion is often non-diffusive on long time scales (e.g., Rypina et al., 2012) due to persistent Lagrangian flow correlations.

Double-particle statistics builds upon the works of Batchelor (1952) and Bennett (1987). The relative diffusivity (the time rate of the mean square pair separation) is

$$\kappa_R(t) \equiv \frac{1}{2} \frac{d}{dt} \langle r^2(t) \rangle = \frac{1}{2} \frac{d}{dt} \left\langle \sum_{m \neq n} [\mathbf{X}^{(m)}(t) - \mathbf{X}^{(n)}(t)]^2 \right\rangle, \quad (34)$$

where the sum is over all pairs of particles ( $m, n$ ). At times longer than the velocity decorrelation time scale, the pair particles move independently from one another, and the relative diffusivity is constant at twice the single particle diffusivity (LaCasce, 2008). Using the relative diffusivity rectifies the problem of the time-mean flow removal by measuring particle relative separation, though it will still be influenced by the mean flow shear. In practice, double-particle statistics are often implemented in terms of cluster or moment methods which are equivalent to double-particle statistics on the plane (LaCasce, 2008).

The single- and double-particle diagnostics derived from simulated trajectories may be used for the following.

- Quantifying the advection by the turbulent mesoscale flows (eddy diffusivity) in eddying models as a function of time and separation, for example for parameterisations of diffusive processes in models that do not resolve eddies (Poje et al., 2010).
- Eddy diffusivity maps obtained by binning (see Section 4.3) quantify regional variability in eddy diffusivity and other derived statistics (eddy length, time scales; e.g., LaCasce et al., 2014; Griesel et al., 2014; 2015).
- Investigating the nature of the oceanic turbulent transport. The relative diffusivity as a function of particle separation is related to the Eulerian kinetic energy spectra. Together with the FSLEs (see Section 4.2), the relative velocity diagnostics and the pair displacement PDFs can be used to check for consistency with quasi-geostrophic turbulence, chaotic advection, and mean shear (LaCasce, 2008; Koszalka et al., 2009).

## 4.2. Lagrangian Coherent Structures

The ocean is full of eddies, jets and other coherent structures, which are visible in ocean tracers such as temperature or chlorophyll. The field of Lagrangian Coherent Structures (LCS) aims to identify the kinematic skeleton of such objects based on the Lagrangian trajectories of the fluid and to study the role of these structures in transport. Here we provide a very brief introduction and overview of the field and refer the interested reader to the more comprehensive review articles on the topic (e.g. Peacock and Dabiri, 2010; Peacock and Haller, 2013; Haller, 2015).

The most developed branch of LCS theory is concerned with identifying distinguished material surfaces which serve as the boundaries of coherent regions in unsteady flows. According to Haller (2015), a method for identifying such surfaces must (a) be objective (i.e. gives the same result in all observer reference frames), (b) be applicable over a finite time interval, (c) describe an actual material surface, and (d) converge with respect to spatial resolution.

Many different LCS diagnostics have been developed to detect different types of structures. A starting point in many LCS identification methods, however, is the finite-time flow map  $F_{t_0}^t(\mathbf{x}_0)$ , which gives the positions at time  $t$  of particles initially located at  $\mathbf{x}_0$  at time  $t_0$ . The flow map can only be calculated by numerically advecting a large ensemble of closely spaced Lagrangian particles. From this flow map, one can compute the Cauchy Green Strain Tensor  $C(\mathbf{x}_0) = [\nabla F_{t_0}^t(\mathbf{x}_0)]^T \nabla F_{t_0}^t(\mathbf{x}_0)$ , which measures the magnitude of the growth in separation of infinitesimal perturbations in the initial position space.  $C$  is characterised by its eigenvalues  $\lambda$  and corresponding eigenvectors.

The original diagnostic of LCSs is the Finite Time Lyapunov Exponent (FTLE). The FTLE is a measure of the exponential rate of separation of trajectories of infinitesimally close initial points over a finite-time interval and is given by

$$FTLE(\mathbf{x}_0, t_0, \tau) = \frac{1}{\tau} \ln \sqrt{\lambda_{max}} \quad (35)$$

with  $\lambda_{max}$  the maximum eigenvalue of  $C$  over the chosen finite integration time  $\tau = t - t_0$ . Early applications of the FTLE were to distinguish regions of high and low predictability in chaotic flows (FTLE; Pierrehumbert and Yang, 1993; Artale et al., 1997). Later, FTLE fields were applied to the identification of attracting and repelling transport barriers (Haller and Yuan, 2000; Lapeyre, 2002). The ridges (i.e. curves of local maxima) of the FTLE field correspond with repelling LCS positions at  $t_0$ ; as regions of extreme local stretching, these structures represent material barriers which remain coherent under advection (unlike general material lines). Attracting LCSs, which represent the Lagrangian skeleton of tracer filaments, can similarly be obtained as ridges of the FTLE field calculated from a *backward* time integration. Haller and Sapsis (2011) review different strategies for calculating

attracting and repelling LCSs from forward- and backward-time FTLEs. A related diagnostic is the Finite Size Lyapunov Exponent (FSLE; Aurell et al., 1997), which represents the *time* required for particle separation to reach a specified size (Fig. 3). FSLEs have also been used widely for LCS identification and can be related to the statistics of turbulent dispersion (LaCasce, 2008). However, Karrasch and Haller (2013) proved that FSLE and FTLE ridges do not coincide in general and argued that FSLEs were less reliable for the identification of LCSs.

The statistics of FTLE and FSLE based on flow maps constructed from Lagrangian particle trajectories have been applied to characterize regimes of dispersion and regional differences in mixing (Drijfhout et al., 2003; Waugh and Abraham, 2008; Haza et al., 2010; Lumpkin and Elipot, 2010; Schroeder et al., 2011; Poje et al., 2014). Instantaneous maps of FTLE and FSLE derived from satellite altimetric velocities have also been used to identify LCS positions in the ocean (d'Ovidio et al., 2004; Olascoaga et al., 2006; Lehahn et al., 2007; Beron Vera et al., 2008). Attracting LCS represent transport barriers, and indeed several studies have confirmed the tight correlation between the detected structures and fronts of advected tracers including sea surface temperature (Abraham and Bowen, 2002; d'Ovidio et al., 2009), chlorophyll concentrations (Lehahn et al., 2007), oxygen (Bettencourt et al., 2015), oil spills (Mezić et al., 2010), and even different dominant phytoplanktonic types (d'Ovidio et al., 2010).

Not all coherent structures relevant for transport can reliably be deduced from the FTLE or FSLE fields. Over the past decade, LCS detection methods have developed increasing precision at discriminating different flavours of structure geometry, resulting in a proliferation of techniques (Haller, 2015). Haller and Beron-Vera (2012) used a variational approach to find the least-stretching material lines in the forward and backward flow maps; the initial positions of these lines (called hyperbolic LCSs) can be identified as the geodesic curves of a Riemannian metric related to the Cauchy-Green strain tensor. Definitions of parabolic and elliptic LCSs, corresponding to jet cores and vortex boundaries, can similarly be made using the tools of differential geometry (Haller and Beron-Vera, 2013; Haller, 2015). Additional methods for vortex identification based on dynamic polar decomposition and Lagrangian-averaged vorticity deviation have recently been proposed (Haller, 2016; Haller et al., 2016), while yet a different class of methods identifies LCS based on a probabilistic transfer function (Froyland et al., 2007). A much needed critical comparison of different methods and their performance in different test cases was recently undertaken by Hadjighasem et al. (2017), which provides valuable practical advice for researchers wishing to implement these techniques.

A central preoccupation of LCS techniques is the identification of coherent mesoscale eddies. Beron-Vera et al. (2013) used the elliptic LCS framework to identify materially coherent Agulhas rings, emphasizing the advantages over Eulerian eddy-identification methods, while

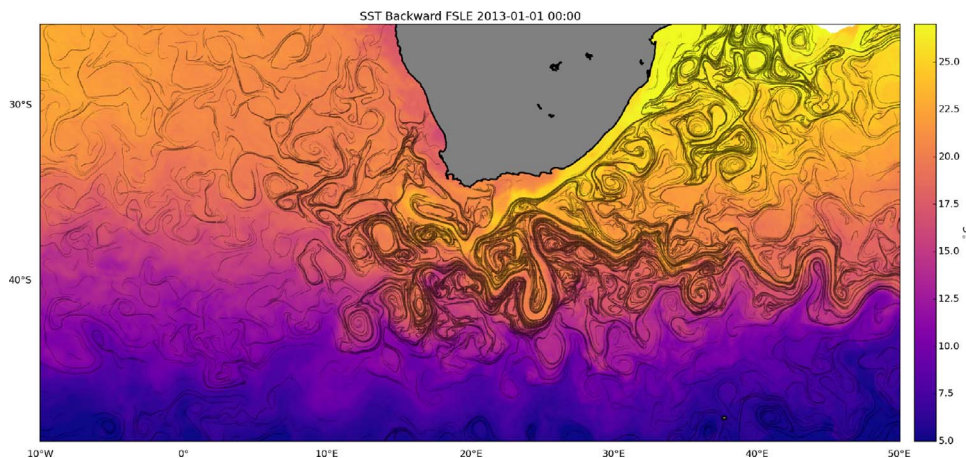


**Fig. 3.** Backward Finite Size Lyapunov Exponents for January 1 2013 computed as in d'Ovidio et al. (2004), with initial separation distance of  $0.01^\circ$  and final separation distance of  $1^\circ$ . The FSLE have been computed using surface absolute geostrophic velocities produced by Ssalto/Duacs and distributed by AVISO, with support from CNES (delayed time, all satellite merged product). Ridges of FSLE ( $\geq 0.3$ ) are overlaid on Multi-scale Ultra-high Resolution (MUR) Sea Surface Temperature (<http://mur.jpl.nasa.gov/>), showing good correspondence between the Lagrangian coherent structures and the distribution of the surface tracer advected by the Agulhas current, the Agulhas retroflection and their associated mesoscale activity.

Froyland et al. (2012) applied the transfer function method to the same region. Wang et al. (2016) and Froyland et al. (2015) used the identified structures to study the transport, origin, and decay of Agulhas ring waters. Abernathy and Haller (2017) used the Lagrangian-averaged vorticity deviation method of Haller et al. (2016) to identify eddies in the eastern Pacific and quantify their role in meridional dispersion. These studies illustrate the value of LCS methods for questions of long-range material transport.

#### 4.3. Probability distributions

A common way to visualize trajectory data is to bin particle positions into histograms. The result is a map of particle density which, when normalised by the total number of particle positions, yields a probability map. Alternatively we can produce probability maps by counting the visit of a particular particle only once per bin and then normalizing by the total number of particles (instead of the total number of particle positions, e.g., van Sebille et al., 2012; von Appen et al., 2014). Both methods offer a useful means to identify flow structure through particle pathways from a set of release points.

Fig. 4 illustrates the use of both methods for studying the flow responsible for the spreading of particles originating in the Agulhas Current. Fig. 4a shows the probability derived from the procedure described at first. Obviously, bins located within the areas of the Agulhas Current (AC), the Agulhas Return Current (ARC), and the Agulhas Ring corridor show the highest probabilities, highlighting the most probable spreading pathways along the major currents and via mesoscale eddies. But even between the AC and ARC there is a region with comparable particle position counts. Fig. 4b reveals that this is not due to a particularly strong circulation feature transporting many particles, but rather due to the recirculation of fewer particles.

One consideration in the choice of bin resolution is aliasing. If either the grid resolution is too fine or the period of particle position updates is too long, trajectories may pass through more than one histogram bin within a given output time step and thus may not be adequately accounted for. The density maps from binning can also be scaled to account for the residence time in bins and the time step of the Lagrangian simulation. One practice is to scale the particle density maps by the time step  $dt$  to obtain the density maps in units of days (e.g., Koszalka et al., 2011). Another is to scale the particle densities in bins with the integral Lagrangian time scale,  $T_L$ , yielding particle distributions in bins in terms of the ‘number of independent observations’:  $N_{ind} = N/\sqrt{T/T_L}$ , where  $T$  is the total time (e.g., Koszalka and

LaCasce, 2010).

Apart from using particle density maps to assess the water mass pathways and connectivity, binning of particle positions and their corresponding properties allows the investigation of mean properties (temperature, density) and their changes along simulated trajectories (e.g., van Sebille et al., 2014). Binning Lagrangian velocities to test the Gaussianity of their distributions and other velocity statistics is yet another application (LaCasce, 2005). The binning is also used to construct maps of eddy diffusivity from particle simulations in high-resolution models (e.g., LaCasce et al., 2014; Griesel et al., 2014; 2015). Using binning to estimate spatially-dependent eddy diffusivities (‘pseudo-Eulerian eddy diffusivity maps’) and other parameters (maps of eddy time and length scales) has been widely used in observational Lagrangian analysis (Bauer et al., 2002; Koszalka et al., 2011; Rypina et al., 2012; Lumpkin and Johnson, 2013; Zhurbas, 2004), as well as in particle simulations in eddy-resolving models (e.g., Berloff et al., 2002; LaCasce et al., 2014; Griesel et al., 2014; 2015)

Binning can be used to verify the spreading of Lagrangian particles by comparing the ensemble particle movement with large-scale distributions of either conserved quantities, such as potential vorticity, or a tracer field whose evolution is explicitly computed online in the OGCM (e.g., Gary et al., 2012). Such evaluations can be statistically formalised using pointwise correlation between the binned histogram and the online tracer (Simons et al., 2013).

Binning is not limited to spatial boxes as particles can be binned by virtually any variable that can be determined along a particle’s path: for example depth, time, density, temperature, salinity, etc. This sort of binning can be useful to highlight along-pathway water mass transformations (e.g., Koszalka et al., 2013b; Iudicone et al., 2011; Gary et al., 2014; van Sebille et al., 2014). Particles can also be binned by the distance from the deployment site. Such a distance metric can be re-defined to account for the topographic steering (Davis, 1998). Finally, an alternative to binning was proposed by Koszalka and LaCasce (2010). Rather than grouping the Lagrangian data in bins of fixed size, they grouped a fixed number of nearest-neighbour particle positions together using a clustering algorithm.

#### 4.4. Water mass ages and transit times

The ‘age’ of ocean water, or the time taken for water to transit between defined regions or reservoirs, is a property of the flow that provides useful understanding of the ocean circulation (Deleersnijder et al., 2001). Such a metric can be easily derived from

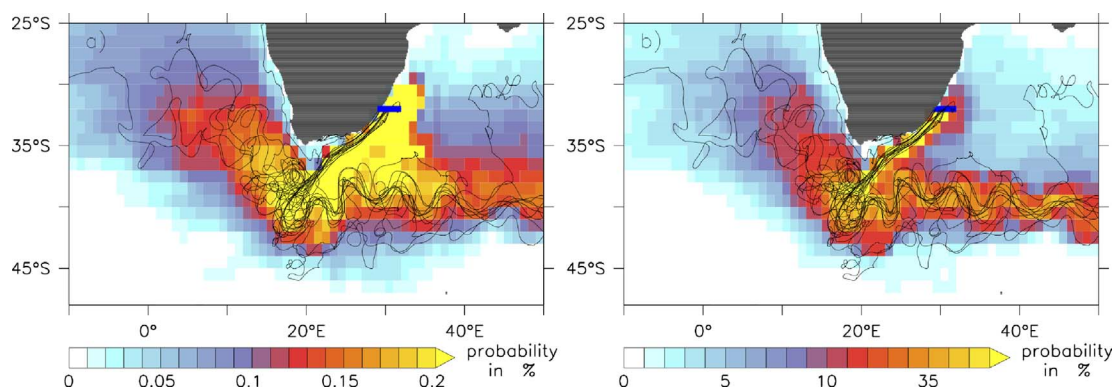


Fig. 4. Lagrangian modelling approach to determine pathways of particles released in the Agulhas Current at 32°S (blue line extending east from Southeast Africa), based on a set of 5-year long trajectories initialized in the year 2000 (some examples visualized as black lines): a) Probability with that a  $1^\circ \times 1^\circ$  bin spanning the whole depth range is occupied by a particle during the considered time span. The probability for each bin has been obtained by counting the number of particles occupying this bin at each time step, summing up this particle counts over the whole integration period and then dividing it by the total number of recorded particle counts for all bins. Thus, the sum of the probabilities of all bins yields 100%; b) Probability that a particle occupies a particular bin at least once during the considered time span. In this case the probability for each bin has been obtained by counting the number of different particles occupying this bin and dividing by the total number of particles. Thus, the probability for each bin can range between 0 and 100%. The Lagrangian analysis was performed with the ARIANE tool using the 3D 5day-mean velocity fields from the high-resolution model INALT01 (Durgadoo et al., 2013). (For interpretation of the references to colour in this figure legend, the reader is referred to the web version of this article.)



Lagrangian calculations by determining the transit time of particles. Since the age of water can also be recovered from float trajectories or observations of chemical tracers (Fine et al., 2002; Waugh et al., 2004), there is the possibility to use the age to evaluate model results in comparison to observations. However, this comparison requires careful interpretation (Khawiwala et al., 2001) and has been rare (e.g. Haines et al., 1999).

The age of a parcel of ocean water, described by numerous particle trajectories, is not unique, since different particles may transit between two regions by distinct pathways, travelling for different lengths of time (Phelps et al., 2013). As such, the age of ocean water is in fact a probability distribution: the transit time distribution (TTD) that an individual particle might take to travel between the two regions (Holzer and Hall, 2000; Deleersnijder et al., 2001; Haine and Hall, 2002). Given a sufficient number of Lagrangian trajectories, a TTD between two regions can be formed from a histogram of the particle ages (see Fig. 5 for an example in the Agulhas region). In Lagrangian ocean analysis, the range, maximum or variance of this TTD is used to understand the inherent timescales of the circulation (e.g. Rühls et al., 2013). However, transit time distributions are highly sensitive to the spatial scales resolved by the numerical model from which Lagrangian trajectories are determined.

In Lagrangian analyses, the ‘age’ can be evaluated as the time since a particle was last within the surface ocean (the ventilation timescale), in which case it reveals the timescales on which the ocean interacts with the atmosphere, and influences global climate. This method has been considered for the global ocean (Blanke and Speich, 2002) as well as specific water masses (Koch-Larrouy et al., 2010). In regional seas (with riverine forcing) an analogue to ventilation with the atmosphere is freshwater age (Phelps et al., 2013). One difficulty is that the ventilation timescale of deep ocean flows (which can be on the order of thousands of years) often exceeds the length of available OGCM output such that the velocity fields must be ‘looped’ to calculate the full TTD (see also Section 3.2).

By considering the entry and exit of particles from an enclosed region, transit times can be interpreted as a residence timescale. For a marginal sea with one point of exchange, such as the Baltic Sea, this has been used as an alternative to the classic box model approach (Döös et al., 2004; Jönsson et al., 2004). Where there are multiple points of exchange, such as the Arctic Ocean, the approach determines the timescales on which these gateways interact (Lique et al., 2010).

Lagrangian transit times are also used to evaluate the timescales on which anomalies in a certain region would influence the flow downstream (e.g., Speich et al., 2001; van Sebille et al., 2011; Rühls et al., 2013), or to determine time-integrated properties of specific flows, such as the average speed (Koszalka et al., 2013b) or the most rapid pathways (Gary et al., 2012).

#### 4.5. Volume transport and Lagrangian streamfunctions

Among the first uses of basin-scale Lagrangian particle tracking was to assess seawater volume transports between chosen sites in the ocean,

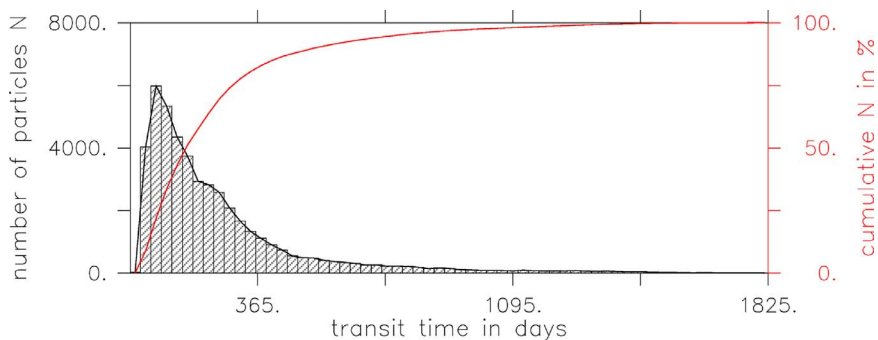


Fig. 5. Example transit time distribution for particles released in the Agulhas Current at 32°S (blue lines in Figs. 4 and 6, extending east from Southeast Africa) in the year 2000 and traced towards the GoodHope line (red line in Fig. 6). The Lagrangian analysis was performed with the ARIANE tool using the 3D 5day-mean velocity fields from the high-resolution model INALT01 (Durgadoo et al., 2013). (For interpretation of the references to colour in this figure legend, the reader is referred to the web version of this article.)

resulting in an effective way of quantifying Lagrangian connectivity. In these applications, each particle is ‘tagged’ with a transport upon release, and that transport is then conserved along the trajectory as per the streamtube discussion in Section 2.4. We can construct volume transport pathways by summing the transports of particles that connect two regions (see Fig. 6 for an illustrative example).

Just like in the Eulerian framework, the concept of volume conservation (as in a Boussinesq fluid discussed in Section 2.4) can be used to ‘collapse’ the full three-dimensional transport into a two-dimensional streamfunction. The unique feature in Lagrangian streamfunctions is that they can be constructed for only that part of the flow that connects the section where particles are released and where they are received. This concept has been applied to study for example the cold and warm water routes into the Atlantic (Speich et al., 2001; 2002; Drijfhout et al., 2003), Agulhas leakage (Durgadoo et al., 2017), the Pacific-to-Indian Ocean connectivity (van Sebille et al., 2014), the Lagrangian decomposition of the Deacon Cell (Döös et al., 2008), and the Atlantic MOC (Thomas et al., 2015b).

The concept of Lagrangian streamfunctions was introduced by Blanke et al. (1999) and is closely tied to the analytical integration method (Section 3.2.3). Consider a domain with open boundaries, such as the Agulhas region around South Africa. Trajectories are initialized along the boundaries of a control volume (box in Fig. 6), and traced until they again reach the boundaries. Each trajectory is associated with a volume transport, and the volume transport is recorded at each grid-wall crossing of a trajectory. This method results in a non-divergent field of volume fluxes through all grid walls that can be integrated to Lagrangian streamfunctions. It is to be noted that this streamfunction represents the mean flow during the whole integration period, i.e. ideally until all trajectories have left the box.

Both Döös et al. (2008) and Kjellsson and Döös (2012a) showed that the total Lagrangian streamfunction is almost identical to the Eulerian streamfunction. One of the main differences is that the Lagrangian streamfunction is based on trajectories with varying residence times ranging from hours to months or even years, while Eulerian streamfunctions are snapshots or time-averages.

#### 4.6. Biological connectivity

Lagrangian particle trajectories can be used to study how water moves around in the ocean. Additionally, Lagrangian particles can be interpreted as passively drifting (biological) particulates. Many marine organisms reproduce with larvae that are dispersed at the whim of the currents. Hydrodynamic connectivity therefore has important implications for population dynamics (e.g., Kool et al., 2013; Thomas et al., 2014). In particular, this connectivity generally allows for longer dispersal and more rapid range expansion than is observed in terrestrial species (Kinlan and Gaines, 2003), as well as directly creating range limits (Gaylord and Gaines, 2000). Understanding these processes and their implications is important for a range of management objectives.

Transport models have provided insights in varied contexts including the creation of robust networks of Marine Protected Areas



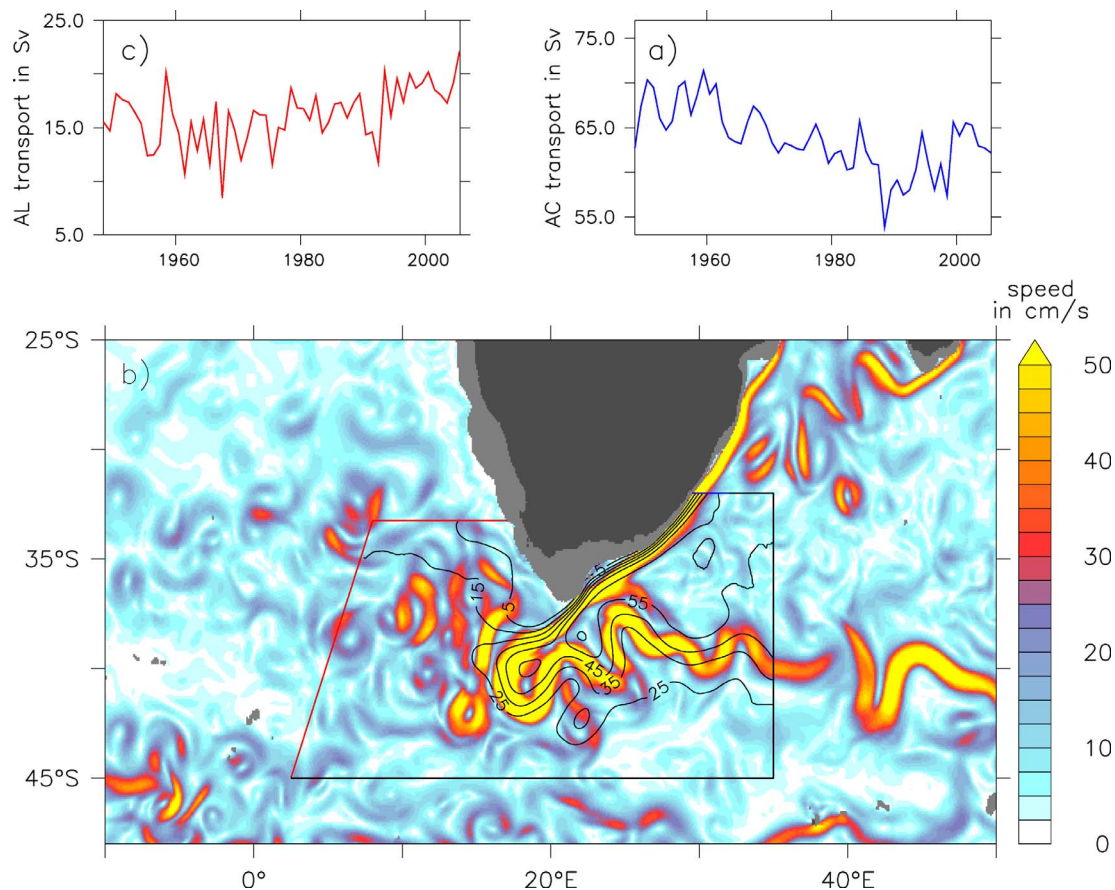


**Fig. 6.** Quantitative Lagrangian modelling approach to determine Agulhas Leakage: a) Time series of the annual Agulhas Current (AC) transport at 32°S, where particles were released continuously proportional to the current volume transport, each particle associated with a fraction of this transport; b) Snapshot (18-Apr-2000) of current speed at 450 m depth in the Agulhas region (colour shading, in cm/s), as well as the horizontal Lagrangian streamfunction (contours, in Sv) for all trajectories initialized in the year 2000 and traced along 3D streamlines towards the control sections (black and red lines); c) Time series of annual Agulhas Leakage (AL) transport, obtained by considering for each release year only the transports of those trajectories, that cross the approximated GoodHope section (red lines) within 5 years. The Lagrangian analysis was performed with the ARIANE tool using the 3D 5day-mean velocity fields from the high-resolution model INALTO1 (Durgadoo et al., 2013). (For interpretation of the references to colour in this figure legend, the reader is referred to the web version of this article.)

(Gaines et al., 2003; Berglund et al., 2012; Burgess et al., 2014), conservation of coral reefs (Trenl et al., 2008; Wood et al., 2013), sustainability of fisheries (Gilbert et al., 2010), competition between biophysical and hydrodynamical controls on larvae retention (Phelps et al., 2015), and spread of invasive species. Similar models are frequently applied in coastal scenarios to understand the spread of aquaculture parasites (Salama and Rabe, 2013) and invasive benthic organisms (Brandt et al., 2008). It is important to note that horizontal resolution and subgrid scale diffusivity of the underlying Eulerian flow field can be a key for the distribution and time scales, as it was the case for the dispersion of European glass eels (Blanke et al., 2012; Baltazar-Soares et al., 2014).

How these larvae interact with the water column depends on a range of characteristics such as size, development rate and behaviour (McManus and Woodson, 2012). Models investigating biological connectivity must therefore account for these characteristics and many others (e.g., Visser, 2008; Paris et al., 2013b), in addition to physical processes. ‘Behaviour’ such as orientation and swimming in response to scent plumes released from suitable habitat (Holstein et al., 2014; Staaterman and Paris, 2013) is often documented, as is vertical migration (Lampert, 1989).

Observations of microchemical markers, genetic microsatellite markers and single nucleotide polymorphisms can provide information on realised connectivity between spatially separated populations. They can provide a direct comparison for Lagrangian tracking predictions (e.g., Pujolar et al., 2013; Wilkins et al., 2013; Teske et al., 2015) in

terms of population similarity, and can provide evidence of biogeographic barriers (for example coral species in the Gulf of Mexico; Sammarco et al., 2012). Recent work hints at the possibility of applying such techniques to understand population connectivity and evaluate predicted patterns at a global scale (e.g., Hellweger et al., 2014; Villar et al., 2015; Jonsson and Watson, 2016).

## 5. Outlook

Lagrangian analysis provides a powerful tool to help interpret output from OGCMs. This power will only increase as OGCMs enter ‘peta-scale’ territory. In this final section, we offer outlooks on where we see new and exciting opportunities and possibilities for the Lagrangian analysis of OGCMs.

### 5.1. The next generation of particle tools

A major challenge with particle tracking is obtaining performance for a large number (order of billions) of particles. For small velocity data sets, offline parallel particle tracking can be employed via a Single Instruction Multiple Data (SIMD) approach, e.g., openMP or GPU-based implementations. However, Input/Output will remain a bottle-neck, with most codes simply reading in the entire velocity field, even if the particles occupy only a subregion of the domain. Recent advances in the NetCDF library toolkit, however, mean that it is now feasible to read in only those parts of the grid where there are particles, so that the

number of Input/Output operations could potentially be reduced by orders of magnitude. Implementation of these new libraries, in combination with better memory management and efficient use of tiered cache levels, will lead to vastly faster codes that also have smaller memory footprints.

Nevertheless, for petabyte-scale velocity data sets such as those from grand challenge climate simulations, online particle tracking is necessary to avoid the unsustainable storage costs associated with off-line particle tracking. The challenge in this arena, however, is utilization of heterogeneous computer architectures. Message-passing (MPI) between computational nodes is essential and a hybrid approach utilising on-node openMP, GPU, or MIC threading will be required on next-generation architectures to obtain peak performance. Task-based parallelism, if implemented for OGCMs, may provide at least a partial solution. However, at present, no definitive framework or “best practice” has been adopted.

Several OGCMs already have on-line particle diagnostics (see Appendix A.2), yet no general library for coupled Lagrangian particle tracking exists so far. As a result, development efforts are disjoint and functionalities are often model-specific. On the other hand, run-time integration with OGCMs requires close coupling with grid data in order to reduce performance overheads, while the variety of grid types makes finding a general abstraction difficult. Moreover, such a library needs to provide parallel performance and scalability, as well as an easily accessible API that allows it to be integrated with different types of ocean models.

## 5.2. A case for standard tests of particle tools

Most of the Lagrangian particle tracking tools described in Section 3.5 have never been compared against each other, which makes it hard to assess their skill and fidelity. While most codes are designed for very different purposes, we propose to develop a set of test cases that we suggest code developers to use when debugging codes. This set of test cases would then also serve to highlight differences in explicit versus analytical time stepping codes, for example, or differences between particle tracking on A, B and C grids. While we envision the set to grow over time, the following would be a minimum requirement.

A first set of tests to consider are those where analytical expressions are known for trajectories.

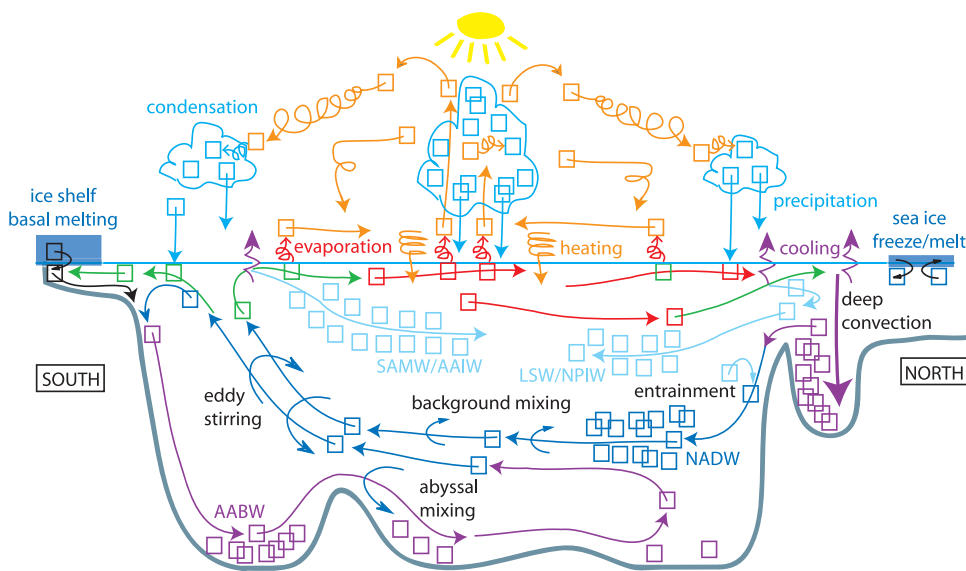


Fig. 7. Illustrating how water particles follow the water cycle in the Earth System. We emphasize here the global ocean conveyor circulation in a pole-to-pole, meridional-vertical plane, coupled to selected and idealized atmospheric circulation in the same plane, omitting land for convenience [terrestrial processes such as evapo-transpiration, storage and runoff are also part of the full water cycle]. Individual water particles are represented by color-coded boxes, advected quickly/chaotically through the atmosphere, and slowly/steadily through the ocean. Particles are stored on a wide range of time-scales: in clouds (hours–days); in sea ice (seasons–years); in the ocean (years–centuries); in ice sheets/shelves (centuries–millennia). In the ocean, colour coding identifies selected water masses and advection thereof: Antarctic Bottom Water (AABW); North Atlantic Deep Water (NADW); Labrador Sea Water (LSW); Antarctic Intermediate Water (AAIW); North Pacific Intermediate Water (NPIW); Subantarctic Mode Water (SAMW). In the atmosphere, colour-coding distinguishes vapour and liquid phases. Highlighted processes involve phase change or ocean-atmosphere exchange: ocean surface heating/cooling; evaporation; condensation; precipitation; sea ice freezing/melting; ice shelf basal melting. Highlighted processes internal to the ocean transform water particle density: deep convection; entrainment; enhanced abyssal mixing; eddy stirring; weak background mixing. (For interpretation of the references to colour in this figure legend, the reader is referred to the web version of this article.)

1. Radial rotation with known period. This setup tests particle trajectories in the simplest-possible flow, without time evolution.
2. Longitudinal shear dispersion flow in a pipe (e.g., Fischer et al., 2013) to ensure that shear dispersion effects are properly represented.
3. Effective lateral diffusion due to an oscillating vertical shear flow (Bowden, 1965) to test particle trajectories in a time-evolving flow.
4. Steady-state flow around a peninsula (Ådlandsvik et al., 2009). This setup tests particle trajectories in a domain with an obstacle, and can be used to test how codes behave near land boundaries.
5. Steady-state flow in a Stommel gyre and western boundary current (Fabbroni, 2009) to test particle trajectories in a domain with large gradients in flow speed.
6. Damped inertial oscillation on a geostrophic flow (Fabbroni, 2009; Döös et al., 2013) to appropriately quantify sub-inertial motion, e.g., loops.
7. For codes that include diffusivity, a simulation of Brownian motion with a given  $K_h$  and  $K_v$  to test for sub-grid parameterizations of diffusivity.

A second set of tests can be considered that do not have an analytical solution, but that test for speed and efficiency of the code in more realistic idealized test cases corresponding to eddy resolving simulations, e.g., as are becoming standard in modern climate models.

8. Zonally-periodic baroclinic channel (Ilıcak et al., 2012; Berloff et al., 2009; Abernathey et al., 2013; Ringler et al., 2016; Wolfram and Ringler, 2017a; 2017b) to explore unconstrained eddy and mean flow interactions, e.g., in an idealized Antarctic Circumpolar Current.
9. Eddying double-gyre flow (Shevchenko and Berloff, 2015; Wolfram et al., 2015) to explore idealized eddying flows constrained within an ocean basin.

Looking forward, a list such as this one might form the basis of a Lagrangian Model Intercomparison Project (LMIP), similar to that used in the climate modelling community through the Coupled Model Intercomparison Project (Eyring et al., 2015) or the Ocean Model Intercomparison Project (Griffies et al., 2016). An LMIP could host the velocity fields and analytical solutions of the set of test cases needed by particle model developers for debugging purposes. To allow for use

across a broad suite of analysis software, we encourage developers of tools to make the trajectory data CF-compliant, as stated at <http://cfconventions.org/Data/cf-conventions/cf-conventions-1.6/build/cf-conventions.html#discrete-sampling-geometries>.

### 5.3. Whole-Earth System and Water Cycle Modelling

Beyond quantifying the pathways of seawater in the ocean, it is tantalising to consider whether Lagrangian methods could be used to track water throughout the entire climate system. Such analysis could be used to quantify coupled thermodynamic cycles (Laliberte et al., 2015; Kjellsson et al., 2014; Zika et al., 2012; Döös et al., 2012), geographical connectivity (Gimeno et al., 2010), and the transport, dilution and fractionation of salt, nutrients and oxygen (Fig. 7). Here we will discuss such prospects including basic requirements and challenges of such analysis.

One important reason for modelling the water cycle is the intensification evident over recent decades in ocean salinity (Hosoda et al., 2009; Helm et al., 2010; Durack et al., 2012). Central to this intensification are changes to moist processes in the atmosphere (Held and Soden, 2006). However, based on observed salinity and in CMIP5 simulations, the hydrological cycle intensifies at around half the rate predicted from moist thermodynamics alone (Skliris et al., 2016), while observations are currently inadequate for an accurate quantification of changes in key processes (Hegerl et al., 2015), including precipitation and evaporation over the oceans (Skliris et al., 2014). With a Lagrangian description of the global water cycle in coupled climate models, it will be possible to fully explore the full range of atmospheric processes that are driving and retarding the observed intensification.

Another motivation is the possibility of tracing stable water isotopes through the Earth system. Stable water isotopes are a cornerstone in paleoclimate reconstructions, since their concentrations can be used to infer the source of the water. For example, water vapour that has evaporated from the ocean has low concentrations of heavy isotopes. Likewise, ice on Antarctica also has very low concentrations of heavy isotopes, so it is likely that the ice originates from evaporated water that precipitated over the continent (Gat, 1996). Hence, an observed decrease in heavy isotope concentrations in the ocean could be due to either less evaporation, or advection of meltwater from ice sheets or land (Roche, 2013). If we could trace the isotopic composition of water as it moves between oceans, atmosphere, land and ice we could reconstruct the hydrological cycles of past climates.

In general, if a Lagrangian code is to exchange particles between ocean and other components of the earth system, it must first deal appropriately with sources and sinks of water within the ocean itself. It is now common for ocean models to have explicit water fluxes at the sea-surface due to evaporation, precipitation and river run-off (Griffies et al., 2000). These sources and sinks of water in the ocean should be accounted for in any Lagrangian framework (e.g., with sources and sinks of particles) regardless of whether water is being traced between components.

Secondly, for water to be consistently traced between components of the climate system, water must be conserved between them. This is for example the case in some sea-ice and iceberg models which are integrated into ocean modelling systems (Martin and Adcroft, 2010; Marsh et al., 2015, some of which incidentally use a Lagrangian framework). However, challenges remain in conserving water consistently between the ocean, atmosphere, terrestrial hydrological systems (e.g. lakes, soil moisture, groundwater and irrigation) and ice-sheets.

Tracking water within each component of the earth system other

than the ocean presents its own challenges. There is, for example, a rich history of Lagrangian methods in meteorology (Stohl, 1998), some having evolved from the oceanographic community (e.g. TRACMASS, see Kjellsson and Döös, 2012a). It is common for such methods to track air masses rather than water itself. Water in the atmosphere comes in three phases: vapour, liquid and ice, making the tracking of water challenging. However, robust methods are in common use (see for example the FLEXPART model; Stohl and James, 2005; Gimeno et al., 2010).

Simulating the movement of water as Lagrangian particles between different components of the earth system is further complicated by vast contrasts in scale both in storage and transport rates between them. The atmosphere for example holds 0.001% of all the water in the climate system while the ocean holds 97%. In contrast, the cycle of evaporation and precipitation over the globe amounts to approximately 16 Sv (i.e. multiplying global mean precipitation of 2.7 mm/day, Trenberth, 1998, by the area of the earth). So while storage of water in the atmosphere is small relative to the ocean its transport of water is equivalent to that of major ocean currents. Differences in scales of motion and numerical description of these systems present great technical challenges beyond the scope of this review.

## 6. Concluding remarks

In this review article, we have presented an extensive overview of the state of the art in Lagrangian particle analysis. We focused on the use of particles determined by integral curves of the velocity field and large-scale open ocean applications. Based on the collective knowledge of the authors, we have identified opportunities and issues for improvements of these methods as we move towards a petascale age of computing. We hope that the guidance provided here can provide a starting point for new users, as well as an impetus for experienced users and developers of these codes.

## Acknowledgements

This review paper is the result of very fruitful discussions during the “Future of Lagrangian Ocean Modelling” workshop, held at Imperial College London, UK, in September 2015. Funding for this workshop was provided through an EPSRC Institutional Sponsorship grant to EvS under reference number EP/N50869X/1. EvS has received funding from the European Research Council (ERC) under the European Unions Horizon 2020 research and innovation programme (grant agreement No 715386). This research for PJW was supported as part of the Energy Exascale Earth System Model (E3SM) project, funded by the U.S. Department of Energy, Office of Science, Office of Biological and Environmental Research. Funding for HFD was provided by Grant No. DE-SC0012457 from the US Department of Energy. PB acknowledges support for this work from NERC grant NE/R011567/1. SFG is supported by NERC National Capability funding through the Extended Ellett Line Programme. ED is an honorary Research Associate with the Belgian Fund for Scientific Research (F.R.S.-FNRS). SR was funded (Grant CP1412) by the Cluster of Excellence 80 “The Future Ocean” within the framework of the Excellence Initiative by the Deutsche Forschungsgemeinschaft (DFG) on behalf of the German federal and state governments. We thank Sergey Danilov (editor), Andrew Shao, François Primeau, Nathaniel Tarshish, and five anonymous reviewers for very helpful comments.

We also wish to thank all the scientists, researchers and programmers who built the Ocean General Circulation and Lagrangian tracking models over the past decades.

## Appendix A. Community tools for Lagrangian ocean analysis

In this appendix, we provide further background on the different community codes, both for offline and online particle tracking, listed in Tables 1 and 2.



## A1. Community-based offline 3D Lagrangian codes

### A1.1. Ariane

Ariane is a numerical diagnostic tool developed at the Laboratoire de Physique des Océans (Brest, France). It is dedicated to the off-line computation of the advective component of 3D trajectories and subsequent volume transport analyses in given velocity and tracer fields, most often obtained from the numerical integration of an ocean general circulation model.

The trajectory integration scheme at the core of the Ariane calculations (Blanke and Raynaud, 1997) dates back to 1992 (Speich, 1992). It takes full advantage of the volume continuity equation expressed on a C-grid (Mesinger and Arakawa, 1976). There are several advantages to the analytical calculation of streamlines on the model grid for successive time intervals, over which the velocity is assumed to be steady-state (see Section 3.2.3). The method only calculates particle positions on the edge of grid cells, and it respects the local three-dimensional non-divergence of the flow. Doing so makes the method both fast and accurate in terms of truncation error relative to an RK4 code. It offers flexibility too, in which backward integrations can be performed to track the origin of a given volume. A trajectory scheme that respects the continuity equation shows excellent capability for volume tracing, following the streamtube perspective discussed in Section 2.4.

Following the methodology proposed by Döös (1995) and taken up by Blanke and Raynaud (1997) to take advantage of such a scheme, water volume transfers between selected control sections can be assessed with great accuracy. They can be portrayed by means of Lagrangian streamfunctions, defined either on a geographic plane (Blanke et al., 1999) or on other sets of coordinates that include the model physical tracers (Blanke et al., 2006).

### A1.2. TRACMASS

The TRACMASS Lagrangian trajectory code was originally developed by Döös (1995) and a thorough documentation was given by Döös et al. (2013) and Döös et al. (2017). TRACMASS has been used to calculate trajectories using velocity and tracer fields from a variety of ocean models. TRACMASS has also been used to study the atmospheric Hadley and Ferrell Cells using ERA-Interim as input (Kjellsson and Döös, 2012a). Hence, TRACMASS can handle a wide variety of vertical grids and data formats.

TRACMASS solves the path of a trajectory through a grid box analytically (see Section 3.2.3). Trajectories are thus unique and if a trajectory is calculated forward and then backward the solution will be the same up to numerical noise due to round-off errors. There are two algorithms for calculating the trajectories. The original from Döös (1995) uses velocities and tracers for trajectory calculations that are assumed piecewise constant in time. Another algorithm was developed by de Vries and Döös (2001) where time-dependence was taken into account by linearly interpolating the velocities in both time and space. Döös et al. (2017) showed that the time-interpolating scheme resulted in much more accurate calculations than the piecewise time-constant scheme.

TRACMASS trajectories have also been used to simulate the behaviour of surface drifters (Kjellsson and Döös, 2012b; Nilsson et al., 2013). Comparing the simulated drifter trajectories with observed surface-drifter trajectories has showed that coarse-resolution ocean models lack variability in the surface currents, which is very likely due to the omission of stochastic noise to mimic subgrid scale diffusion.

### A1.3. Octopus

Octopus is an offline particle tracking code first written to conduct offline particle simulation using the Southern Ocean State Estimation (Mazloff et al., 2010), which makes use of the MITgcm. The code was used to study tracer evolution (Wang et al., 2016) observed during the Diapycnal and Isopycnal Mixing Experiment in the Southern Ocean (DIMES; Gille et al., 2007; Ledwell et al., 2011). It was later used in simulating Argo floats as a component of observational system planning for the Southern Ocean Carbon and Climate Observations and Modeling project (SOCCOM, <http://soccom.princeton.edu>) and in studies of watermass pathways in the Southern Ocean.

The interpolation scheme is linear in time and trilinear in space. The RK4 scheme is used for time integration. The boundary condition is reflective at the surface and solid walls. The model is currently written in Fortran for structured C-grids. OpenMP is implemented for shared-memory parallel calculation.

### A1.4. LAMTA software package

The Lagrangian Manifolds and Trajectories Analyser (LAMTA) consists of a set of functions developed for gnu-octave and intended for the analysis of two-dimensional velocity fields, in particular for oceanic current datasets. The source code is freely available and distributed under a GPL license upon direct request to the authors (d'Ovidio and Nencioli).

The package provides routines to compute particle trajectories and Lagrangian diagnostics based on user defined velocity fields (which include analytical test cases, numerical model results and altimetry-based surface geostrophic currents). The trajectories are computed using a Runge–Kutta fourth order advection scheme (Section 3.2.1). Particle advection can be performed either forward or backward in time. The scheme applies bi-linear interpolation of velocities in space and, if necessary, linear interpolation in time. Lagrangian diagnostics include Finite Time/Size Lyapunov Exponents, eddy retention, origin of water particles, age of a water particles from a given bathymetry.

The package has been applied to investigate the relationship between satellite-based Lagrangian coherent structures and ocean surface tracers in the open ocean (d'Ovidio et al., 2004; 2009; Lehahn et al., 2007), the retention of mesoscale structures (Smetacek et al., 2012; Martin et al., 2013), the impact of horizontal advection in structuring ecological niches (d'Ovidio et al., 2010) up to top predators (Cotté et al., 2011; De Monte et al., 2012; Bon et al., 2015; Cotté et al., 2015) and for contextualizing biodiversity genomic data (Sunagawa et al., 2015). LAMTA has been recently included in the SPASSO (Software Package for an Adaptive Satellite-based Sampling for Ocean campaigns) software package<sup>14</sup> developed to guide the in-situ sampling strategy as well as the interpretation of collected observations from (sub)mesoscale oriented field experiments. The package has been used to support experiments in the NW Mediterranean (LATEX, e.g. Nencioli et al., 2011; 2013), tropical North Atlantic (STRASSE, Reverdin et al., 2015) and Southern Indian ocean: KEOPS2 (d'Ovidio et al., 2015) and LOHAFEX (Martin et al., 2013). The code has also been integrated in the package used by Cnes/AVISO to produce global maps of Lyapunov exponents and vectors from altimetry data.

<sup>14</sup> <http://www.mio.univ-amu.fr/~doglioli/spasso.htm>.



### A1.5. The Connectivity Modeling System (CMS)

The Connectivity Modelling System (CMS Paris et al., 2013b) is an open-source Fortran toolbox, created at the University of Miami, for the multi-scale tracking of biotic and abiotic particles in the ocean. The tool is inherently multiscale, allowing for the seamless moving of particles between grids at different resolutions.

The CMS has been used on velocity fields from OFES, HYCOM, NEMO, MITgcm, UVic, ECCO2, SOSE, MOM and many other ocean models to compute dispersion, connectivity and fate in applications including large scale oceanography, marine reserve planning, and movement of marine biota all across the world.

The CMS uses RK4 timestepping and tricubic interpolation and is designed to be modular and probabilistic, meaning that it is relatively easy to add additional ‘behaviours’ to the particles, with attributed randomly assigned for a distribution of traits. Modules distributed with the code include random walk diffusion, mortality, vertical migration, mixed layer mixing, and a seascape module designed to generate a connectivity matrix output from the source to the final destination of the particles.

### A1.6. Other Biotic-particle models

While the CMS discussed above is also used for physical oceanography applications, the code has been developed as a so-called Individual Based Model (IBM), which serve predominantly biophysical applications. Another widely-used example of an IBM is ICHTYOP (Lett et al., 2008, <http://www.ichthyop.org/>). We will not cover IBMs in this discussion, as a very good recent overview can be found in Lynch et al. (2014).

### A1.7. Parcels

Parcels is an experimental prototype code aimed at exploring novel approaches for Lagrangian tracking of virtual ocean tracer particles in the petascale age. Parcels, which is currently under development, is designed from the ground up to be efficient and fast for the next generation of ocean circulation models. These ocean models are so big and massively parallel, and they produce so much data, that in a few years we may face a situation where many of the Lagrangian frameworks cannot be used on the latest data any more (see also Section 5.1).

The user interface of Parcels is written in python, while the computational intensive integration is Just-In-Time (JIT) compiled into C. The code is formed around a flexible and customisable API that allows rapid model development, based on discrete time-stepping algorithms (Section 3.2.1). It has a high-level abstraction that hides complexities from the user (field sampling, efficient loop scheduling, file I/O, etc.). This allows computer architecture experts to optimise underlying methods without changing the high-level description of the model.

## A2. Online tools within OGCMs

### A2.1. LIGHT within MPAS-O

The Los Alamos National Laboratory Model for Prediction Across Scales Ocean (MPAS-O) (Ringler et al., 2013) is a fully unstructured C-grid ocean model capable of multiscale ocean simulation that is part of the Energy Exascale Earth System Model (E3SM), formerly known as Accelerated Climate model for Energy (ACME). MPAS-O uses an online diagnostic particle tracking technique called LIGHT (Wolfram et al., 2015), for Lagrangian, in Situ, Global, High-performance particle Tracking, which is integrated within the MPAS framework and uses different particle advection modes corresponding to different vertical interpolation schemes. For example, particles can be advected along isopycnally-constrained trajectories. Time advancement uses a generalized Runge–Kutta sub-stepping scheme. Horizontal interpolation with Wachspress interpolation (Gillette et al., 2012) occurs following reconstruction of the full velocity vector via an inverse multi-quadratic radial basis function approach (Baudisch et al., 2006). Particles are implemented in linked-lists on each processor to conserve memory for large particle simulations and parallelism is via MPI. Parallel communication occurs during the computational step between spatially-adjacent processors for particles advecting from one processor to another and global parallel communication is reserved for Input and Output (I/O) tasks. Processor exchange lists for I/O may either be incrementally updated or globally computed to minimize communication overhead in different particle tracking configurations. LIGHT provides the capability to advect the same number of particles as cells to obtain a complementary Lagrangian description of the flow computed by the Eulerian prognostic solver in MPAS-O. A version of MPAS-O that includes LIGHT will be available via the public release of the U.S. Department of Energy’s Energy Exascale Earth System Model (E3SM).

### A2.2. NEMO

NEMO (the Nucleus for European Modelling of the Ocean) model (Madec and NEMO team, 2016) includes both Lagrangian floats (Madec, 2008) and interactive icebergs, module ICB (both RK4). In addition to the online icebergs option (NEMO-ICB; Marsh et al., 2015), icebergs can be forced in offline mode (for tracking purposes) using the Stand-Alone Surface forced (SAS) option, as SAS-ICB. In both NEMO-ICB and SAS-ICB, implementation exploits available MPI parallelism.

### A2.3. MITgcm

The Massachusetts Institute of Technology General Circulation model (MITgcm Marshall et al., 1997b; 1997c) is a generalized level coordinate ocean model with a wide range of configuration possibilities. The MITgcm includes a package for Lagrangian particle advection. The Lagrangian package, named `flt`, is however poorly documented and not described in the literature. Nevertheless, this package provides a convenient way to integrate Lagrangian analysis into existing MITgcm setups, thereby taking advantage of the MPI parallelism of the model. Numerically, floats are advected using RK4. A fixed memory buffer is allocated for floats on each tile, implying that memory is wasted for sparse particle ensembles. Because of MITgcm’s “offline mode” (Adcroft et al., 2014), which enables loading of velocity fields from files, MITgcm can be effectively used as a general-purpose Lagrangian model. Numerous studies have employed this configuration for simulating Lagrangian trajectories from satellite-derived geostrophic velocities (Klocker et al., 2012b; 2012a; Klocker and Abernathy, 2014) and three-dimensional model output (Abernathy et al., 2013).

### A2.4. HYCOM

HYCOM (the HYbrid Coordinate Ocean Model) is a generalized (hybrid) vertical coordinate ocean model (isopycnal, terrain following, and/or pressure). It is isopycnal in the open stratified ocean, but reverts smoothly to a terrain-following coordinate in shallow coastal regions, and to pressure coordinates near the surface in the mixed layer (Bleck, 2002; Chassignet et al., 2003; 2006). HYCOM includes online code designed to follow numerical particles during model run time (Halliwell and Garraffo, 2002; Wallcraft et al., 2009). In addition to the ability to follow a fluid

particle in three dimensions, one can also release both isobaric and isopycnic floats. Isobaric floats remain at prescribed pressure levels while isopycnic floats remain on prescribed density surfaces.

Because of the generalized (or hybrid) vertical coordinate of HYCOM, one has to be especially attentive when performing vertical and horizontal interpolations/advections. The horizontal, vertical, and temporal interpolation schemes used in HYCOM to advect the floats are adapted from Garraffo et al. (2001a); 2001b). Horizontal interpolation is performed using a sixteen-point grid box surrounding the float when a sufficient number of good grid points are available (bilinear interpolation otherwise). Vertical interpolation first locates the bounding pressure interfaces and all properties are then linearly interpolated to the float location. Temporal interpolation is performed using RK4. Since the vertical velocity is not a prognostic variable in HYCOM, it is diagnosed using the continuity equation (see Halliwell and Garraffo (2002) and Wallcraft et al. (2009) for details on the implementation).

### A2.5. ROMS

ROMS (Regional Ocean Model System, <https://www.myroms.org/>) is a free surface, hydrostatic primitive equations ocean model with terrain-following vertical coordinates that allow differential stretching (Shchepetkin and McWilliams, 2005; Haidvogel et al., 2008). It is an open source parallel Fortran code coupled to several models including biogeochemistry, waves, sediments, bio-optical and sea ice. It offers great flexibility for configuration and is widely used by the scientific community for a diverse range of applications. ROMS includes a module called floats, which allows the release and tracking of numerical particles during model run time. Passive floats can be of 3 different types: neutral density 3D Lagrangian, isobaric (remain at prescribed pressure level) or geopotential (remain at prescribed depth). The numerical scheme used to time-step simulated floats trajectories is a fourth-order Milne predictor and fourth-order Hamming corrector. It is possible to add a random walk to the floats to simulate subgrid scale vertical diffusion. The random walk component is implemented considering spatially variable diffusivity following Hunter et al. (1993). Floats can either reflect or ‘stick’ when they hit the surface/bottom boundaries. Clusters of floats with user defined distributions can be released at specified locations. It is possible to release particles multiple times, at defined time intervals throughout the run. Recently new subroutines have been implemented to allow for ‘biological floats’ that behave according to user defined parameters. The complex biology of oyster larvae, including variable growth rates and vertical swimming dependent on food, salinity, temperature and turbidity has been implemented (Narvaez et al., 2012a; 2012b), and is available with the latest ROMS release.

### Appendix B. Tracer trajectories with isopycnal diffusion

We here illustrate the stochastic differential equation discussion from Section 3.3.1. We consider the calculation of Lagrangian tracer trajectories in a 3D benchmark for diffusive tracer transport from Shah et al. (2011; 2013). Note that in two dimensions, the approach is slightly different (see Appendix C). For this purpose, let  $x$  and  $y$  denote the horizontal coordinates, while  $z$  denotes the vertical coordinate and assume zero diapycnal diffusion. If  $\rho$  is the potential density field (assume linear equation of state), then the isopycnal diffusion tensor (Redi, 1982) reads

$$\mathbf{K} = \frac{K_I}{\rho_x^2 + \rho_y^2 + \rho_z^2} \begin{pmatrix} \rho_y^2 + \rho_z^2 & -\rho_x\rho_y & -\rho_x\rho_z \\ -\rho_y\rho_x & \rho_x^2 + \rho_z^2 & -\rho_y\rho_z \\ -\rho_z\rho_x & -\rho_z\rho_y & \rho_x^2 + \rho_y^2 \end{pmatrix}. \tag{36}$$

Here  $K_I$  represents the isopycnal diffusion coefficient and  $\rho$  is given by

$$\rho(x, y, z) = \rho_0 \left[ 1 - \frac{N^2 z}{g} + \alpha_x \sin(\kappa_x x) + \alpha_y \sin(\kappa_y y) \right]. \tag{37}$$

Note that the vertical density gradient is assumed to be constant, but the horizontal one is not, so that the isopycnal surfaces are not flat.

The concentration satisfies the following initial value problem:

$$\frac{\partial C}{\partial t} = \frac{\partial}{\partial x_i} \left( K_{ij} \frac{\partial C}{\partial x_j} \right), \quad t_0 \leq t \leq T$$

$$C(\mathbf{x}, t) = C_0(\mathbf{x}). \tag{38}$$

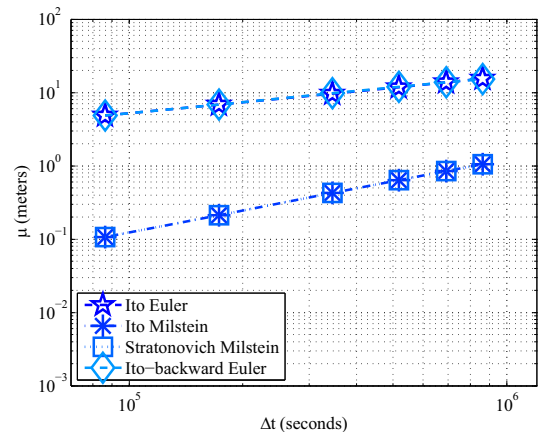
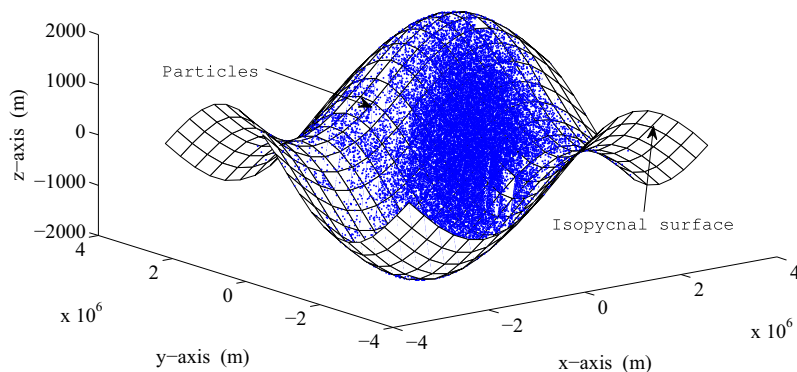


Fig. 8. (a) Simulated position of Lagrangian particles at a certain time on the non-flat isopycnal surface and (b) the spurious diapycnal diffusivity for different Lagrangian schemes.

To solve this problem with the stochastic model given by Eq. (27), one needs to decompose the diffusion tensor  $\mathbf{K}$  in the form  $2K_{ij} = \sigma_{ik} \sigma_{jk}$ . Using a Cholesky decomposition method, the components of the matrix  $\sigma$  can be determined. This decomposition leads to the following stochastic differential equations describing the behaviour of the individual particles (note that due to the use of Cholesky decomposition, the components  $\sigma_{xy}$ ,  $\sigma_{xz}$  and  $\sigma_{yz}$  of the matrix  $\sigma$  are zero)

$$\begin{aligned} dX(t) &= a_x dt + \sqrt{2} \sigma_{xx} dW_x(t), \\ dY(t) &= a_y dt + \sqrt{2} \sigma_{yx} dW_x(t) + \sqrt{2} \sigma_{yy} dW_y(t), \\ dZ(t) &= a_z dt + \sqrt{2} \sigma_{zx} dW_x(t) + \sqrt{2} \sigma_{zy} dW_y(t), \\ X(t_0) &= X_0, \quad Y(t_0) = Y_0, \quad Z(t_0) = Z_0, \end{aligned} \quad (39)$$

where the drift coefficients  $a_x$ ,  $a_y$  and  $a_z$  are given by

$$a_x = \frac{\partial K_{xx}}{\partial x} + \frac{\partial K_{xy}}{\partial y}, \quad a_y = \frac{\partial K_{yx}}{\partial x} + \frac{\partial K_{yy}}{\partial y} \quad \text{and} \quad a_z = \frac{\partial K_{zx}}{\partial x} + \frac{\partial K_{zy}}{\partial y}. \quad (40)$$

In Fig. 8a results of a simulation are shown for parameter values that are relevant for ocean transport problems (Shah et al., 2011; 2013). Here the particles have been released at the origin  $(x, y, z) = (0, 0, 0)$ , a point that belongs to the isopycnal surface. The position vector  $[x_j(t), y_j(t), z_j(t)]$ ,  $j = 1, 2 \dots J$ , of each particle is simulated by means of a Lagrangian scheme. Because the diapycnal diffusion is zero, the particles should not leave the isopycnal surface. However, numerical errors are unavoidable and their magnitude can be estimated by means of a spurious diapycnal diffusivity. The results presented in Fig. 8b show that the higher order Milstein scheme performs better than the Euler scheme.

### Appendix C. Diffusion in two-dimensional models and associated Lagrangian tracer trajectories

This review article deals with Lagrangian methods for large-scale open-ocean applications in oceanography. This is why the theoretical developments and the flows dealt with are essentially three-dimensional. There are, however, difficulties inherent in one- or two-dimensional transport models, which cannot be regarded as an idealisation or simplification of three-dimensional models. Some aspect thereof are outlined below.

Let  $H$ ,  $u_i$  ( $i = 1, 2$ ) and  $C$  be functions of the time and horizontal coordinates representing the height of the water column, the depth-averaged horizontal velocity and the depth-averaged concentration of a passive tracer, respectively. Then, the continuity equation is

$$\partial_t H + \partial_i (H u_i) = 0 \quad (41)$$

and the equation obeyed by the concentration reads (e.g. Vanderborgh et al., 2007)

$$\partial_t (H C) + \partial_i (H C u_i) = \partial_i (H K_{ij} \partial_j C) \quad (42)$$

where the diffusivity tensor  $K_{ij}$  is symmetric and positive definite. The latter partial differential equation may be transformed into a Fokker–Planck equation in which  $HC$  (rather than  $C$ ) should be viewed as the unknown:

$$\partial_t (H C) + \partial_i (H C u_i^{\text{drift}}) = \partial_i \partial_j (K_{ij} H C) \quad (43)$$

where the drift velocity is (Heemink, 1990)

$$u_i^{\text{drift}} = u_i + H^{-1} \partial_j (H K_{ij}) = u_i + \partial_i (K_{ij}) + K_{ij} H^{-1} \partial_j H. \quad (44)$$

The first two terms on the right-hand-side of Eq. (44) are equivalent to those used in three-dimensional models, whilst the last one is specific to depth-integrated models.

If the last term in (44) is not taken into account in a Lagrangian model, then particles might tend to concentrate into the shallowest areas, which clearly is unphysical and may lead to erroneous conclusions (e.g. Spagnol et al., 2002). A test case was designed by Deleersnijder (2015) that includes an analytical solution for diffusion in a depth-varying domain, and implemented numerically by Thomas et al. (2015a). This exact solution exhibits a somewhat counter-intuitive behaviour, with the location of the maximum of the concentration and the tracer patch centre of mass moving in opposite directions.

Somewhat similar developments are made when designing a one-dimensional, cross section-averaged transport model. Such models are often used to simulate transport processes in elongated domains such as rivers or estuaries (e.g. Everbecq et al., 2001; Hofmann et al., 2008). In this case all the variables and parameters depend on time and the along-flow coordinate  $x$ . If  $S$ ,  $u$  and  $C$  denote the cross-sectional area, the cross-section-averaged velocity and the cross-section-averaged concentration, respectively, then the one-dimensional counterparts to Eqs. (41)–(44) are

$$\partial_t S + \partial_x (S u) = 0 \quad (45a)$$

$$\partial_t (S C) + \partial_x (S C u) = \partial_x (S K \partial_x C) \quad (45b)$$

$$\partial_t (S C) + \partial_x (S C u^{\text{drift}}) = \partial_x \partial_x (K S C) \quad (45c)$$

where

$$u^{\text{drift}} = u + S^{-1} \partial_x (S K) = u + \partial_x K + K S^{-1} \partial_x S \quad (46)$$

is the drift velocity, and  $K$  is the along-flow diffusivity.

In depth- and section-averaged models, the diffusion term is rarely meant to represent turbulent diffusion per se. Instead, it is essentially the effect of shear dispersion (e.g. Young and Jones, 1991) that is to be parameterized, i.e. the impact on the resolved (reduced-dimension) processes of the combined effect of sheared-advection and turbulent diffusion in the transversal direction. As a consequence, the diffusivity coefficients are often significantly larger than those that would be used in a three-dimensional model of the same domain.

## References

- Abernathy, R., Ferreira, D., Klocker, A., 2013. Diagnostics of isopycnal mixing in a circumpolar channel. *Ocean Modell.* 72, 1–16. <http://dx.doi.org/10.1016/j.oceomod.2013.07.004>.
- Abernathy, R., Haller, G., 2017. Transport by lagrangian vortices in the eastern pacific. Arxiv: 1705.08487. In revision at *J. Phys. Oceanogr.*
- Abraham, E.R., Bowen, M.M., 2002. Chaotic stirring by a mesoscale surface-ocean flow. *Chaos* 12 (2), 373–381. <http://dx.doi.org/10.1063/1.1481615>.
- Adcroft, A., Campin, J., Dutkiewicz, S., Evangelinos, C., Ferreira, D., Forget, G., Fox-Kemper, B., Heimbach, P., Hill, C., Hill, E., et al., 2014. *Mitgcm User Manual*.
- Ådlandsvik, B., Bartsch, J., Brickman, D., Browman, H.I., Edwards, K., Fiksen, Ø., Gallego, A., Hermann, A.J., Hinckley, S., Houde, E., Huret, M., Irsson, J.-O., Lacroix, G., Leis, J.M., McClohrrie, P., Megrey, B.A., Miller, T., Van der Molen, J., Mullon, C., North, E.W., Parada, C., Paris, C.B., Pepin, P., Petigas, P., Rose, K., Thygesen, U.H., Werner, C., 2009. Manual of Recommended Practices for Modelling Physical – Biological Interactions During Fish Early Life. Technical Report. IFREMER, Dépt., EMH BP 21105 FR-44311 Nantes, Cedex 03, France.
- von Appen, W.-J., Koszalka, I.M., Pickart, R.S., Haine, T.W.N., Mastopole, D., Magaldi, M.G., 2014. East Greenland Spill Jet as important part of the AMOC. *Deep Sea Res.* 192, 75–84. <http://dx.doi.org/10.1016/j.dsr.2014.06.002>.
- Aris, R., 1962. *Vectors, Tensors and the Basic Equations of Fluid Mechanics*. Dover Publishing, New York.
- Artale, V., Boffetta, G., Celani, A., Cencini, M., Vulpiani, A., 1997. Dispersion of passive tracers in closed basins: beyond the diffusion coefficient. *Phys. Fluids* 9 (11), 3162–3171.
- Aurell, E., Boffetta, G., Crisanti, A., Paladin, G., Vulpiani, A., 1997. Predictability in the large: an extension of the concept of Lyapunov exponent. *J. Phys. A* 30 (1), 1.
- Awaji, T., Imasato, N., Kunishi, H., 1980. Tidal exchange through a strait: a numerical experiment using a simple model basin. *J. Phys. Oceanogr.* 10 (10), 1499–1508.
- Baltazar-Soares, M., Biastoch, A., Harrod, C., Hanel, R., Marohn, L., Prigge, E., Evans, D., Bodles, K., Behrens, E., Böning, C.W., 2014. Recruitment collapse and population structure of the European eel shaped by local ocean current dynamics. *Current Biology* 24 (1), 104–108.
- Batchelor, G., 1952. Diffusion in a field of homogeneous turbulence. *Mathematical Proceedings of the Cambridge Philosophical Society*. 48–02. Cambridge Univ Press, pp. 345–362.
- Batchelor, G.K., 1967. *An Introduction to Fluid Dynamics*. Cambridge University Press, Cambridge, England.
- Bates, M.L., Griffies, S.M., England, M.H., 2012. A dynamic, embedded Lagrangian model for ocean climate models. Part I: Theory and implementation. *Ocean Modell.* 59–60 (C), 41–59.
- Baudisch, J., Bonaventura, L., Iske, A., Miglio, E., 2006. Matrix Valued Radial Basis Functions for Local Vector Field Reconstruction: Applications to Computational Fluid Dynamic Models. MOX Report, pp. 75.
- Bauer, S., Swenson, M.S., Griffa, A., 2002. Eddy mean flow decomposition and eddy diffusivity estimates in the tropical Pacific Ocean: 2. Results. *J. Geophys. Res.* 107 (C10), 3154.
- Bennett, A.F., 1987. A lagrangian analysis of turbulent diffusion. *Reviews of Geophysics* 25 (4), 799–822.
- Bennett, A.F., 2006. *Lagrangian Fluid Dynamics*. Cambridge University Press, Cambridge.
- Berglund, M., Nilsson Jacobi, M., Jonsson, P.R., 2012. Optimal selection of marine protected areas based on connectivity and habitat quality. *Ecological Modelling* 240, 105–112. <http://dx.doi.org/10.1016/j.ecolmodel.2012.04.011>.
- Berloff, P., Kamenkovich, I., Pedlosky, J., 2009. A model of multiple zonal jets in the oceans: dynamical and kinematical analysis. *J. Phys. Oceanogr.* 39 (11), 2711–2734.
- Berloff, P., McWilliams, J., 2003. Material transport in oceanic gyres. Part iii: randomized stochastic models. *J. Phys. Oceanogr.* 33, 1416–1445.
- Berloff, P., McWilliams, J., Bracco, A., 2002. Material transport in oceanic gyres. Part i: phenomenology. *J. Phys. Oceanogr.* 32, 764–796.
- Berloff, P.S., McWilliams, J.C., 2002. Material transport in oceanic gyres. Part ii: hierarchy of stochastic models. *J. Phys. Oceanogr.* 32 (3), 797–830.
- Beron-Vera, F.J., LaCasce, J.H., 2016. Statistics of simulated and observed pair separations in the Gulf of Mexico. *J. Phys. Oceanogr.* 46 (7), 2183–2199. <http://dx.doi.org/10.1175/JPO-D-15-0127.1>.
- Beron Vera, F.J., Olascoaga, M.J., Goni, G.J., 2008. Oceanic mesoscale eddies as revealed by Lagrangian coherent structures. *Geophys. Res. Lett.* 35 (12). <http://dx.doi.org/10.1029/2008GL033957>.
- Beron-Vera, F.J., Wang, Y., Olascoaga, M.J., Goni, G.J., Haller, G., 2013. Objective detection of oceanic eddies and the agulhas leakage. *J. Phys. Oceanogr.* 43 (7), 1426–1438.
- Bettencourt, J.H., López, C., Hernández-García, E., Montes, I., Sudre, J., Dewitte, B., Paulmier, A., Garçon, V., 2015. Boundaries of the peruvian oxygen minimum zone shaped by coherent mesoscale dynamics. *Nat. Geosci.* 8, 937–940.
- Blanke, B., Arhan, M., Madec, G., Roche, S., 1999. Warm water paths in the equatorial Atlantic as diagnosed with a general circulation model. *J. Phys. Oceanogr.* 29, 2753–2768.
- Blanke, B., Arhan, M., Speich, S., 2006. Salinity changes along the upper limb of the Atlantic thermohaline circulation. *Geophys. Res. Lett.* 33, L06609.
- Blanke, B., Bonhommeau, S., Grima, N., Drillet, Y., 2012. Sensitivity of advective transfer times across the North Atlantic Ocean to the temporal and spatial resolution of model velocity data: Implication for European eel larval transport. *Dyn. Atmos. Ocean.* 55–56, 22–44. <http://dx.doi.org/10.1016/j.dynatmoce.2012.04.003>.
- Blanke, B., Raynaud, S., 1997. Kinematics of the Pacific equatorial undercurrent: an Eulerian and Lagrangian approach from GCM results. *J. Phys. Oceanogr.* 27 (6), 1038–1053.
- Blanke, B., Speich, S., 2002. A global diagnostic of interior ocean ventilation. *Geophys. Res. Lett.* 29 (8), 1–4. <http://dx.doi.org/10.1029/2001GL013727>.
- Bleck, R., 2002. An oceanic general circulation model framed in hybrid isopycnic-Cartesian coordinates. *Ocean Modell.* 4 (1), 55–88.
- Bon, C., Della Penna, A., d'Ovidio, F., Arnould, J.Y., Poupart, T., Bost, C.-A., 2015. Influence of oceanographic structures on foraging strategies: macaroni penguins at crozet islands. *Movement Ecol.* 3 (1), 1–11.
- Böning, C.W., Cox, M.D., 1988. Particle dispersion and mixing of conservative properties in an eddy-resolving model. *J. Phys. Oceanogr.* 18, 320–338.
- Bowden, K.F., 1965. Horizontal mixing in the sea due to a shearing current. *J. Fluid Mech.* 21 (2), 83–95.
- Bower, A.S., Lozier, M.S., Gary, S.F., Böning, C.W., 2009. Interior pathways of the North Atlantic meridional overturning circulation. *Nature* 459, 243–248.
- Brandt, G., Wehrmann, A., Wirtz, K.W., 2008. Rapid invasion of *Crassostrea gigas* into the German Wadden Sea dominated by larval supply. *J. Sea Res.* 59 (4), 279–296. <http://dx.doi.org/10.1016/j.seares.2008.03.004>.
- Burgess, S.C., Nickols, K.J., Griesemer, C.D., Barnett, L.A.K., Dedrick, A.G., Satterthwaite, E.V., Yamane, L., Morgan, S.G., White, J.W., Botsford, L.W., 2014. Beyond connectivity: how empirical methods can quantify population persistence to improve marine protected-area design. *Ecol. Appl.* 24 (2), 257–270.
- Butcher, J.C., 2016. *Numerical Methods for Ordinary Differential Equations*. John Wiley & Sons.
- Cetina-Heredia, P., Roughan, M., van Sebille, E., Feng, M., Coleman, M.A., 2015. Strengthened currents override the effect of warming on lobster larval dispersal & survival. *Global Change Biol.* 21, 4377–4386.
- Chassignet, E., Smith, L.T., Halliwell, G., Bleck, R., 2003. North Atlantic simulations with the Hybrid Coordinate Ocean Model (HYCOM): impact of the vertical coordinate choice, reference pressure, and therobaricity. *J. Phys. Oceanogr.* 33 (12), 2504–2526.
- Chassignet, E.P., Hurlburt, H., Smedstad, O.M., Halliwell, G., Wallcraft, A.J., Metzger, E.J., Blanton, B., Lozano, C., Rao, D., Hogan, P., Srinivasan, A., 2006. Generalized vertical coordinates for eddy-resolving global and coastal ocean forecasts. *Oceanography* 19 (1), 118–129.
- Chenillat, F., Blanke, B., Grima, N., Franks, P.J.S., Capet, X., Rivière, P., 2015. Quantifying tracer dynamics in moving fluids: a combined Eulerian-Lagrangian approach. *Front. Environ. Sci.* 3, 1–15.
- Chu, P.C., Fan, C., 2014. Accuracy progressive calculation of Lagrangian trajectories from a gridded velocity field. *J. Atmos. Ocean. Technol.* 31 (7), 1615–1627.
- Cotté, C., d'Ovidio, F., Chaigneau, A., Lévy, M., Taupier Letage, I., Mate, B., Guinet, C., 2011. Scale-dependent interactions of Mediterranean whales with marine dynamics. *Limnol. Oceanogr.* 106 (20), 219–232. <http://dx.doi.org/10.4319/lo.2011.56.1.0219>.
- Cotté, C., d'Ovidio, F., Dragon, A.-C., Guinet, C., Lévy, M., 2015. Flexible preference of southern elephant seals for distinct mesoscale features within the antarctic circumpolar current. *Prog. Oceanogr.* 131, 46–58.
- Cowen, R.K., Paris, C.B., Srinivasan, A., 2006. Scaling of connectivity in marine populations. *Science* 311, 522–527.
- Cummins, S.J., Silvester, T.B., Cleary, P.W., 2012. Three-dimensional wave impact on a rigid structure using smoothed particle hydrodynamics. *Int. J. Numer. Methods Fluids* 68 (12), 1471–1496. <http://dx.doi.org/10.1002/fld.2539>.
- Danabasoglu, G., 2004. A comparison of global ocean general circulation model solutions obtained with synchronous and accelerated integration methods. *Ocean Modell.* 7, 323–341.
- Davis, R.E., 1982. On relating eulerian and lagrangian velocity statistics: single particles in homogeneous flows. *J. Fluid Mech.* 114, 1–26. <http://dx.doi.org/10.1017/S0022112082000019>.
- Davis, R.E., 1983. Oceanic property transport, lagrangian particle statistics, and their prediction. *J. Marine Res.* 41, 163–194. <http://dx.doi.org/10.1357/002224083788223018>.
- Davis, R.E., 1985. Drifter observations of coastal surface currents during code: The statistical and dynamical views. *J. Geophys. Res.* 90 (C3), 4756–4772. <http://dx.doi.org/10.1029/JC090iC03p04756>.
- Davis, R.E., 1987. Modeling eddy transport of passive tracers. *J. Marine Res.* 45 (3), 635–666.
- Davis, R.E., 1991. Observing the general circulation with floats. *Deep Sea Res.* 38, 531–571.
- Davis, R.E., 1998. Preliminary results from directly measuring mid-depth circulation in the Tropical and South Pacific. *J. Geophys. Res.* 103, 24619–24639.
- Dawson, M.N., Sen Gupta, A., England, M.H., 2005. Coupled biophysical global ocean model and molecular genetic analyses identify multiple introductions of cryptogenic species. *Proc. Natl. Acad. Sci.* 102 (34), 11968–11973.
- De Monte, S., Cotté, C., d'Ovidio, F., Lévy, M., Le Corre, M., Weimerskirch, H., 2012. Frigatebird behaviour at the ocean-atmosphere interface: integrating animal behaviour with multi-satellite data. *J. R. Soc. Interface* 9 (77), 3351–3358.
- DeGroot, S.R., Mazur, P., 1984. *Non-Equilibrium Thermodynamics*. Dover Publications, New York, pp. 510.
- Deleersnijder, E., 2015. A Depth-Integrated Diffusion Problem in a Depth-Varying, Unbounded Domain for Assessing Lagrangian Schemes. Technical Report. Université Catholique de Louvain. <http://hdl.handle.net/2078.1/160980>.
- Deleersnijder, E., Campin, J.M., Delhez, E.J.M., 2001. The concept of age in marine modelling I. Theory and preliminary model results. *J. Marine Syst.* 28, 229–267. [http://dx.doi.org/10.1016/S0924-7963\(01\)00026-4](http://dx.doi.org/10.1016/S0924-7963(01)00026-4).
- Döös, K., 1995. Inter-ocean exchange of water masses. *J. Geophys. Res.* 100, 13499–13514.
- Döös, K., Jönsson, B., Kjellsson, J., 2017. Evaluation of oceanic and atmospheric



- trajectory schemes in the TRACMASS trajectory model v6.0. *Geosci. Model Dev.* 10 (4), 1733–1749. <http://dx.doi.org/10.5194/gmd-10-1733-2017>.
- Döös, K., Kjellsson, J., Jönsson, B., 2013. TRACMASSa Lagrangian trajectory model. *Preventive Methods for Coastal Protection*. Springer International Publishing, Heidelberg, pp. 225–249.
- Döös, K., Meier, H.E.M., Döscher, R., 2004. The Baltic haline conveyor belt or the overturning circulation and mixing in the Baltic. *Ambio* 33 (4–5), 261–266. <http://dx.doi.org/10.1579/0044-7447-33.4.261>.
- Döös, K., Nilsson, J., Nycander, J., Brodeau, L., Ballarotta, M., 2012. The World Ocean thermohaline circulation. *J. Phys. Oceanogr.* 42 (9), 1445–1460.
- Döös, K., Nycander, J., Coward, A.C., 2008. Lagrangian decomposition of the Deacon Cell. *J. Geophys. Res. Ocean.* 113 (C7), C07028. <http://dx.doi.org/10.1029/2007JC004351>.
- Dormand, J., Prince, P., 1980. A family of embedded Runge-Kutta formulae. *J. Comput. Appl. Math.* 6 (1), 19–26. [http://dx.doi.org/10.1016/0771-050X\(80\)90013-3](http://dx.doi.org/10.1016/0771-050X(80)90013-3).
- d'Ovidio, F., De Monte, S., Alvain, S., Dandonneau, Y., Lévy, M., 2010. Fluid dynamical niches of phytoplankton types. *Proc. Nat. Acad. Sci.* 107 (43), 18366–18370.
- d'Ovidio, F., Fernández, V., Hernández García, E., López, C., 2004. Mixing structures in the Mediterranean Sea from finite-size Lyapunov exponents. *Geophys. Res. Lett.* 31, L17203. <http://dx.doi.org/10.1029/2004GL020328>.
- d'Ovidio, F., Isern Fontanet, J., López, C., Hernández García, E., García Ladona, E., 2009. Comparison between Eulerian diagnostics and finite-size Lyapunov exponents computed from altimetry in the Algerian basin. *Deep Sea Res.* 156 (1), 15–31. <http://dx.doi.org/10.1016/j.dsr.2008.07.014>.
- d'Ovidio, F., Della Penna, A., Trull, T.W., Nencioli, F., Pujol, M.-I., Rio, M.-H., Park, Y.-H., Cotté, C., Zhou, M., Blain, S., 2015. The biogeochemical structuring role of horizontal stirring: Lagrangian perspectives on iron delivery downstream of the Kerguelen Plateau. *Biogeosciences* 12 (19), 5567–5581. <http://dx.doi.org/10.5194/bg-12-5567-2015>.
- Drijfhout, S., de Vries, P., Döös, K., Coward, A., 2003. Impact of eddy-induced transport on the lagrangian structure of the upper branch of the thermohaline circulation. *J. Phys. Oceanogr.* 24, 2141–2155.
- Drijfhout, S.S., Maier-Reimer, E., Mikolajewicz, U., 1996. Tracing the conveyor belt in the Hamburg large-scale geostrophic ocean general circulation model. *J. Geophys. Res.* 101, 22563–22575.
- Durack, P.J., Wijffels, S.E., Matear, R.J., 2012. Ocean salinities reveal strong global water cycle intensification during 1950 to 2000. *Science* 336 (6080), 455–458.
- Durgadoo, J.V., Loveday, B.R., Reason, C.J.C., Penven, P., Biastoch, A., 2013. Agulhas leakage predominantly responds to the southern hemisphere westerlies. *J. Phys. Oceanogr.* 43 (10), 2113–2131. <http://dx.doi.org/10.1175/JPO-D-13-047.1>.
- Durgadoo, J.V., Rühs, S., Biastoch, A., Böning, C.W.B., 2017. Indian ocean sees of agulhas leakage. *J. Geophys. Res.* 122, 3481–3499. <http://dx.doi.org/10.1002/2016JC012676>.
- Durran, D.R., 1999. *Numerical Methods for Wave Equations in Geophysical Fluid Dynamics*. Springer Verlag, Berlin, pp. 470.
- Eckart, C., 1948. An analysis of the stirring and mixing processes in incompressible fluids. *J. Marine Res.* 7, 265–275.
- England, M., 1995. The age of water and ventilation timescales in a global ocean model. *J. Phys. Oceanogr.* 25, 2756–2777.
- Everbecq, E., Gosselain, V., Viroux, L., Descy, J.P., 2001. Potamon: a dynamic model for predicting phytoplankton composition and biomass in lowland rivers. *Water Res.* 35 (4), 901–912.
- Eyring, V., Bony, S., Meehl, J., Senior, C., Stevens, B., Stouffer, R., Taylor, K., 2015. Overview of the coupled model intercomparison project phase 6 (cmip6) experimental design and organisation. *Geosci. Model Dev. Discuss.* 2015, 10539–10583. <http://dx.doi.org/10.5194/gmd-2015-265>.
- Fabbroni, N., 2009. *Numerical Simulations of Passive Tracers Dispersion in the Sea*. Università di Bologna Ph.D. thesis.
- Farazmand, M.M., Haller, G., 2012. Computing lagrangian coherent structures from their variational theory. *Chaos* 22. <http://dx.doi.org/10.1063/1.369015>.
- Fine, R.A., Rhein, M., Adrié, C., 2002. Using a CFC effective age to estimate propagation and storage of climate anomalies in the deep western North Atlantic Ocean. *Geophys. Res. Lett.* 29 (24), 80–81. <http://dx.doi.org/10.1029/2002GL015618>.
- Fischer, H.B., List, J.E., Koh, C.R., Imberger, J., Brooks, N.H., 2013. *Mixing in Inland and Coastal Waters*. Elsevier.
- Fox-Kemper, B., Lumpkin, R., Bryan, F., 2013. Lateral transport in the ocean interior. In: Siedler, G., Griffies, S.M., Gould, J., Church, J. (Eds.), *Ocean Circulation and Climate*, 2nd Edition: A 21st Century Perspective. International Geophysics Series, vol. 103. Academic Press, pp. 185–209.
- Froyland, G., Horenkamp, C., Rossi, V., Santitissadeekorn, N., Sen Gupta, A., 2012. Three-dimensional characterization and tracking of an Agulhas Ring. *Ocean Modell.* 52–53, 69–75.
- Froyland, G., Horenkamp, C., Rossi, V., van Sebille, E., 2015. Studying an Agulhas ring's long-term pathway and decay with finite-time coherent sets. *Chaos* 25 (8), 083119.
- Froyland, G., Padberg-Gehle, K., England, M.H., Treguier, A.-M., 2007. Detection of coherent oceanic structures via transfer operators. *Phys. Rev. Lett.* 98 (22), 224503.
- Fujio, S., Imasato, N., 1991. Diagnostic calculation for circulation and water mass movement in the deep pacific. *J. Geophys. Res.* 96 (C1), 759–774.
- Fujio, S., Kadowaki, T., Imasato, N., 1992. World ocean circulation diagnostically derived from hydrographic and wind stress fields: 2. the water movement. *J. Geophys. Res.* 97 (C9), 14439–14452.
- Gaines, S.D., Gaylord, B., Largier, J.L., 2003. Avoiding current oversights in marine reserve design. *Ecol. Appl.* 13 (sp1), 32–46. [http://dx.doi.org/10.1890/1051-0761\(2003\)013\[0032:ACOIMR\]2.0.CO;2](http://dx.doi.org/10.1890/1051-0761(2003)013[0032:ACOIMR]2.0.CO;2).
- Gardiner, C.W., 1985. *Handbook of stochastic models*, second ed. Springer, Heidelberg.
- Garraffo, Z.D., Griffa, A., Mariano, A.J., Chassignet, E.P., 2001. Lagrangian data in a high-resolution numerical simulation of the North Atlantic II. on the pseudo-Eulerian averaging of Lagrangian data. *J. Marine Syst.* 29 (1–4), 177–200.
- Garraffo, Z.D., Mariano, A.J., Griffa, A., Veneziani, C., Chassignet, E.P., 2001. Lagrangian data in a high-resolution numerical simulation of the North Atlantic I. Comparison with in situ drifter data. *J. Marine Syst.* 29 (1–4), 157–176.
- Gary, S.F., Lozier, M.S., Biastoch, A., Bning, C.W., 2012. Reconciling tracer and float observations of the export pathways of Labrador Sea Water. *Geophys. Res. Lett.* 39 (November), 1–5. <http://dx.doi.org/10.1029/2012GL053978>.
- Gary, S.F., Lozier, M.S., Kwon, Y.-O., J., P.J., 2014. The fate of north atlantic subtropical mode water in the flame model. *J. Phys. Oceanogr.* 44 (5).
- Gat, J.R., 1996. Oxygen and hydrogen isotopes in the hydrologic cycle. *Annu. Rev. Earth Planet. Sci.* 24, 225–262.
- Gaylord, B., Gaines, S.D., 2000. Temperature or transport? range limits in marine species mediated solely by flow. *Am. Nat.* 155 (6), 769–789.
- Gilbert, C.S., Gentleman, W.C., Johnson, C.L., DiBacco, C., Pringle, J.M., Chen, C., 2010. Modelling dispersal of sea scallop (*Placopecten magellanicus*) larvae on Georges Bank: the influence of depth-distribution, planktonic duration and spawning seasonality. *Prog. Oceanogr.* 87 (1–4), 37–48. <http://dx.doi.org/10.1016/j.pocan.2010.09.021>.
- Gille, S.T., Speer, K., Ledwell, J.R., Garabato, A.C.N., 2007. Mixing and Stirring in the Southern Ocean. *Eos Trans. Am. Geophys. Union* 88, 382. <http://dx.doi.org/10.1029/2007EO390002>.
- Gillette, A., Rand, A., Bajaj, C., 2012. Error estimates for generalized barycentric interpolation. *Adv. Comput. Math.* 37 (3), 417–439.
- Gimeno, L., Drumond, A., Nieto, R., Trigo, R.M., Stohl, A., 2010. On the origin of continental precipitation. *Geophys. Res. Lett.* 37 (13), L13804.
- Graham, F., McDougall, T., 2013. Quantifying the nonconservative production of conservative temperature, potential temperature, and entropy. *J. Phys. Oceanogr.* 43, 838–862.
- Gräwe, U., Deleersnijder, E., Shah, S.H.A.M., Heemink, A.W., 2012. Why the euler-scheme in particle-tracking is not enough: the shallow sea test case. *Ocean Dyn.* 62 (4), 501–514.
- Griesel, A., Eden, C., Koopmann, N., Yulaeva, E., 2015. Comparing isopycnal eddy diffusivities in the southern ocean with predictions from linear theory. *Ocean Modell.* 94, 33–45.
- Griesel, A., McClean, J., Gille, S., Sprintall, J., Eden, C., 2014. Eulerian and lagrangian isopycnal eddy diffusivities in the southern ocean of an eddying model. *J. Phys. Oceanogr.* 44, 644–661.
- Griffa, A., 1996. Applications of stochastic particle models to oceanographic problems. *Stochastic Modelling in Physical Oceanography*. Springer, pp. 113–140.
- Griffies, S.M., 1998. The Gent-McWilliams skew-flux. *J. Phys. Oceanogr.* 28, 831–841.
- Griffies, S.M., Böning, C.W., Bryan, F.O., Chassignet, E.P., Gerdes, R., Hasumi, H., Hirst, A.C., Treguier, A.-M., Webb, D.J., 2000. Developments in ocean climate modelling. *Ocean Modell.* 2, 123–192.
- Griffies, S.M., Danabasoglu, G., Durack, P.J., Adcroft, A.J., Balaji, V., Böning, C.W., Chassignet, E.P., Curchitser, E., Deshayes, J., Drange, H., Fox-Kemper, B., Gleckler, P., Gregory, J., Haak, H., Hallberg, R., Heimbach, P., Hewitt, H., Holland, D., Ilyina, T., Jungclaus, J., Komuro, Y., Krasting, J., Large, W., Marsland, S., Masina, S., McDougall, T., Nurser, A.G., Orr, J., Pirani, A., Qiao, F., Stouffer, R., Taylor, K., Treguier, A.M., Tsujino, H., Uotila, P., Valdivieso, M., Wang, Q., Winton, M., Yeager, S., 2016. OMP contribution to CMIP6: experimental and diagnostic protocol for the physical component of the Ocean Model Intercomparison Project. *Geosci. Model Dev.* 9, 3231–3296. <http://dx.doi.org/10.5194/gmd-9-3231-2016>.
- Hadjighasem, A., Farazmand, M., Blazevski, D., Froyland, G., Haller, G., 2017. A critical comparison of lagrangian methods for coherent structure detection. *Chaos* 27 (5), 053104. <http://dx.doi.org/10.1063/1.4982720>.
- Haertel, P.T., Fedorov, A., 2012. The ventilated ocean. *J. Phys. Oceanogr.* 42 (1), 141–164.
- Haertel, P.T., Randall, D.A., 2002. Could a pile of slippery sacks behave like an ocean? *Mon. Weather Rev.* 130 (12), 2975–2988.
- Haidvogel, D., Arango, H., Budgell, W., Cornuelle, B., Curchitser, E., Lorenzo, E.D., Fennel, K., Geyer, W., Hermann, A., Lanerolle, L., Levin, J., McWilliams, J., Miller, A., Moore, A., Powell, T., Shchepetkin, A., Sherwood, C., Signell, R., Warner, J., Wilkin, J., 2008. Ocean forecasting in terrain-following coordinates: formulation and skill assessment of the regional ocean modeling system. *J. Comput. Phys.* 227 (7), 3595–3624. Predicting weather, climate and extreme events, doi:10.1016/j.jcp.2007.06.016.
- Haine, T.W., Hall, T.M., 2002. A generalized transport theory: water-mass composition and age. *J. Phys. Oceanogr.* 32 (6), 1932–1946.
- Haines, M.A., Fine, R.A., Luther, M.E., Ji, Z., 1999. Particle trajectories in an Indian Ocean model and sensitivity to seasonal forcing. *J. Phys. Oceanogr.* 29 (4), 584–598. [http://dx.doi.org/10.1175/1520-0485\(1999\)029<0584:PTIAIO>2.0.CO;2](http://dx.doi.org/10.1175/1520-0485(1999)029<0584:PTIAIO>2.0.CO;2).
- Hairer, E., Lubich, C., Wanner, G., 2006. *Geometric Numerical Integration: Structure-Preserving Algorithms for Ordinary Differential Equations*. vol. 31 Springer Science & Business Media.
- Haller, G., 2015. Lagrangian coherent structures. *Annu. Rev. Fluid Mech.* 47 (1), 137–162. <http://dx.doi.org/10.1146/annurev-fluid-010313-141322>.
- Haller, G., 2016. Dynamic rotation and stretch tensors from a dynamic polar decomposition. *J. Mech. Phys. Solids* 86, 70–93.
- Haller, G., Beron-Vera, F.J., 2012. Geodesic theory of transport barriers in two-dimensional flows. *Physica D* 241 (20), 1680–1702.
- Haller, G., Beron-Vera, F.J., 2013. Coherent Lagrangian vortices: the black holes of turbulence. *J. Fluid Mech.* 731, 69–10.
- Haller, G., Hadjighasem, A., Farazmand, M., Huhn, F., 2016. Defining coherent vortices objectively from the vorticity. *J. Fluid Mech.* 795, 136–173.
- Haller, G., Sapsis, T., 2011. Lagrangian coherent structures and the smallest finite-time

- lyapunov exponent. *Chaos* 21 (2), 023115.
- Haller, G., Yuan, G., 2000. Lagrangian coherent structures and mixing in two-dimensional turbulence. *Physica D* 147 (3–4), 352–370. [http://dx.doi.org/10.1016/S0167-2789\(00\)00142-1](http://dx.doi.org/10.1016/S0167-2789(00)00142-1).
- Halliwel, G., Garraffo, Z.D., 2002. Synthetic Floats, Drifters, and Moorings in HYCOM. Technical Report. HYCOM Consortium.
- Haza, A., Özgökmen, T., Hogan, P., 2016. Impact of submesoscales on surface material distribution in a gulf of mexico mesoscale eddy. *Ocean Modell.* 107, 28–47. <http://dx.doi.org/10.1016/j.ocemod.2016.10.002>.
- Haza, A.C., Özgökmen, T.M., Griffa, A., Molcard, A., Poulain, P.-M., Peggion, G., 2010. Transport properties in small-scale coastal flows: relative dispersion from VHF radar measurements in the Gulf of La Spezia. *Ocean Dyn.* 60 (4), 861–882. <http://dx.doi.org/10.1007/s10236-010-0301-7>.
- Heemink, A.W., 1990. Stochastic modeling of dispersion in shallow-water. *Stochastic Hydrol. Hydraul.* 4 (2), 161–174.
- Hegerl, G.C., Black, E., Allan, R.P., Ingram, W.J., Polson, D., Trenberth, K.E., Chadwick, R.S., Arkin, P.A., Sarojini, B.B., Becker, A., Dai, A., Durack, P.J., Easterling, D., Fowler, H.J., Kendon, E.J., Huffman, G.J., Liu, C., Marsh, R., New, M., Osborn, T.J., Skliris, N., Stott, P.A., Vidale, P.-L., Wijffels, S.E., Wilcox, L.J., Willett, K.M., Zhang, X., 2015. Challenges in quantifying changes in the global water cycle. *Bull. Am. Meteorol. Soc.* 96 (7), 1097–1115.
- Held, I.M., Soden, B.J., 2006. Robust responses of the hydrological cycle to global warming. *J. Climate* 19 (21), 5686–5699.
- Hellweger, F.L., van Sebille, E., Fredrick, N.D., 2014. Biogeographic patterns in ocean microbes emerge in a neutral agent-based model. *Science* 345, 1346–1349.
- Helm, K.P., Bindoff, N.L., Church, J.A., 2010. Changes in the global hydrological-cycle inferred from ocean salinity. *Geophys. Res. Lett.* 37.
- Hofmann, A.F., Soetaert, K., Middelburg, J.J., 2008. Present nitrogen and carbon dynamics in the Scheldt estuary using a novel 1-D model. *Biogeosciences* 5 (4), 981–1006.
- Holstein, D.M., Paris, C.B., Mumby, P.M., 2014. Consistency and inconsistency in multispecies population network dynamics of coral reef ecosystems. *Marine Ecol. Prog. Ser.* 499, 1–18. <http://dx.doi.org/10.3354/meps10647>.
- Holzer, M., Hall, T.M., 2000. Transit-time and tracer-age distributions in geophysical flows. *J. Atmos. Sci.* 57 (21), 3539–3558. [http://dx.doi.org/10.1175/1520-0469\(2000\)057<3539:TTATAD>2.0.CO;2](http://dx.doi.org/10.1175/1520-0469(2000)057<3539:TTATAD>2.0.CO;2).
- Hosoda, S., Suga, T., Shikama, N., Mizuno, K., 2009. Global surface layer salinity change detected by argo and its implication for hydrological cycle intensification. *J. Oceanogr.* 65 (4), 579–586.
- Hunter, J., Craig, P., Phillips, H., 1993. On the use of random walk models with spatially variable diffusivity. *J. Comput. Phys.* 106 (2), 366–376. [http://dx.doi.org/10.1016/S0021-9991\(83\)71114-9](http://dx.doi.org/10.1016/S0021-9991(83)71114-9).
- Ihcak, M., Adcroft, A.J., Griffies, S.M., Hallberg, R.W., 2012. Spurious diapycnal mixing and the role of momentum closure. *Ocean Modell.* 45, 37–58.
- Imasato, N., Awaji, T., Kunishi, H., 1980. Tidal exchange through naruto, akashi and kitan straits. *J. Oceanogr. Soc. Jpn.* 36 (3), 151–162.
- Imasato, N., Qiu, B., 1987. An event in water exchange between continental shelf and the kuroshio off southern Japan: Lagrangian tracking of a low-salinity water mass on the kuroshio. *J. Phys. Oceanogr.* 17 (7), 953–968.
- Iudicone, D., Rodgers, K., Stendaro, I., Aumont, O., Madec, G., Bopp, L., Mangoin, O., d'Alcala, M.R., 2011. Water masses as a unifying framework for understanding the Southern Ocean Carbon Cycle. *Biogeosciences* 8, 1031–1052.
- Jazwinski, A.H., 1970. *Stochastic Processes and Filtering Theory*. Academic Press, New York.
- Jones, B.T., Solow, A., Ji, R., 2016. Resource allocation for lagrangian tracking. *J. Atmos. Ocean. Technol.* 33 (6), 1225–1235. <http://dx.doi.org/10.1175/JTECH-D-15-0115.1>.
- Jönsson, B.F., Lundberg, P.A., Döös, K., 2004. Baltic sub-basin turnover times examined using the Rossby Centre Ocean model. *Ambio* 33 (4–5), 257–260. <http://dx.doi.org/10.1579/0044-7447-33.4.257>.
- Jönsson, B.F., Salisbury, J.E., Mahadevan, A., 2011. Large variability in continental shelf production of phytoplankton carbon revealed by satellite. *Biogeosciences* 8 (5), 1213–1223.
- Jonsson, B.F., Watson, J.R., 2016. The timescales of global surface-ocean connectivity. *Nat. Commun.* 7, 1–6.
- Jutzeler, M., Marsh, R., Carey, R.J., White, J.D.L., Talling, P.J., Karlstrom, L., 2014. On the fate of pumice rafts formed during the 2012 Havre submarine eruption. *Nat. Commun.* 5, 3660.
- Kamenkovich, I., Rypina, I.I., Berloff, P., 2015. Properties and origins of the anisotropic eddy-induced transport in the north atlantic. *J. Phys. Oceanogr.* 45 (3), 778–791.
- Karrasch, D., Haller, G., 2013. Do finite-size lyapunov exponents detect coherent structures? *Chaos* 23 (4), 043126.
- Khatiwala, S., Visbeck, M., Schlosser, P., 2001. Age tracers in an ocean GCM. *Deep-Sea Res. Part I* 48 (6), 1423–1441. [http://dx.doi.org/10.1016/S0967-0637\(00\)00094-7](http://dx.doi.org/10.1016/S0967-0637(00)00094-7).
- Kinlan, B., Gaines, S., 2003. Propagule dispersal in marine and terrestrial environments: a community perspective. *Ecology* 84 (8), 2007–2020.
- Kjellsson, J., Döös, K., 2012. Lagrangian decomposition of the hadley and ferrel cells. *Geophys. Res. Lett.* 39, L15807. <http://dx.doi.org/10.1029/2012GL052420>.
- Kjellsson, J., Döös, K., 2012. Surface drifters and model trajectories in the baltic sea. *Boreal Environ. Res.* 17, 447–459.
- Kjellsson, J., Doos, K., Laliberte, F.B., Zika, J.D., 2014. The atmospheric general circulation in thermodynamical coordinates. *J. Atmos. Sci.* 71 (3), 916–928.
- Klocker, A., Abernathy, R., 2014. Global patterns of mesoscale eddy properties and diffusivities. *J. Phys. Oceanogr.* 44, 1030–1047. <http://dx.doi.org/10.1175/JPO-D-13-0159.1>.
- Klocker, A., Ferrari, R., LaCasce, J.H., 2012. Estimating suppression of eddy mixing by mean flow. *J. Phys. Oceanogr.* 9, 1566–1576.
- Klocker, A., Ferrari, R., LaCasce, J.H., Merrifield, S.T., 2012. Reconciling float-based and tracer-based estimates of lateral diffusivities. *J. Marine Res.* 70 (4), 569–602.
- Kloeden, P.E., Platen, E., 1992. *Numerical Solutions of Stochastic Differential Equations. Application of Mathematics, Stochastic Modelling and applied probability*. Springer-Verlag, Berlin Heidelberg.
- Koch-Larrouy, A., Morrow, R., Penduff, T., Juza, M., 2010. Origin and mechanism of Subantarctic Mode Water formation and transformation in the Southern Indian Ocean. *Ocean Dyn.* 60 (3), 563–583. <http://dx.doi.org/10.1007/s10236-010-0276-4>.
- Kool, J.T., Moilanen, A., Trem, E.A., 2013. Population connectivity: recent advances and new perspectives. *Landscape Ecol.* 28 (2), 165–185. <http://dx.doi.org/10.1007/s10980-012-9819-z>.
- Koszalka, I., LaCasce, J.H., 2010. Lagrangian analysis by clustering. *Ocean Dyn.* 60(4), 957–972. <http://dx.doi.org/10.1007/s10236-010-0306-2>.
- Koszalka, I., LaCasce, J.H., Andersson, M., Orvik, K.A., Mauritzen, C., 2011. Surface circulation in the Nordic Seas from clustered drifters. *Deep Sea Res. I* 58(4), 468–485. <http://dx.doi.org/10.1016/j.dsr2.2011.01.007>.
- Koszalka, I., LaCasce, J.H., Mauritzen, C., 2013. In pursuit of anomalies - analyzing the poleward transport of Atlantic Water with surface drifters. *Deep Sea Res. II* 85, 96–108. <http://dx.doi.org/10.1016/j.dsr2.2012.07.035>.
- Koszalka, I., LaCasce, J.H., Orvik, K.A., 2009. Relative dispersion in the Nordic Seas. *J. Mar. Res.* 67, 411–433.
- Koszalka, I.M., Haine, T.W.N., Magaldi, M.G., 2013. Fates and travel times of Denmark Strait Overflow Water in the Irminger Basin. *J. Phys. Oceanogr.* 43 (12), 2611–2628. <http://dx.doi.org/10.1175/JPO-D-13-023.1>.
- Krugger-Emden, H., Sturm, M., Wirtz, S., Scherer, V., 2008. Selection of an appropriate time integration scheme for the discrete element method (DEM). *Comput. Chem. Eng.* 32 (10), 2263–2279. <http://dx.doi.org/10.1016/j.compchemeng.2007.11.002>.
- Kundu, P.K., Cohen, I.M., Dowling, D.R., 2012. Chapter 3 - kinematics. *Fluid Mechanics*, fifth ed. Academic Press, Boston, pp. 65–93. <http://dx.doi.org/10.1016/B978-0-12-382100-3.10003-4>.
- LaCasce, J., 2008. Statistics from lagrangian observations. *Prog. Oceanogr.* 77 (1), 1–29.
- LaCasce, J.H., 2005. Eulerian and Lagrangian velocity distributions in the North Atlantic. *J. Phys. Oceanogr.* 35 (12), 2327–2336.
- LaCasce, J.H., Ferrari, R., Marshall, J., Tulloch, R., Balwada, D., Speer, K., 2014. Float-Derived Isopycnal Diffusivities in the DIMES Experiment. *J. Phys. Oceanogr.* 44 (2), 764–780.
- Laliberte, F., Zika, J.D., Mudryk, L., Kushner, P.J., Kjellsson, J., Döös, K., 2015. Constrained work output of the moist atmospheric heat engine in a warming climate. *Science* 347 (6221), 540–543.
- Lampert, W., 1989. The adaptive significance of diel vertical migration of zooplankton. *Funct. Ecol.* 3 (1), 21–27. <http://dx.doi.org/10.2307/2389671>.
- Lange, M., van Sebille, E., 2017. Parcels v0.9: prototyping a lagrangian ocean analysis framework for the petascale age. *Geosci. Model Dev.* 10, 4175–4186. <http://dx.doi.org/10.5194/gmd-10-4175-2017>.
- Lapeyre, G., 2002. Characterization of finite-time lyapunov exponents and vectors in two-dimensional turbulence. *Chaos* 12 (3), 688–698.
- Lebedev, K.V., Yoshinari, H., Maximenko, N.A., Hacker, P., 2007. YoMaHa'05: Velocity Data Derived from Trajectories of Argo Floats at Parking Level and At the Sea Surface. Technical Report. IPRC Technical Note.
- Lebreton, L.C.M., Greer, S.D., Borerro, J.C., 2012. Numerical modelling of floating debris in the world's oceans. *Marine Pollut. Bull.* 64, 653–661.
- Ledwell, J.R., St. Laurent, L.C., Girtin, J.B., Toole, J.M., 2011. Diapycnal mixing in the antarctic circumpolar current. *J. Phys. Oceanogr.* 41 (11), 241–246. <http://dx.doi.org/10.1175/2010JPO4557.1>.
- Lehahn, Y., d'Ovidio, F., Levy, M., Heifetz, E., 2007. Stirring of the northeast Atlantic spring bloom: a Lagrangian analysis based on multisatellite data. *J. Geophys. Res.* 112 (C8), C08005. <http://dx.doi.org/10.1029/2006JC003927>.
- Leimkuhler, B., Reich, S., 2004. *Simulating Hamiltonian Dynamics*. vol. 14 Cambridge University Press.
- Lett, C., Verley, P., Mullen, C. e., 2008. A lagrangian tool for modelling ichthyoplankton dynamics. *Environ. Model Softw.* 23, 1210–1214. <http://dx.doi.org/10.1016/j.envsoft.2008.02.005>.
- Lique, C., Treguier, A.M., Blanke, B., Grima, N., 2010. On the origins of water masses exported along both sides of Greenland: a Lagrangian model analysis. *J. Geophys. Res.* 115 (C5), C05019. <http://dx.doi.org/10.1029/2009JC005316>.
- Liu, G., Chua, V.P., 2016. A SUNTANS-based unstructured grid local exact particle tracking model. *Ocean Dyn.* 1–11.
- Lumpkin, R., Elipot, S., 2010. Surface drifter pair spreading in the North Atlantic. *J. Geophys. Res.* 115. <http://dx.doi.org/10.1029/2010JC006338>.
- Lumpkin, R., Johnson, G.C., 2013. Global ocean surface velocities from drifters: mean, variance, enso response, and sea-sonal cycle. *J. Geophys. Res.* 118, 2992–3006. <http://dx.doi.org/10.1002/jgrc.20210>.
- Lumpkin, R., Pazos, M., 2007. Measuring surface currents with surface velocity program drifters: the instrument, its data, and some recent results. In: Griffa, A., Kirwan Jr.A.D., Mariano, A.J., Rossby, H.T. (Eds.), *Lagrangian Analysis and Prediction of Coastal and Ocean Dynamics*. Cambridge University Press.
- Lynch, D.R., Greenberg, D.A., Bilgili, A., McGillicuddy Jr., D.J., Manning, J.P., Arctabaleta, A.L., 2014. Individual-based models – biotic particles. *Particles in the Coastal Ocean Theory and Applications*. Cambridge University Press.
- Madec, G., 2008. NEMO Ocean Engine. Technical Report. Note du Pole de modélisation de l'Institut Pierre-Simon No 27, ISSN no.
- Madec, G., NEMO team, 2016. NEMO Ocean Engine. Technical Report. Institut Pierre-Simon Laplace (IPSL).
- Marsden, J.E., Pekarsky, S., Shkoller, S., 1999. Stability of relative equilibria of point vortices on a sphere and symplectic integrators. *Nuovo Cimento Della Società Italiana di Fisica. C* 22 (6), 793–802.

- Marsh, R., Ivchenko, V.O., Skliris, N., Alderson, S., Bigg, G.R., Madec, G., Blaker, A.T., Aksenov, Y., Sinha, B., Coward, A.C., Le Sommer, J., Merino, N., Zalesny, V.B., 2015. NEMO-ICB (v1.0): interactive icebergs in the NEMO ocean model globally configured at eddy-permitting resolution. *Geosci. Model Dev.* 8 (5), 1547–1562.
- Marshall, J., Adcroft, A., Hill, C., Perelman, L., Heisey, C., 1997. A finite-volume, incompressible Navier Stokes model for studies of the ocean on parallel computers. *J. Geophys. Res.* 102 (C3), 5753–5766.
- Marshall, J., Adcroft, A., Hill, C., Perelman, L., Heisey, C., 1997. A finite-volume, incompressible navier stokes model for studies of the ocean on parallel computers. *J. Geophys. Res.* 102, 5753–5766.
- Marshall, J., Hill, C., Perelman, L., Adcroft, A., 1997. Hydrostatic, quasi-hydrostatic, and non-hydrostatic ocean modeling. *J. Geophys. Res.* 102, 5733–5752.
- Martin, P., Loeff, M.R., Cassar, N., Vandromme, P., d'Ovidio, F., Stemmann, L., Rengarajan, R., Soares, M., González, H.E., Ebersbach, F., et al., 2013. Iron fertilization enhanced net community production but not downward particle flux during the southern ocean iron fertilization experiment lohafex. *Global Biogeochem. Cycles* 27 (3), 871–881.
- Martin, T., Adcroft, A., 2010. Parameterizing the fresh-water flux from land ice to ocean with interactive icebergs in a coupled climate model. *Ocean Modell.* 34 (3–4), 111–124.
- Mazloff, M.R., Heimbach, P., Wunsch, C., 2010. An Eddy-permitting southern ocean state estimate. *J. Phys. Oceanogr.* 40 (5), 880–899. <http://dx.doi.org/10.1175/2009JPO4236.1>.
- McDougall, T.J., 2003. Potential enthalpy: a conservative oceanic variable for evaluating heat content and heat fluxes. *J. Phys. Oceanogr.* 33, 945–963.
- McLachlan, R.I., 1999. Area preservation in computational fluid dynamics. *Phys. Lett. A* 264 (1), 36–44.
- McManus, M.A., Woodson, C.B., 2012. Plankton distribution and ocean dispersal. *J. Exp. Biol.* 215 (6), 1008–1016.
- Mesinger, F., Arakawa, A., 1976. Numerical Methods Used in Atmospheric Models. GARP Publications, World Meteorological Organization.
- Mezić, I., Loire, S., Fonoberov, V.A., Hogan, P., 2010. A new mixing diagnostic and gulf oil spill movement. *Science* 330 (6003), 486–489. <http://dx.doi.org/10.1126/science.1194607>.
- Middleton, J.F., Loder, J.W., 1989. Skew fluxes in polarized wave fields. *J. Phys. Oceanogr.* 19, 68–76.
- Monaghan, J.J., 1992. Smoothed particle hydrodynamics. *Annu. Rev. Astron. Astrophys.* 30, 543–574. <http://dx.doi.org/10.1146/annurev.aa.30.090192.002551>.
- Mouchet, A., Cornaton, F., Deleersnijder, E., Delhez, E., 2016. Partial ages: diagnosing transport processes by means of multiple clocks. *Ocean Dyn.* 66, 367–386.
- Narvaez, D.A., Klinck, J.M., Powell, E.N., Hofmann, E.E., Wilkin, J., Haidvogel, D.B., 2012. Circulation and behavior controls on dispersal of eastern oyster (*Crassostrea virginica*) larvae in Delaware Bay. *J. Marine Res.* 70 (2–3), 411–440.
- Narvaez, D.A., Klinck, J.M., Powell, E.N., Hofmann, E.E., Wilkin, J., Haidvogel, D.B., 2012. Modeling the dispersal of eastern oyster (*Crassostrea virginica*) larvae in Delaware Bay. *J. Marine Res.* 70 (2–3), 381–409.
- Nencioli, F., d'Ovidio, F., Doglioli, A.M., Petrenko, A.A., 2011. Surface coastal circulation patterns by in-situ detection of Lagrangian coherent structures. *Geophys. Res. Lett.* 38 (17), L17604. <http://dx.doi.org/10.1029/2011GL048815>.
- Nencioli, F., d'Ovidio, F., Doglioli, A.M., Petrenko, A.A., 2013. In situ estimates of sub-mesoscale horizontal eddy diffusivity across an ocean front. *J. Geophys. Res.* 118 (12), 7066–7080. <http://dx.doi.org/10.1002/2013JC009252>.
- Nilsson, J.A.U., Döös, K., Ruti, P.M., Artale, V., Coward, A.C., Brodeur, L., 2013. Observed and modeled global ocean turbulence regimes as deduced from surface trajectory data. *J. Phys. Oceanogr.* 43, 2249–2269. <http://dx.doi.org/10.1175/JPO-D-12-0193.1>.
- Olascoaga, M.J., Rypina, I.I., Brown, M.G., Beron Vera, F.J., Kocak, H., Brand, L.E., Halliwell, G.R., Shay, L.K., 2006. Persistent transport barrier on the West Florida Shelf. *Geophys. Res. Lett.* 33 (22). <http://dx.doi.org/10.1029/2006GL027800>.
- Ollitrault, M., Rannou, J.-P., 2013. ANDRO: an argo-based deep displacement dataset. *J. Atmos. Oceanic Technol.* 30 (4), 759–788.
- Paris, C.B., Atema, J., Irissou, J.-O., Kingsford, M., Gerlach, G., Guigand, C.M., 2013. Reef Odor: a wake up call for navigation in reef fish larvae. *PLOS One* 8 (8), e72808–8.
- Paris, C.B., Cowen, R.K., Claro, R., Lindeman, K.C., 2005. Larval transport pathways from Cuban snapper (*Lutjanidae*) spawning aggregations based on biophysical modeling. *Marine Ecol.-Prog. Ser.* 296, 93–106.
- Paris, C.B., Helgers, J., van Sebille, E., Srinivasan, A., 2013. Connectivity modeling system: a probabilistic modeling tool for the multi-scale tracking of biotic and abiotic variability in the ocean. *Environ. Modell. Software* 42, 47–54. <http://dx.doi.org/10.1016/j.envsoft.2012.12.006>.
- Paris, C.B., Le Hénaff, M., Aman, Z.M., Subramaniam, A., Helgers, J., Wang, D.-P., Kourafalou, V.H., Srinivasan, A., 2012. Evolution of the Macondo well blowout: simulating the effects of the circulation and synthetic dispersants on the subsea oil transport. *Environ. Sci. Technol.* 42, 47–54.
- Pavia, E.G., Cushman-Roisin, B., 1988. Modelling of oceanic fronts using a particle method. *J. Geophys. Res.* 93, 3554–3562.
- Peacock, T., Dabiri, J., 2010. Introduction to focus issue: Lagrangian coherent structures. *Chaos* 20 (1), 017501. <http://dx.doi.org/10.1063/1.3278173>.
- Peacock, T., Haller, G., 2013. Lagrangian coherent structures: the hidden skeleton of fluid flows. *Phys. Today* 66 (2), 41.
- Perot, B., 2000. Conservation properties of unstructured staggered mesh schemes. *J. Comput. Phys.* 159 (1), 58–89.
- Phelps, J.J., Polton, J.A., Souza, A.J., Robinson, L.A., 2013. Hydrodynamic timescales in a hyper-tidal region of freshwater influence. *Cont. Shelf Res.* 63, 13–22. <http://dx.doi.org/10.1016/j.csr.2013.04.027>.
- Phelps, J.J.C., Polton, J.A., Souza, A.J., Robinson, L.A., 2015. Behaviour influences larval dispersal in shelf sea gyres: Nephrops norvegicus in the Irish Sea. *Marine Ecol. Prog. Ser.* 518, 177–191. <http://dx.doi.org/10.3354/meps11040>.
- Piñones, A., Hofmann, E.E., Dinniman, M.S., Klinck, J.M., 2011. Lagrangian simulation of transport pathways and residence times along the western Antarctic Peninsula. *Deep Sea Res. Part II* 58 (13–16), 1524–1539. <http://dx.doi.org/10.1016/j.dsr2.2010.07.001>.
- Pierrehumbert, R., Yang, H., 1993. Global chaotic mixing on isentropic surfaces. *J. Atmos. Sci.* 50 (15), 2462–2480.
- Poje, A.C., Haza, A.C., Özgökmen, T.M., Magaldi, M.G., Garraffo, Z.D., 2010. Resolution dependent relative dispersion statistics in a hierarchy of ocean models. *Ocean Modell.* 31 (1–2), 36–50.
- Poje, A.C., Özgökmen, T.M., Lipphardt, B.L., Haus, B.K., Ryan, E.H., Haza, A.C., Jacobs, G.A., Reniers, A.J.H.M., Olascoaga, M.J., Novelli, G., Griffa, A., Beron Vera, F.J., Chen, S.S., Coelho, E., Hogan, P.J., Kirwan, A.D., Huntley, H.S., Mariano, A.J., 2014. Submesoscale dispersion in the vicinity of the Deepwater Horizon spill. *Proc. Natl. Acad. Sci.* 111 (35), 12693–12698. <http://dx.doi.org/10.1073/pnas.1402452111>.
- Pujolar, J.M., Schiavina, M., Di Franco, A., Melià, P., Guidetti, P., Gatto, M., De Leo, G.A., Zane, L., 2013. Understanding the effectiveness of marine protected areas using genetic connectivity patterns and Lagrangian simulations. *Divers. Distrib.* 19 (12), 1531–1542. <http://dx.doi.org/10.1111/ddi.12114>.
- Qin, X., van Sebille, E., Gupta, A.S., 2014. Quantification of errors induced by temporal resolution on lagrangian particles in an eddy-resolving model. *Ocean Modell.* 76, 20–30.
- Redi, M.H., 1982. Oceanic isopycnal mixing by coordinate rotation. *J. Phys. Oceanogr.* 12 (10), 1154–1158.
- Reverdin, G., Morisset, S., Marié, L., Bourras, D., Sutherland, G., Ward, B., Salvador, J., Font, J., Cuypers, Y., Centurioni, L., Hormann, V., Koldziejczyk, N., Boutin, J., D'Ovidio, F., Nencioli, F., Martin, N., Diverres, D., Alory, G., Lumpkin, R., 2015. Surface salinity in the North Atlantic subtropical gyre during the STRASSE/SPURS summer 2012 cruise. *Oceanography* 28, 114–123. <http://dx.doi.org/10.5670/oceanog.2015.09>.
- Ringler, T., Petersen, M., Higdon, R.L., Jacobsen, D., Jones, P.W., Maltrud, M., 2013. A multi-resolution approach to global ocean modeling. *Ocean Modell.* 69, 211–232.
- Ringler, T.D., Saenz, J.A., Wolfram, P.J., van Roekel, L., 2016. A thickness-weighted average perspective of force balance in an idealized circumpolar current. *J. Phys. Oceanogr.*
- Roche, D.M., 2013.  $\delta^{18}\text{O}$  water isotope in the iloveclim model (version 1.0) - part 1: implementation and verification. *Geosci. Model Dev.* 6 (5), 1481–1491. <http://dx.doi.org/10.5194/gmd-6-1481-2013>.
- Ross, O.N., Sharples, J., 2004. Recipe for 1-D Lagrangian particle tracking models in space-varying diffusivity. *Limnol. Oceanogr.* 289–302.
- Rossi, V., van Sebille, E., Sen Gupta, A., Garçon, V., England, M.H., 2013. Multi-decadal projections of surface and interior pathways of the Fukushima Cesium-137 radioactive plume. *Deep-Sea Res. Part I* 80 (C), 37–46.
- Rühs, S., Durgadoo, J.V., Behrens, E., Biastoch, A., 2013. Advective timescales and pathways of Agulhas leakage. *Geophys. Res. Lett.* 40 (15), 3997–4000. <http://dx.doi.org/10.1002/grl.50782>.
- Rypina, I., Kamenkovich, I., Berloff, P., Pratt, L., 2012. Eddy-induced particle dispersion in the upper-ocean north atlantic. *J. Phys. Oceanogr.* 42, 2206–2228.
- Rypina, I., Scott, S., Pratt, L., Brown, M., 2011. Investigating the connection between complexity of isolated trajectories and lagrangian coherent structures. *Nonlinear Processes Geophys.* 18 (6), 977–987.
- Salama, N.K.G., Rabe, B., 2013. Developing models for investigating the environmental transmission of disease-causing agents within open-cage salmon aquaculture. *Aquacult. Environ. Interact.* 4 (2), 91–115. <http://dx.doi.org/10.3354/aei00077>.
- Salmon, R., 1998. Lectures on Geophysical Fluid Dynamics. Oxford University Press, Oxford, England. 378 + xiii pp.
- Sammarco, P.W., Brazeau, D.A., Sinclair, J., 2012. Genetic connectivity in scleractinian corals across the northern gulf of mexico: Oil/gas platforms, and relationship to the flower garden banks. *PLoS ONE* 7 (4), e30144. <http://dx.doi.org/10.1371/journal.pone.0030144>.
- Schroeder, K., Haza, A.C., Griffa, A., Özgökmen, T.M., Poulain, P.M., Gerin, R., Peggion, G., Rixen, M., 2011. Relative dispersion in the Liguro-Provençal basin: from sub-mesoscale to mesoscale. *Deep Sea Res.* 158 (3), 209–228. <http://dx.doi.org/10.1016/j.dsr.2010.11.004>.
- Scott, R., Biastoch, A., Roder, C., Stiebens, V.A., Eizaguirre, C., 2014. Nano-tags for neonates and ocean-mediated swimming behaviours linked to rapid dispersal of hatchling sea turtles. *Proc. R. Soc. B* 281 (1796), 20141209–20141209.
- van Sebille, E., Beal, L.M., Johns, W.E., 2011. Advective time scales of Agulhas leakage to the North Atlantic in surface drifter observations and the 3D OFES model. *J. Phys. Oceanogr.* 41 (2002), 1026–1034. <http://dx.doi.org/10.1175/2011>.
- van Sebille, E., Johns, W.E., Beal, L.M., 2012. Does the vorticity flux from Agulhas rings control the zonal pathway of NADW across the South Atlantic? *J. Geophys. Res.* 29, 2753–2768.
- van Sebille, E., Scussolini, P., Durgadoo, J.V., Peeters, F.J.C., Biastoch, A., Weijer, W., Turney, C.S.M., Paris, C.B., Zahn, R., 2015. Ocean currents generate large footprints in marine palaeoclimate proxies. *Nat. Commun.* 6, 6521.
- van Sebille, E., Spence, P., Mazloff, M.R., England, M.H., Rintoul, S.R., Saenko, O.A., 2013. Abyssal connections of Antarctic Bottom Water in a Southern Ocean State Estimate. *Geophys. Res. Lett.* 40.
- van Sebille, E., Sprintall, J., Schwarzkopf, F.U., Sen Gupta, A., Santoso, A., England, M.H., Biastoch, A., Böning, C.W., 2014. Pacific-to-Indian Ocean connectivity: Tasman leakage, Indonesian Throughflow, and the role of ENSO. *J. Geophys. Res. Ocean.* 119 (2), 1365–1382. <http://dx.doi.org/10.1002/2013JC009525>.
- Shah, S., Primeau, F., Deleersnijder, E., Heemink, A., 2017. Tracing the ventilation pathways of the deep North Pacific Ocean using Lagrangian particles and Eulerian



- tracers. *J. Phys. Oceanogr.* 47, 1261–1280. <http://dx.doi.org/10.1175/JPO-D-16-0098.1>.
- Shah, S.H.A.M., Heemink, A.W., Deleersnijder, E., 2011. Assessing lagrangian schemes for simulating diffusion on non-flat isopycnal surfaces. *Ocean Modell.* 39 (3–4), 351–361.
- Shah, S.H.A.M., Heemink, A.W., Gräwe, U., Deleersnijder, E., 2013. Adaptive time stepping algorithm for lagrangian transport models: theory and idealised test cases. *Ocean Modell.* 68, 9–21.
- Shchepetkin, A.F., McWilliams, J.C., 2005. The regional oceanic modeling system (ROMS): a split-explicit, free-surface, topography-following-coordinate oceanic model. *Ocean Modell.* 9 (4), 347–404. <http://dx.doi.org/10.1016/j.ocemod.2004.08.002>.
- Shevchenko, I.V., Berloff, P.S., 2015. Multi-layer quasi-geostrophic ocean dynamics in Eddy-resolving regimes. *Ocean Modell.* 94 (C), 1–14.
- Simons, R.D., Siegel, D.A., Brown, K.S., 2013. Model sensitivity and robustness in the estimation of larval transport: a study of particle tracking parameters. *J. Marine Syst.* 119.
- Skirris, N., Marsh, R., Josey, S.A., Good, S.A., Liu, C., Allan, R.P., 2014. Salinity changes in the World Ocean since 1950 in relation to changing surface freshwater fluxes. *Climate Dyn.* 43 (3–4), 709–736.
- Skirris, N., Zika, J., Nurser, A., Josey, S.A., Marsh, R., 2016. Global water cycle amplifying at less than the Clausius-Clapeyron rate. *Sci. Rep.* 6. <http://dx.doi.org/10.1038/srep38752>. Article number: 38752.
- Smetacek, V., Klaas, C., Strass, V.H., Assmy, P., Montresor, M., Cisewski, B., Savoye, N., Webb, A., d'Ovidio, F., Arrieta, J.M., Bathmann, U., Bellerby, R., Berg, G.M., Croot, P., Gonzalez, S., Henjes, J., Herndl, G.J., Hoffmann, L.J., Leach, H., Losch, M., Mills, M.M., Neill, C., Peeken, I., Rottgers, R., Sachs, O., Sauter, E., Schmidt, M.M., Schwarz, J., Terbruggen, A., Wolf Gladrow, D., 2012. Deep carbon export from a Southern Ocean iron-fertilized diatom bloom. *Nature* 487 (7407), 313–319. <http://dx.doi.org/10.1038/nature11229>.
- Spagnol, S., Wolanski, E., Deleersnijder, E., Brinkman, R., McAllister, F., Cushman-Roisin, B., Hanert, E., 2002. An error frequently made in the evaluation of advective transport in two-dimensional Lagrangian models of advection-diffusion in coral reef waters. *Marine Ecol. Prog. Ser.* 235, 299–302.
- Speich, S., 1992. Etude du Forçage de la Circulation Oceanique par Les Detroits: Cas de la Mer d'Alboran. Ph.D. thesis. Université de Paris 06.
- Speich, S., Blanke, B., Madec, G., 2001. Warm and cold water routes of an OGCM thermohaline conveyor belt. *Geophys. Res. Lett.* 28 (2), 311–314.
- Speich, S., Blanke, B., de Vries, P., Drijfhout, S.S., Döös, K., Ganachaud, A., Marsh, R., 2002. Tasman leakage: a new route in the global ocean conveyor belt. *Geophys. Res. Lett.* 29 (10), 1416.
- Spivakovskaya, D., Heemink, A.W., Deleersnijder, E., 2007. The backward Itô method for the lagrangian simulation of transport processes with large space variations of the diffusivity. *Ocean Sci.* 3, 525–535.
- Spivakovskaya, D., Heemink, A.W., Deleersnijder, E., 2007. Lagrangian modelling of multidimensional advection-diffusion with space-varying diffusivities: theory and idealized test cases. *Ocean Dyn.* 57 (3), 189–203.
- Spivakovskaya, D., Heemink, A.W., Milstein, G.N., Schoenmakers, J.G.M., 2005. Simulation of the transport particles in coastal waters using forward and reverse time diffusion. *Adv. Water Resour.* 28 (9), 927–938.
- Staaterman, E., Paris, C.B., 2013. Modelling larval fish navigation: the way forward. *ICES J. Marine Sci. fst103*. <http://dx.doi.org/10.1093/icesjms/fst103>.
- Stohl, A., 1998. Computation, accuracy and applications of trajectories: a review and bibliography. *Atmos. Environ.* 32 (6), 947–966. [http://dx.doi.org/10.1016/S1352-2310\(97\)00457-3](http://dx.doi.org/10.1016/S1352-2310(97)00457-3).
- Stohl, A., James, P., 2005. A Lagrangian analysis of the atmospheric branch of the global water cycle. Part II: Moisture transports between earth's ocean basins and river catchments. *J. Hydrometeorol.* 6 (6), 961–984.
- Stouffer, R.J., 2004. Time scales of climate response. *J. Climate* 17, 209–217.
- Sunagawa, S., Coelho, L.P., Chaffron, S., Kultima, J.R., Labadie, K., Salazar, G., Djahanschiri, B., Zeller, G., Mende, D.R., Alberti, A., et al., 2015. Structure and function of the global ocean microbiome. *Science* 348 (6237), 1261359.
- Swift, D.D., Riser, S.C., 1994. RAFOS floats: defining and targeting surfaces of neutral buoyancy. *J. Atmos. Oceanic Tech.* 11 (4), 1079–1092.
- Taylor, G.I., 1921. Diffusion by continuous movements. *Proc. London Math. Soc.* 20, 196–212.
- Teske, P.R., Sandoval-Castillo, J., van Sebille, E., Waters, J., Beheregaray, L.B., 2015. On-shelf larval retention limits population connectivity in a coastal broadcast spawner. *Marine Ecol.-Prog. Ser.* 532, 1–12.
- Thomas, C., et al., 2015. Modelling Marine Connectivity in the Great Barrier Reef and Exploring its Ecological Implications. UCL Ph.D. thesis.
- Thomas, C.J., Lambrechts, J., Wolanski, E., Traag, V.A., Blondel, V.D., Deleersnijder, E., Hanert, E., 2014. Numerical modelling and graph theory tools to study ecological connectivity in the Great Barrier Reef. *Ecological Modell.* 272, 160–174.
- Thomas, M.D., Tréguier, A.-M., Blanke, B., Deshayes, J., Voldoire, A., 2015. A Lagrangian method to isolate the impacts of mixed layer subduction on the meridional overturning circulation in a numerical model. *J. Clim.* 28, 7503–7517.
- Tremli, E.A., Halpin, P.N., Urban, D.L., Pratson, L.F., 2008. Modeling population connectivity by ocean currents, a graph-theoretic approach for marine conservation. *Landscape Ecol.* 23, 19–36. <http://dx.doi.org/10.1007/s10980-007-9138-y>.
- Trenberth, K.E., 1998. Atmospheric moisture residence times and cycling: Implications for rainfall rates and climate change. *Clim. Change* 39 (4), 667–694.
- Ullman, D.S., O'Donnell, J., Kohut, J., Fake, T., Allen, A., 2006. Trajectory prediction using HF radar surface currents: Monte Carlo simulations of prediction uncertainties. *J. Geophys. Res.* 111 (C12), C12005–14.
- Valdivieso Da Costa, M., Blanke, B., 2004. Lagrangian methods for flow climatologies and trajectory error assessment. *Ocean Modell.* 6 (3–4), 335–358.
- Vallis, G.K., 2006. *Atmospheric and Oceanic Fluid Dynamics: Fundamentals and Large-scale Circulation*, first ed. Cambridge University Press, Cambridge. 745 + xxv pp.
- Vanderborght, J.-P., Folmer, I.M., Aguilera, D.R., Uehnholt, T., Regnier, P., 2007. Reactive-transport modelling of C, N, and O<sub>2</sub> in a river-estuarine-coastal zone system: Application to the Scheldt estuary. *Marine Chem.* 106 (1–2), 92–110.
- Veneziani, M., Griffa, A., Reynolds, A.M., Mariano, A.J., 2004. Oceanic turbulence and stochastic models from subsurface lagrangian data for the northwest atlantic ocean. *J. Phys. Oceanogr.* 34 (8), 1884–1906.
- Villar, E., Farrant, G.K., Follows, M., Garczarek, L., Speich, S., Audic, S., Bittner, L., Blanke, B., Brum, J.R., Brunet, C., Casotti, R., Chase, A., Dolan, J.R., d'Ortenzio, F., Gattuso, J.-P., Grima, N., Guidi, L., Hill, C.N., Jahn, O., Jamet, J.-L., Le Goff, H., Lepoivre, C., Malviya, S., Pelletier, E., Romagnan, J.-B., Roux, S., Santini, S., Scalco, E., Schwenck, S.M., Tanaka, A., Testor, P., Vannier, T., Vincent, F., Zingone, A., Dimier, C., Picheral, M., Searson, S., Kandels-Lewis, S., Tara Oceans Coordinators, Acinas, S.G., Bork, P., Boss, E., de Vargas, C., Gorsky, G., Ogata, H., Pesant, S., Sullivan, M.B., Sunagawa, S., Wincker, P., Karsenti, E., Bowler, C., Not, F., Hingamp, P., Iudicone, D., 2015. Environmental characteristics of Agulhas rings affect inter-ocean plankton transport. *Science* 348 (6237). <http://dx.doi.org/10.1126/science.1261447>.
- Visser, A.W., 1997. Using random walk models to simulate the vertical distribution of particles in a turbulent water column. *Marine Ecol. Prog. Ser.* 158, 275–281.
- Visser, A.W., 2008. Lagrangian modelling of plankton motion: From deceptively simple random walks to Fokker-Planck and back again. *J. Marine Syst.* 70 (3–4), 287–299.
- de Vries, P., Döös, K., 2001. Calculating lagrangian trajectories using time-dependent velocity fields. *J. Atmos. Ocean. Technol.* 18 (6), 1092–1101.
- Wallcraft, A.J., Metzger, E.J., Carroll, S.N., 2009. Software Design Description for the Hybrid Coordinate Ocean Model (HYCOM) Version 2.2. Technical Report, NRL/MR/7320-09-9166. NRL.
- Wang, B., Zhao, G., Fringer, O., 2011. Reconstruction of vector fields for semi-lagrangian advection on unstructured, staggered grids. *Ocean Modell.* 40 (1), 52–71.
- Wang, J., Mazloff, M.R., Gille, S.T., 2016. Cross-stream transport near the Drake Passage. *J. Phys. Oceanogr.* 88. (submitted)
- Wang, Y., Beron-Vera, F.J., Olascoaga, M.J., 2016. The life cycle of a coherent Lagrangian Agulhas ring. *J. Geophys. Res.* 1–11.
- Waugh, D.W., Abraham, E.R., 2008. Stirring in the global surface ocean. *Geophys. Res. Lett.* 35 (20). <http://dx.doi.org/10.1029/2008GL035526>.
- Waugh, D.W., Haine, T.W.N., Hall, T.M., 2004. Transport times and anthropogenic carbon in the subpolar North Atlantic Ocean. *Deep Sea Res. Part I* 51 (11), 1475–1491. <http://dx.doi.org/10.1016/j.dsr.2004.06.011>.
- Welander, P., 1955. Studies on the general development of motion in a two-dimensional, ideal fluid. *Tellus* 7 (2), 141–156.
- Wilkins, D., van Sebille, E., Rintoul, S.R., Lauro, F.M., Cavicchioli, R., 2013. Advection shapes Southern Ocean microbial assemblages independent of distance and environment effects. *Nat. Commun.* 4, 1–7.
- Wolfram, P.J., Ringler, T.D., 2017. Computing eddy-driven effective diffusivity using Lagrangian particles. *Ocean Modell.* 118 (Supplement C), 94–106. <http://dx.doi.org/10.1016/j.ocemod.2017.08.008>.
- Wolfram, P.J., Ringler, T.D., 2017. Quantifying residual, eddy, and mean flow effects on mixing in an idealized circumpolar current. *J. Phys. Oceanogr.* 47 (8), 1897–1920.
- Wolfram, P.J., Ringler, T.D., Maltrud, M.E., Jacobsen, D.W., Petersen, M.R., 2015. Diagnosing isopycnal diffusivity in an eddying, idealized midlatitude ocean basin via Lagrangian, in Situ, Global, High-Performance Particle Tracking (LIGHT). *J. Phys. Oceanogr.* 45 (8), 2114–2133.
- Wood, S., Paris, C.B., Ridgwell, A., Hendy, E.J., 2013. Modelling dispersal and connectivity of broadcast spawning corals at the global scale. *Global Ecol. Biogeogr.* 23, 1–11. <http://dx.doi.org/10.1111/geb.12101>.
- Young, W.R., Jones, S., 1991. Shear dispersion. *Phys. Fluids A* 3 (5), 1087–1101.
- Zhurbas, V., 2004. Drifter-derived maps of lateral diffusivity in the Pacific and Atlantic oceans in relation to surface circulation patterns. *J. Geophys. Res.* 109 (C5), C05015.
- Zika, J.D., England, M.H., Sijp, W.P., 2012. The ocean circulation in thermohaline coordinates. *J. Phys. Oceanogr.* 42 (5), 708–724.